

Steady-State Micro-Bunching based on Transverse-Longitudinal Coupling*

X. J. Deng,^{1,†} A. W. Chao,¹ W. H. Huang,² Z. Z. Li,² Z. L. Pan,² and C. X. Tang²

¹*Institute for Advanced Study, Tsinghua University, Beijing 100084, China*

²*Department of Engineering Physics, Tsinghua University, Beijing 100084, China*

In this paper, three specific scenarios of a novel accelerator light source mechanism called steady-state micro-bunching (SSMB) have been studied, i.e., longitudinal weak focusing, longitudinal strong focusing and generalized longitudinal strong focusing (GLSF). At present, GLSF is the most promising among them in realizing high-power short-wavelength coherent radiation with a mild requirement on the modulation laser power. Its essence is to exploit the ultrasmall natural vertical emittance of an electron beam in a planar storage ring for efficient microbunching formation, like a partial transverse-longitudinal emittance exchange at the optical laser wavelength range. Based on indepth investigation of related beam physics, a solution of a GLSF SSMB storage ring which can deliver 1 kW-average-power EUV light is presented. The work in this paper, such as the generalized Courant-Snyder formalism, the analysis of theoretical minimum emittances, transverse-longitudinal coupling dynamics, and the derivation of the bunching factor and modulation strengths for laser-induced microbunching schemes, is expected to be useful not only for the development of SSMB but also for future accelerator light sources in general that demand increasingly precise electron beam phase space manipulations.

Keywords: Steady-state micro-bunching, extreme ultraviolet, ARPES, generalized Courant-Snyder formalism, theoretical minimum emittances, longitudinal weak focusing, longitudinal strong focusing, generalized longitudinal strong focusing, transverse-longitudinal coupling, damping wiggler

I. INTRODUCTION

Accelerator as light source is arguably the most active driving force for accelerator development at the moment. There are presently two types of workhorses for these sources, namely storage ring-based synchrotron radiation sources and linear accelerator (linac)-based free-electron lasers (FELs). They deliver light with high repetition rate and high peak power or brilliance, respectively. What we are trying to develop is a new storage ring-based light source mechanism called steady-state micro-bunching (SSMB) [1–19], which hopefully can combine the advantages of such two kind of sources and promise both high-repetition and high-power radiation, realizing an accelerator-based fully coherent light source. The schematic layout of an SSMB storage ring and its comparison to the present synchrotron radiation source and FEL is shown in Fig. 1. In a conventional storage ring, the electron bunches are longitudinally focused by one or multiple radio-frequency (RF) cavities, while in SSMB such bunching system is replaced by one or several optical laser modulation systems. The wavelength of laser is six orders of magnitude smaller than that of an RF. The bunch length or structure created by laser is very short, thus the term microbunching. When a beam becomes microbunched, it can radiate coherently and strongly, like that in a laser. But note that in SSMB, there is no exponential growth of the radiation power as that in a high-gain FEL [20] or conventional quantum laser. The term laser in this context mainly reflects that the radiation is coherent, both transversely and longitudi-

nally. To ensure the electron beam property can preserve turn by turn, the SSMB radiator length is comparatively short, typically at meter level, and the peak current of electron beam in SSMB is also lower than that in a high-gain FEL. The radiation back reaction on electron beam is therefore not violent and can be balanced by radiation damping in the ring.

Once realized, such an SSMB ring can produce EUV radiation with greatly enhanced power and flux, allowing sub-meV energy resolution in angle-resolved photoemission spectroscopy (ARPES) and providing new opportunities for fundamental physics research, like revealing key electronic structures in topological materials. A kilowatt (kW)-level EUV source based on such a scheme is also promising to EUV lithography for high-volume chip manufacturing. The reward of such an SSMB ring is therefore tremendous. But one can imagine there are problems to be investigated and solved on the road of every new concept into a reality. To generate coherent EUV radiation in a storage ring, the electron bunch length should reach nm level, which is not at all a trivial task if one keeps in mind that the typical bunch length in present electron storage rings is at mm level. This paper is about our efforts in accomplishing this challenging goal.

The work in this paper is organized as follows. In Sec. II, to build the foundation for the following analysis, we first introduce the generalized Courant-Snyder formalism which applies to a 3D general coupled lattice and present its application in electron storage ring physics. In Sec. III, based on the formalism we derive the theoretical minimum longitudinal emittance in an electron storage ring to provide the basis for later investigation since SSMB is about obtaining short bunch length and small longitudinal emittance. Following this, in Sec. IV, we conduct some key analysis of three specific SSMB scenarios along the thinking of realizing nm bunch length and high-average-power EUV radiation, i.e., longitudinal weak focusing (LWF), longitudinal strong focusing (LSF) and generalized longitudinal strong focusing (GLSF). A short summary of these three schemes is: a LWF

* Supported by the National Key Research and Development Program of China (Grant No. 2022YFA1603401), the National Natural Science Foundation of China (NSFC Grant No. 12035010 and No. 12342501), the Beijing Outstanding Young Scientist Program (No. JWZQ20240101006) and the Tsinghua University Dushi Program.

† dengxiujie@mail.tsinghua.edu.cn

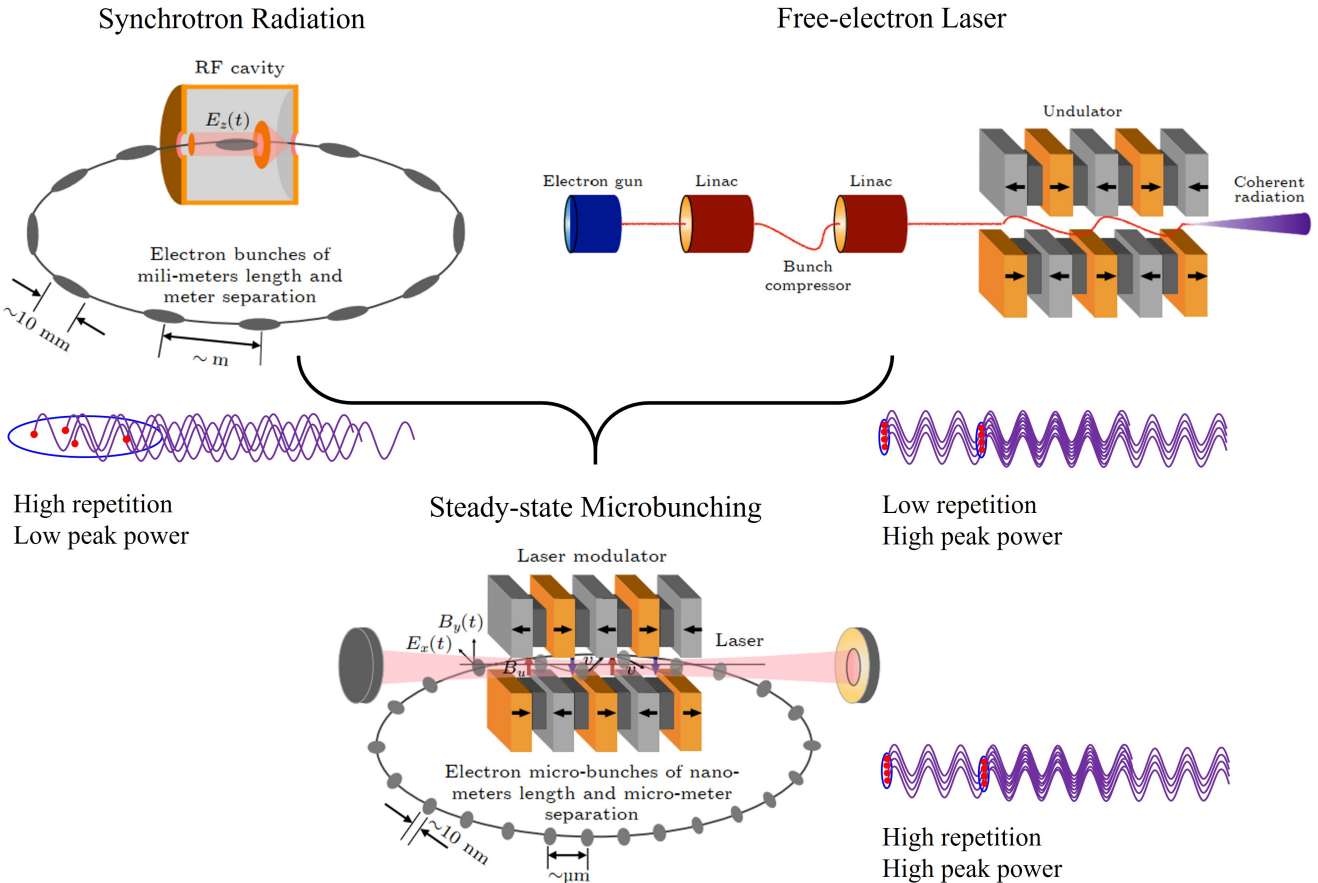


Fig. 1. A schematic layout of an SSMB storage ring, and comparison to a synchrotron radiation source and free-electron laser. (Figure adapted from Ref. [19])

66 SSMB ring can be used to generate bunches with a bunch
 67 length of a couple of 10 nm, thus can be used to generate
 68 coherent visible and infrared radiation. If we want to push
 69 the bunch length to an even shorter value, the required phase
 70 slippage factor of the LWF ring will be too small from an en-
 71 gineering viewpoint. As a comparison, a LSF SSMB ring
 72 can create bunches with a bunch length of nm level, thus
 73 to generate coherent EUV radiation. However, the required
 74 modulation laser power is at gigawatt (GW) level, and makes
 75 the laser modulator, which typically consists of an optical en-
 76 hancement cavity with an incident laser and an undulator and
 77 is used to longitudinally focus the electron beam at the laser
 78 wavelength scale, can only work at a low duty cycle pulsed
 79 mode, thus limiting the average output EUV radiation power.
 80 At present, a GLSF SSMB ring is the most promising among
 81 these three to obtain nm bunch length with a mild modulation
 82 laser power, thus allowing high-average-power radiation out-
 83 put. The basic idea of GLSF is to exploit the ultrasmall ver-
 84 tical emittance in a planar ring and apply partial transverse-
 85 longitudinal emittance for bunch compression with a shallow
 86 energy modulation strength, thus a small modulation laser
 87 power. The backbone of such an GLSF ring is the transverse-
 88 longitudinal coupling (TLC) dynamics, which is analyzed in
 89 depth in this paper. Following this analysis, before going into

90 the concrete examples, we prove three theorems in Sec. V
 91 about TLC-based bunch compression or harmonic generation
 92 schemes. After that, we then go into the details of various
 93 TLC schemes, with Sec. VI devoted to energy modulation-
 94 based schemes and Sec. VII dedicated to angular modulation-
 95 based schemes. We have derived the bunching factors and the
 96 required modulation laser powers for them. The conclusion
 97 from the analysis is that the energy modulation-based cou-
 98 pling is favored for our application in GLSF SSMB. Based on
 99 the investigations and other critical physical considerations,
 100 an example parameter set of a 1 kW-average-power EUV light
 101 source is finally presented in Sec. VIII. A short summary is
 102 given in Sec. IX.

103 II. GENERALIZED COURANT-SNYDER FORMALISM

104 In this section, to provide the basis for the following dis-
 105 cussions, we introduce a generalized Courant-Snyder for-
 106 malism for storage ring physics. Particle state vector $\mathbf{X} =$
 107 $(x \ x' \ y \ y' \ z \ \delta)^T$ is used throughout this paper, with its com-
 108 ponents meaning the horizontal position, horizontal angle,
 109 vertical position, vertical angle, longitudinal position, and

¹¹⁰ $\delta = \Delta E/E_0$ the relative energy deviation of a particle with
¹¹¹ respect to the reference particle, respectively. E_0 is the en-
¹¹² ergy of the reference particle. The superscript T means the
¹¹³ transpose of a vector or matrix.

¹⁴⁴ their definitions take the real and imaginary part of $\mathbf{E}_{ki}\mathbf{E}_{kj}^*$,
¹⁴⁵ respectively. We use the symbol $\hat{\cdot}$ on the top of these func-
¹⁴⁶ tions to indicate ‘imaginary’. Further we can define the real
¹⁴⁷ and imaginary generalized 6×6 Twiss matrices of a storage
¹⁴⁸ ring lattice corresponding to each eigen mode as

¹⁴⁹ A. Generalized Beta Functions in a General Coupled Lattice

¹⁵⁰ Inspired by Chao’s solution by linear matrix (SLIM) for-
¹⁵¹ malism [21], we introduce the definition of the generalized
¹⁵² beta functions in a 3D general coupled storage ring lattice as

$$\begin{aligned} \beta_{ij}^k &= 2\text{Re}(\mathbf{E}_{ki}\mathbf{E}_{kj}^*), \\ k &= \pm I, II, III, \\ i, j &= 1, 2, 3, 4, 5, 6, \end{aligned} \quad (1)$$

¹⁵³ where $*$ means the complex conjugate, the sub or superscript
¹⁵⁴ k is the eigenmode index, $\text{Re}()$ means the real component of
¹⁵⁵ a complex number or matrix, \mathbf{E}_{ki} is the i -th component of the
¹⁵⁶ vector \mathbf{E}_k which is the eigenvector of the 6×6 symplectic
¹⁵⁷ one-turn map \mathbf{M} of storage ring with the eigenvalue $e^{i2\pi\nu_k}$

$$\mathbf{M}\mathbf{E}_k = e^{i2\pi\nu_k}\mathbf{E}_k, \quad (2)$$

¹⁵⁸ satisfying the following normalization condition

$$\mathbf{E}_k^\dagger \mathbf{S} \mathbf{E}_k = \begin{cases} i, & k = I, II, III, \\ -i, & k = -I, -II, -III, \end{cases} \quad (3)$$

¹⁵⁹ and

$$\mathbf{E}_k^\dagger \mathbf{S} \mathbf{E}_j = 0 \text{ for } k \neq j, \quad (4)$$

¹⁶⁰ where i here means the imaginary unit, \dagger means complex con-
¹⁶¹ jugate transpose, and

$$\mathbf{S} = \begin{pmatrix} 0 & 1 & 0 & 0 & 0 & 0 \\ -1 & 0 & 0 & 0 & 0 & 0 \\ 0 & 0 & 0 & 1 & 0 & 0 \\ 0 & 0 & -1 & 0 & 0 & 0 \\ 0 & 0 & 0 & 0 & 0 & 1 \\ 0 & 0 & 0 & 0 & -1 & 0 \end{pmatrix}. \quad (5)$$

¹⁶² This normalization condition can be preserved around the
¹⁶³ ring due to the symplecticity of the transfer matrix. Since the
¹⁶⁴ one-turn map is a real symplectic matrix, for a stable motion,
¹⁶⁵ we have

$$\nu_{-k} = -\nu_k, \mathbf{E}_{-k} = \mathbf{E}_k^*, \quad (6)$$

¹⁶⁶ where ν_k are the eigen tunes.

¹⁶⁷ Similar to the real generalized beta function, here we define
¹⁶⁸ the imaginary generalized beta functions as

$$\hat{\beta}_{ij}^k = 2\text{Im}(\mathbf{E}_{ki}\mathbf{E}_{kj}^*), \quad (7)$$

¹⁶⁹ where $\text{Im}()$ means the imaginary component of a complex
¹⁷⁰ number or matrix. Note that $\hat{\beta}_{ij}^k$ as a value is actually real, just
¹⁷¹ like β_{ij}^k . The name ‘real’ and ‘imaginary’ here reflects that

$$(\mathbf{T}_k)_{ij} = \beta_{ij}^k, (\hat{\mathbf{T}}_k)_{ij} = \hat{\beta}_{ij}^k. \quad (8)$$

¹⁷² From their definitions we have

$$\begin{aligned} \mathbf{T}_{-k} &= \mathbf{T}_k, \mathbf{T}_k^* = \mathbf{T}_k, \mathbf{T}_k^T = \mathbf{T}_k, \\ \hat{\mathbf{T}}_{-k} &= -\hat{\mathbf{T}}_k, \hat{\mathbf{T}}_k^* = \hat{\mathbf{T}}_k, \hat{\mathbf{T}}_k^T = -\hat{\mathbf{T}}_k. \end{aligned} \quad (9)$$

¹⁷³ So we know that \mathbf{T}_k is a real symmetric matrix, while $\hat{\mathbf{T}}_k$ is
¹⁷⁴ a real anti-symmetric matrix. Further, we can prove that

$$\sum_{k=I,II,III} \hat{\mathbf{T}}_k = -\mathbf{S}. \quad (10)$$

¹⁷⁵ The generalized Twiss matrices at different places around the
¹⁷⁶ ring are related to each other according to

$$\begin{aligned} \mathbf{T}_k(s_2) &= \mathbf{R}(s_2, s_1)\mathbf{T}_k(s_1)\mathbf{R}^T(s_2, s_1), \\ \hat{\mathbf{T}}_k(s_2) &= \mathbf{R}(s_2, s_1)\hat{\mathbf{T}}_k(s_1)\mathbf{R}^T(s_2, s_1). \end{aligned} \quad (11)$$

¹⁷⁷ where $\mathbf{R}(s_2, s_1)$ is the symplectic transfer matrix of the state
¹⁷⁸ vector \mathbf{X} from s_1 to s_2

$$\mathbf{X}(s_2) = \mathbf{R}(s_2, s_1)\mathbf{X}(s_1), \quad (12)$$

¹⁷⁹ and we have

$$\mathbf{T}_k(s + C_0) = \mathbf{T}_k(s), \hat{\mathbf{T}}_k(s + C_0) = \hat{\mathbf{T}}_k(s) \quad (13)$$

¹⁸⁰ where C_0 is the circumference of the ring.

¹⁸¹ With the help of the generalized Twiss matrices and eigen
¹⁸² tunes, the one-turn map \mathbf{M} can be parametrized as

$$\begin{aligned} \mathbf{M} &= e^{\mathbf{S}(\sum_{k=I,II,III} \mathbf{G}_k \Phi_k)} \\ &= \left(\sum_{k=I,II,III} [\mathbf{T}_k \sin \Phi_k + \hat{\mathbf{T}}_k \cos \Phi_k] \right) \mathbf{S}, \end{aligned} \quad (14)$$

¹⁸³ where

$$\mathbf{G}_k \equiv \mathbf{S}^T \mathbf{T}_k \mathbf{S}, \quad (15)$$

¹⁸⁴ and $\Phi_k = 2\pi\nu_k$ is the phase advance of the corresponding
¹⁸⁵ mode in one turn. For \mathbf{M}^n we only need to replace the above
¹⁸⁶ Φ_k with $n\Phi_k$. We can write the matrix terms of the one-turn
¹⁸⁷ map more explicitly as

$$\begin{aligned} \mathbf{M}_{ij} &= (-1)^j \sum_{k=I,II,III} \left[\beta_{i(j-(-1)^j)}^k \sin \Phi_k \right. \\ &\quad \left. + \hat{\beta}_{i(j-(-1)^j)}^k \cos \Phi_k \right]. \end{aligned} \quad (16)$$

¹⁸⁸ Applying $\beta_{ij}^k = \beta_{ji}^k, \hat{\beta}_{ij}^k = -\hat{\beta}_{ji}^k$, we have

$$\begin{aligned}\mathbf{M}_{12} &= \sum_{k=I,II,III} \beta_{11}^k \sin \Phi_k, \\ \mathbf{M}_{21} &= - \sum_{k=I,II,III} \beta_{22}^k \sin \Phi_k, \\ \mathbf{M}_{34} &= \sum_{k=I,II,III} \beta_{33}^k \sin \Phi_k, \\ \mathbf{M}_{43} &= - \sum_{k=I,II,III} \beta_{44}^k \sin \Phi_k, \\ \mathbf{M}_{56} &= \sum_{k=I,II,III} \beta_{55}^k \sin \Phi_k, \\ \mathbf{M}_{65} &= - \sum_{k=I,II,III} \beta_{66}^k \sin \Phi_k.\end{aligned}$$

175

Using the generalized Twiss matrices, the actions or generalized Courant-Snyder invariants of a particle are defined according to

$$J_k \equiv \frac{\mathbf{X}^T \mathbf{G}_k \mathbf{X}}{2}.$$

It is easy to prove that J_k are invariants of a particle when it travels around the ring, from Eqs. (11), (12), and the symplecticity of the transfer matrix

$$\mathbf{R}^T \mathbf{S} \mathbf{R} = \mathbf{S}.$$

For a beam with N_p particles, the three beam invariants can then be defined according to

$$\epsilon_k \equiv \langle J_k \rangle = \frac{\sum_{i=1}^{N_p} J_{k,i}}{N_p}, \quad k = I, II, III,$$

where $J_{k,i}$ means the k -th mode invariant of the i -th particle. These invariants are the generalized root-mean-square (RMS) emittances of beam in the ring.

The beam emittances defined above are based on the eigen-mode motion of particles in the storage ring. Another definition of emittance is based directly on the second moments matrix of a particle beam

$$\Sigma = \langle \mathbf{X} \mathbf{X}^T \rangle,$$

where $\langle \rangle$ here means particle ensemble average. The beam second moment matrix at different places are related according to

$$\Sigma(s_2) = \mathbf{R}(s_2, s_1) \Sigma(s_1) \mathbf{R}^T(s_2, s_1).$$

From the symplecticity of \mathbf{R} , we can prove that the eigenvalues of $\Sigma(-i\mathbf{S})$ are unchanged with the beam transport in a linear symplectic lattice. The beam eigen emittances can thus be defined as the positive eigen values of $\Sigma(-i\mathbf{S})$.

When the particle beam matches the storage ring lattice, which means the beam distribution at a given location repeats itself turn by turn, we have

$$\Sigma(s + C_0) = \mathbf{M}(s) \Sigma(s) \mathbf{M}^T(s) = \Sigma(s).$$

It can be proven that for a matched beam the RMS emittances defined in Eq. (20) are the eigenvalues of $\Sigma(-i\mathbf{S})$ with the eigenvector \mathbf{E}_k , i.e.,

$$\Sigma(-i\mathbf{S}) \mathbf{E}_k = \text{sgn}(k) \epsilon_k \mathbf{E}_k, \quad (24)$$

where we have used $\epsilon_{-k} \equiv \epsilon_k$ and

$$\text{sgn}(k) = \begin{cases} 1, & k = I, II, III, \\ -1, & k = -I, -II, -III. \end{cases} \quad (25)$$

Using the generalized Twiss and second moments matrices, the eigen emittances for a matched beam can be calculated as

$$\epsilon_k = \text{Tr}(\mathbf{T}_k \mathbf{S} \Sigma \mathbf{S}^T) = \text{Tr}(\mathbf{G}_k \Sigma). \quad (26)$$

Using the generalized Twiss matrices, the actions or generalized Courant-Snyder invariants of a particle are defined according to

$$J_k \equiv \frac{\mathbf{X}^T \mathbf{G}_k \mathbf{X}}{2}.$$

It is easy to prove that J_k are invariants of a particle when it travels around the ring, from Eqs. (11), (12), and the symplecticity of the transfer matrix

$$\mathbf{R}^T \mathbf{S} \mathbf{R} = \mathbf{S}.$$

For a beam with N_p particles, the three beam invariants can then be defined according to

$$\epsilon_k \equiv \langle J_k \rangle = \frac{\sum_{i=1}^{N_p} J_{k,i}}{N_p}, \quad k = I, II, III,$$

where $J_{k,i}$ means the k -th mode invariant of the i -th particle. These invariants are the generalized root-mean-square (RMS) emittances of beam in the ring.

The beam emittances defined above are based on the eigen-mode motion of particles in the storage ring. Another definition of emittance is based directly on the second moments matrix of a particle beam

$$\Sigma = \langle \mathbf{X} \mathbf{X}^T \rangle,$$

where $\langle \rangle$ here means particle ensemble average. The beam second moment matrix at different places are related according to

$$\Sigma(s_2) = \mathbf{R}(s_2, s_1) \Sigma(s_1) \mathbf{R}^T(s_2, s_1).$$

From the symplecticity of \mathbf{R} , we can prove that the eigenvalues of $\Sigma(-i\mathbf{S})$ are unchanged with the beam transport in a linear symplectic lattice. The beam eigen emittances can thus be defined as the positive eigen values of $\Sigma(-i\mathbf{S})$.

When the particle beam matches the storage ring lattice, which means the beam distribution at a given location repeats itself turn by turn, we have

$$\Sigma(s + C_0) = \mathbf{M}(s) \Sigma(s) \mathbf{M}^T(s) = \Sigma(s).$$

where $\text{Tr}()$ means the trace of a matrix.

To ensure that the eigenvectors \mathbf{E}_k are uniquely defined all around the ring once they are determined at a given location, we will let

$$\mathbf{E}_k(s_2) = e^{-i \frac{s_2 - s_1}{C_0} \Phi_k} \mathbf{R}(s_2, s_1) \mathbf{E}_k(s_1). \quad (27)$$

Following this definition, we have

$$\mathbf{E}_k(s + C_0) = e^{-i \Phi_k} \Sigma(s) \mathbf{E}_k(s) = \mathbf{E}_k(s). \quad (28)$$

Using the generalized beta function, we can write the eigen-vector component in an amplitude-phase form

$$\mathbf{E}_{kj} = \sqrt{\frac{\beta_{jj}^k}{2}} e^{i \phi_j^k}. \quad (29)$$

where $J_{k,i}$ means the k -th mode invariant of the i -th particle. These invariants are the generalized root-mean-square (RMS) emittances of beam in the ring.

The beam emittances defined above are based on the eigen-mode motion of particles in the storage ring. Another definition of emittance is based directly on the second moments matrix of a particle beam

$$\Sigma = \langle \mathbf{X} \mathbf{X}^T \rangle,$$

where $\langle \rangle$ here means particle ensemble average. The beam second moment matrix at different places are related according to

$$\Sigma(s_2) = \mathbf{R}(s_2, s_1) \Sigma(s_1) \mathbf{R}^T(s_2, s_1).$$

From the symplecticity of \mathbf{R} , we can prove that the eigenvalues of $\Sigma(-i\mathbf{S})$ are unchanged with the beam transport in a linear symplectic lattice. The beam eigen emittances can thus be defined as the positive eigen values of $\Sigma(-i\mathbf{S})$.

When the particle beam matches the storage ring lattice, which means the beam distribution at a given location repeats itself turn by turn, we have

$$\Sigma(s + C_0) = \mathbf{M}(s) \Sigma(s) \mathbf{M}^T(s) = \Sigma(s).$$

And according to the definition we have

$$\beta_{ij}^k = \sqrt{\beta_{ii}^k \beta_{jj}^k} \cos(\phi_i^k - \phi_j^k). \quad (30)$$

Using the generalized Courant-Snyder invariants and beta functions, we can express the phase space coordinate of a particle at s as

$$\mathbf{X}_i(s) = \sum_{k=I,II,III} \sqrt{2 J_k \beta_{ii}^k(s)} \cos [\psi_i^k(s)], \quad (31)$$

with ψ_i^k determined by the initial condition of particle state.

The phase term ψ_i^k at different locations are related according to

$$\psi_i^k(s_2) = \psi_i^k(s_1) + \frac{s_2 - s_1}{C_0} \Phi_k + \phi_i^k(s_2) - \phi_i^k(s_1). \quad (32)$$

In particular, after n revolutions in the ring, we have

$$\mathbf{X}_i(s + nC_0) = \sum_{k=I,II,III} \sqrt{2 J_k \beta_{ii}^k(s)} \cos [\psi_i^k(s) + n\Phi_k]. \quad (33)$$

238

B. Perturbations

278

C. Application to Electron Storage Rings

239 After considering the parametrization of a general coupled
 240 lattice and the prescribed particle motion in it, let us now
 241 add perturbations, that from the lattice and also that from the
 242 beam. Assume there is a perturbation \mathbf{K} to the one-turn map
 243 \mathbf{M} , i.e.,

$$244 \quad \mathbf{M}_{\text{per}} = (\mathbf{I} + \mathbf{K})\mathbf{M}_{\text{unp}}, \quad (34)$$

245 where \mathbf{I} is the identity matrix, the subscripts ‘per’ and ‘unp’
 246 mean ‘perturbed’ and ‘unperturbed’, respectively. When the
 247 perturbation is small, from canonical perturbation theory,
 248 the tune shift of the k -th eigen mode can be calculated as

$$249 \quad \Delta\nu_k = -\frac{1}{4\pi} \text{Tr} \left[\left(\text{sgn}(k)\mathbf{T}_k + i\hat{\mathbf{T}}_k \right) \mathbf{S}\mathbf{K} \right]. \quad (35)$$

250 This tune shift formula can be used to calculate the real and
 251 imaginary tune shifts due to symplectic (for example lattice
 252 error) and non-symplectic (for example radiation damping)
 253 perturbations. For example, given the radiation damping ma-
 254 trix \mathbf{D} around the ring, the damping rate of each eigen mode
 255 per turn is

$$256 \quad \alpha_k = -\frac{1}{2} \oint \text{Tr} \left(\hat{\mathbf{T}}_k \mathbf{S}\mathbf{D} \right) ds, k = I, II, III, \quad (36)$$

257 where \oint means integration around the ring. Note that the
 258 damping rates here are those for the corresponding eigenvec-
 259 tors. The damping rates for particle actions or beam eigen
 260 emittances are a factor of two larger, since they are quadratic
 261 with respect to the phase space coordinates.

262 Apart from the radiation damping, there are also various
 263 beam diffusion effects in the ring, like quantum excitation and
 264 intra-beam scattering. Using Eq. (26), once we know the dif-
 265 fusion and damping matrix \mathbf{N} around the ring, the emittance
 266 growth per turn due to diffusion is

$$267 \quad \Delta\epsilon_k = \frac{1}{2} \oint \text{Tr}(\mathbf{G}_k \mathbf{N}) ds = -\frac{1}{2} \oint \text{Tr}(\mathbf{T}_k \mathbf{S}\mathbf{N}\mathbf{S}) ds, \quad (37)$$

268 The equilibrium eigen emittance between a balance of diffu-
 269 sion and damping can be calculated as

$$270 \quad \epsilon_k = \frac{\Delta\epsilon_k}{2\alpha_k} = \frac{\frac{1}{2} \oint \text{Tr}(\mathbf{G}_k \mathbf{N}) ds}{-\oint \text{Tr}(\hat{\mathbf{T}}_k \mathbf{S}\mathbf{D}) ds} \\ (38) \quad = \frac{-\frac{1}{2} \sum_{i,j} \oint \beta_{ij}^k (\mathbf{S}\mathbf{N}\mathbf{S})_{ij} ds}{\sum_{i,j} \oint \beta_{ij}^k (\mathbf{S}\mathbf{D})_{ij} ds}.$$

271 It can be proven that the equilibrium beam distribution in 6D
 272 phase space given by such a balance in a linear lattice is Gaus-
 273 sian [22], with $\langle \mathbf{X} \rangle = \mathbf{0}$. After getting the equilibrium eigen
 274 emittances, the second moments of beam can be written as

$$275 \quad \Sigma_{ij} = \langle \mathbf{X}_i \mathbf{X}_j \rangle = \sum_{k=I,II,III} \epsilon_k \beta_{ij}^k, \quad (39)$$

276 or in matrix form as

$$277 \quad \Sigma = \sum_{k=I,II,III} \epsilon_k \mathbf{T}_k. \quad (40)$$

279 In an electron storage ring, the intrinsic diffusion and
 280 damping are both from the emission of photons, namely the
 281 so-called quantum excitation and radiation damping. For
 282 quantum excitation, we have all the other components of the
 283 diffusion matrix \mathbf{N} zero except that

$$284 \quad N_{66} = \frac{\left\langle \dot{\mathcal{N}} \frac{u^2}{E_0^2} \right\rangle}{c} = \frac{2C_L\gamma^5}{c|\rho|^3}, \quad (41)$$

285 where $\dot{\mathcal{N}}$ is the number of photons emitted per unit time, u is
 286 the photon energy, $C_L = \frac{55}{48\sqrt{3}} \frac{r_e \hbar}{m_e}$ with r_e being the classical
 287 electron radius, \hbar being the reduced Planck’s constant, m_e
 288 being the electron mass, γ is the Lorentz factor, c is the speed
 289 of light in free space, ρ is the bending radius. We take the
 290 convention that the sign of ρ is positive when the bending is
 291 inward, and negative when the bending is outward. $\langle \dot{\mathcal{N}} u^2 \rangle$ in
 292 the above formula is a result of Campbell’s theorem [23, 24].

293 For damping effect, we have two sources, i.e., dipole mag-
 294 nets and RF cavity. For a horizontal dipole, we have all the
 295 other components of damping matrix \mathbf{D} zero except that

$$296 \quad D_{66} = -\frac{C_\gamma E_0^3}{\pi} \frac{1}{\rho^2}, \quad D_{61} = -\frac{C_\gamma E_0^3}{2\pi} \frac{1-2n}{\rho^3}, \quad (42)$$

297 where $C_\gamma = \frac{4\pi}{3} \frac{r_e}{(m_e c^2)^3} = 8.85 \times 10^{-5} \frac{\text{m}}{\text{GeV}^2}$, $n = -\frac{\rho}{B_y} \frac{\partial B_y}{\partial x}$
 298 is the transverse field gradient index. The physical origin of
 299 D_{66} is the fact that a higher energy particle tends to radiate
 300 more photon energy in a given magnetic field, while D_{61} is
 301 due to the fact that a transverse displacement of particle will
 302 affect its path length in the dipole and when there is transverse
 303 field gradient also the magnetic field strength observed, thus
 304 the radiation energy loss. For an RF cavity, we have all the
 305 other damping matrix terms of \mathbf{D} zero except that

$$306 \quad D_{22} = D_{44} = -\frac{eV_{RF} \sin \phi_{RF}}{E_0} \delta(s_{RF}), \quad (43)$$

307 where e is the elementary charge and is assumed positive in
 308 this paper, V_{RF} and ϕ_{RF} are the RF voltage and phase, re-
 309 spectively, $\delta(s)$ means Dirac’s delta function. Here we have
 310 assumed that the RF cavity is a zero-length one. The physical
 311 origin of these damping terms is that the momentum boost
 312 of a particle in the RF cavity is along the longitudinal direc-
 313 tion, while the transverse momentums of the particle are un-
 314 changed. Therefore, there is a damping effect on the horizon-
 315 tal and vertical angle of the particle. We remind the readers
 316 that if we use the horizontal and vertical particle momentum
 317 p_x and p_y , instead of x' and y' , as the phase space coordinates,
 318 then the damping happens only at bending magnets since the
 319 RF acceleration does not affect $p_{x,y}$.

320 In an electron storage ring, the RF acceleration compen-
 321 sates the radiation energy loss of electrons. If there are N
 322 cavities in the ring, we have

$$323 \quad \sum_{i=1}^N eV_{RF,i} \sin \phi_{RF,i} = U_0, \quad (44)$$

³²⁴ where

$$\text{325} \quad U_0 = \frac{C_\gamma E_0^4}{2\pi} I_2 \quad (45)$$

³²⁶ is the radiation energy loss per particle per turn, with

$$\text{327} \quad I_2 = \oint \frac{1}{\rho^2} ds. \quad (46)$$

³²⁸ If the ring consists of iso-bending magnets, then $U_0 = C_\gamma \frac{E_0^4}{\rho}$.

³²⁹ From Eq. (42), we have

$$\text{330} \quad \oint D_{66}(s) ds = -\frac{2U_0}{E_0}. \quad (47)$$

³³¹ Similarly, based on Eqs. (43) and (44), we have

$$\text{332} \quad \oint D_{22}(s) ds = \oint D_{44}(s) ds = -\frac{U_0}{E_0}. \quad (48)$$

³³³ Combing with Eqs. (10) and (36), it is easy to show that for

³³⁴ radiation damping, we have

$$\begin{aligned} \sum_{k=I,II,III} \alpha_k &= -\frac{1}{2} \oint \text{Tr} \left[\left(\sum_{k=I,II,III} \hat{\mathbf{T}}_k \right) \mathbf{SD} \right] ds \\ &= -\frac{1}{2} \oint \text{Tr}(\mathbf{D}) ds \\ &= -\frac{1}{2} \oint (D_{22} + D_{44} + D_{66}) ds \\ &= \frac{2U_0}{E_0}, \end{aligned} \quad (49)$$

³³⁵ which is the well-known Robinson's sum rule [25].

³³⁶ The above formulation applies for a 3D general coupled lattice. For a ring without x - y coupling and when the RF cavity is placed at dispersion-free location, we can express the normalized eigenvectors using the classical Courant-Snyder functions [26] α, β, γ and dispersion D and dispersion angle

³⁴¹ D' as

$$\mathbf{E}_I = \frac{1}{\sqrt{2}} \begin{pmatrix} \frac{\sqrt{\beta_x}}{-\alpha_x+i} \\ \frac{\sqrt{\beta_x}}{0} \\ 0 \\ 0 \\ \frac{-(\alpha_x D_x + \beta_x D'_x) + i D_x}{\sqrt{\beta_x}} \\ 0 \end{pmatrix} e^{i\Psi_I}, \quad \mathbf{E}_{II} = \frac{1}{\sqrt{2}} \begin{pmatrix} 0 \\ 0 \\ \frac{\sqrt{\beta_y}}{-\alpha_y+i} \\ \frac{\sqrt{\beta_y}}{0} \\ \frac{-(\alpha_y D_y + \beta_y D'_y) + i D_y}{\sqrt{\beta_y}} \\ 0 \end{pmatrix} e^{i\Psi_{II}}, \quad \mathbf{E}_{III} = \frac{1}{\sqrt{2}} \begin{pmatrix} \frac{-\alpha_z+i}{\sqrt{\beta_z}} D_x \\ \frac{-\alpha_z+i}{\sqrt{\beta_z}} D'_x \\ \frac{-\alpha_z+i}{\sqrt{\beta_z}} D_y \\ \frac{-\alpha_z+i}{\sqrt{\beta_z}} D'_y \\ \frac{\sqrt{\beta_z}}{-\alpha_z+i} \\ \frac{\sqrt{\beta_z}}{-\alpha_z+i} \end{pmatrix} e^{i\Psi_{III}}, \quad (50)$$

³⁴³

³⁴⁴ where the subscripts x, y, z correspond to the horizontal, vertical and longitudinal dimensions, respectively, and $\Psi_{I,II,III}$ are ³⁴⁵ the phase factors of the eigenvectors. There is flexibility in choosing these phase factors as they ³⁴⁶ do not affect the calculation of our defined Twiss matrices and physical quantities. But note that once they are set at one location, then their values all around ³⁴⁷ the ring are determined according to Eq. (27). In this case, the real and imaginary generalized Twiss matrices can be obtained ³⁴⁸ explicitly

$$\begin{aligned} \mathbf{T}_I &= \begin{pmatrix} \beta_x & -\alpha_x & 0 & 0 & -\alpha_x D_x - \beta_x D'_x & 0 \\ -\alpha_x & \gamma_x & 0 & 0 & \gamma_x D_x + \alpha_x D'_x & 0 \\ 0 & 0 & 0 & 0 & 0 & 0 \\ 0 & 0 & 0 & 0 & 0 & 0 \\ -\alpha_x D_x - \beta_x D'_x & \gamma_x D_x + \alpha_x D'_x & 0 & 0 & \mathcal{H}_x & 0 \\ 0 & 0 & 0 & 0 & 0 & 0 \end{pmatrix}, \quad \hat{\mathbf{T}}_I = \begin{pmatrix} 0 & -1 & 0 & 0 & -D_x & 0 \\ 1 & 0 & 0 & 0 & -D'_x & 0 \\ 0 & 0 & 0 & 0 & 0 & 0 \\ 0 & 0 & 0 & 0 & 0 & 0 \\ D_x & D'_x & 0 & 0 & 0 & 0 \\ 0 & 0 & 0 & 0 & 0 & 0 \end{pmatrix}, \\ \mathbf{T}_{II} &= \begin{pmatrix} 0 & 0 & 0 & 0 & 0 & 0 \\ 0 & 0 & 0 & 0 & 0 & 0 \\ 0 & 0 & \beta_y & -\alpha_y & -\alpha_y D_y - \beta_y D'_y & 0 \\ 0 & 0 & -\alpha_y & \gamma_y & \gamma_y D_y + \alpha_y D'_y & 0 \\ 0 & 0 & -\alpha_y D_y - \beta_y D'_y & \gamma_y D_y + \alpha_y D'_y & \mathcal{H}_y & 0 \\ 0 & 0 & 0 & 0 & 0 & 0 \end{pmatrix}, \quad \hat{\mathbf{T}}_{II} = \begin{pmatrix} 0 & 0 & 0 & 0 & 0 & 0 \\ 0 & 0 & 0 & 0 & 0 & 0 \\ 0 & 0 & 0 & -1 & -D_y & 0 \\ 0 & 0 & 1 & 0 & -D'_y & 0 \\ 0 & 0 & D_y & D'_y & 0 & 0 \\ 0 & 0 & 0 & 0 & 0 & 0 \end{pmatrix}, \\ \mathbf{T}_{III} &= \begin{pmatrix} \gamma_z D_x^2 & \gamma_z D_x D'_x & \gamma_z D_x D_y & \gamma_z D_x D'_y & -\alpha_z D_x & \gamma_z D_x \\ \gamma_z D_x D'_x & \gamma_z D_x'^2 & \gamma_z D'_x D_y & \gamma_z D'_x D'_y & -\alpha_z D'_x & \gamma_z D'_x \\ \gamma_z D_x D_y & \gamma_z D'_x D_y & \gamma_z D_y^2 & \gamma_z D_y D'_y & -\alpha_z D_y & \gamma_z D_y \\ \gamma_z D_x D'_y & \gamma_z D'_x D'_y & \gamma_z D_y D'_y & \gamma_z D_y'^2 & -\alpha_z D'_y & \gamma_z D'_y \\ -\alpha_z D_x & -\alpha_z D'_x & -\alpha_z D_y & -\alpha_z D'_y & \beta_z & -\alpha_z \\ \gamma_z D_x & \gamma_z D'_x & \gamma_z D_y & \gamma_z D'_y & -\alpha_z & \gamma_z \end{pmatrix}, \quad \hat{\mathbf{T}}_{III} = \begin{pmatrix} 0 & 0 & 0 & 0 & D_x & 0 \\ 0 & 0 & 0 & 0 & D'_x & 0 \\ 0 & 0 & 0 & 0 & D_y & 0 \\ 0 & 0 & 0 & 0 & D'_y & 0 \\ -D_x & -D'_x & -D_y & -D'_y & 0 & -1 \\ 0 & 0 & 0 & 0 & 1 & 0 \end{pmatrix}. \end{aligned} \quad (51)$$

³⁴⁹

³⁵⁰ Correspondingly, the generalized Courant-Snyder invariants are given by

$$\begin{aligned}
J_I &\equiv \frac{(\mathbf{S}\mathbf{X})^T \mathbf{T}_I \mathbf{S}\mathbf{X}}{2} = \frac{(x - D_x \delta)^2 + [\alpha_x (x - D_x \delta) + \beta_x (x' - D'_x \delta)]^2}{2\beta_x}, \\
J_{II} &\equiv \frac{(\mathbf{S}\mathbf{X})^T \mathbf{T}_{II} \mathbf{S}\mathbf{X}}{2} = \frac{(y - D_y \delta)^2 + [\alpha_y (y - D_y \delta) + \beta_y (y' - D'_y \delta)]^2}{2\beta_y}, \\
J_{III} &\equiv \frac{(\mathbf{S}\mathbf{X})^T \mathbf{T}_{III} \mathbf{S}\mathbf{X}}{2} = \frac{(z + D'_x x - D_x x' + D'_y y - D_y y')^2 + [\alpha_z (z + D'_x x - D_x x' + D'_y y - D_y y') + \beta_z \delta]^2}{2\beta_z},
\end{aligned} \tag{52}$$

352 The equilibrium emittances determined by the balance of
353 quantum excitation and radiation damping in an electron stor-
354 age in this case reduce to the classical Sands radiation inte-
355 grals formalism found in textbooks [27]

$$\begin{aligned}
\epsilon_x &\equiv \langle J_I \rangle = \frac{C_L \gamma^5}{2c\alpha_I} \oint \frac{\beta_{55}^I}{|\rho|^3} ds = C_q \frac{\gamma^2}{J_x} \frac{I_{5x}}{I_2}, \\
\epsilon_y &\equiv \langle J_{II} \rangle = \frac{C_L \gamma^5}{2c\alpha_{II}} \oint \frac{\beta_{55}^{II}}{|\rho|^3} ds = C_q \frac{\gamma^2}{J_y} \frac{I_{5y}}{I_2}, \\
\epsilon_z &\equiv \langle J_{III} \rangle = \frac{C_L \gamma^5}{2c\alpha_{III}} \oint \frac{\beta_{55}^{III}}{|\rho|^3} ds = C_q \frac{\gamma^2}{J_z} \frac{I_{5z}}{I_2},
\end{aligned} \tag{53}$$

357 with $C_q = \frac{55\lambda_e}{32\sqrt{3}} = 3.8319 \times 10^{-13}$ m for electrons, $\lambda_e =$
358 $\frac{\lambda_e}{2\pi} = \frac{\hbar c}{m_e c^2} = 386$ fm is the reduced Compton wavelength of
359 electron, and the radiation integrals are given by

$$\begin{aligned}
I_2 &= \oint \frac{1}{\rho^2} ds, \quad I_{4x} = \oint D_x \left(\frac{1 - 2n}{\rho^3} \right) ds, \\
I_{5x} &= \oint \frac{\mathcal{H}_x}{|\rho|^3} ds, \quad I_{5y} = \oint \frac{\mathcal{H}_y}{|\rho|^3} ds, \quad I_{5z} = \oint \frac{\beta_z}{|\rho|^3} ds,
\end{aligned} \tag{54}$$

361 where

$$\mathcal{H}_{x,y} = \beta_{55}^{I,II} = \frac{D_{x,y}^2 + (\alpha_{x,y} D_{x,y} + \beta_{x,y} D'_{x,y})^2}{\beta_{x,y}} \tag{55}$$

363 are the horizontal and vertical dispersion invariant, and $\beta_z =$
364 β_{55}^{III} is the longitudinal beta function [8]. The damping rate
365 of three eigen modes are given by

$$\alpha_I = \frac{U_0}{2E_0} J_x, \quad \alpha_{II} = \frac{U_0}{2E_0} J_y, \quad \alpha_{III} = \frac{U_0}{2E_0} J_z, \tag{56}$$

367 where $J_{x,y,z}$ are the damping partition numbers

$$J_x = 1 - \frac{I_{4x}}{I_2}, \quad J_y = 1, \quad J_z = 2 + \frac{I_{4x}}{I_2}. \tag{57}$$

369 The Robinson's sum rule corresponds then to

$$J_x + J_y + J_z = 4. \tag{58}$$

371 The horizontal, vertical, longitudinal radiation damping times
372 are

$$\tau_{x,y,z} = \frac{T_0}{\alpha_{x,y,z}}, \tag{59}$$

374 where T_0 is the particle revolution period time in the ring.

375 After getting the equilibrium emittance, the beam second
376 moments can be obtained using Eq. (39). For example,

$$\begin{aligned}
\sigma_x^2 &= \langle x^2 \rangle = \epsilon_x \beta_x + \epsilon_z \gamma_z D_x^2 = \epsilon_x \beta_x + \sigma_\delta^2 D_x^2, \\
\sigma_z^2 &= \langle z^2 \rangle = \epsilon_z \beta_z + \epsilon_x \mathcal{H}_x + \epsilon_y \mathcal{H}_y.
\end{aligned} \tag{60}$$

378 We remind the readers that the generalized Courant-Snyder
379 formalism presented in this section has been briefly reported
380 before in Ref. [28].

III. THEORETICAL MINIMUM EMITTANCES

382 After introducing the generalized Courant-Snyder formal-
383 ism, we now apply it to analyze the theoretical minimum lon-
384 gitudinal emittance in an electron storage ring. This work
385 serves as the basis for the following investigation of SSMB,
386 since the longitudinal weak focusing and strong focusing
387 SSMB to be introduced soon are about lowering the equilib-
388 rium bunch length and longitudinal emittance in an electron
389 storage ring. For completeness, here in this section we also
390 present the analysis of theoretical minimum transverse emit-
391 tance since they can be treated within a single framework.

A. Theoretical Minimum Horizontal Emittance

393 From Eq. (53) we can see that \mathcal{H}_x and β_z , i.e., β_{55}^I and
394 β_{55}^{III} as defined by us, at the bending magnets are of vital im-
395 portance in determining the horizontal and longitudinal emit-
396 tance, respectively. Therefore, we need to know how they
397 evolve inside a bending magnet. The transfer matrix of the
398 particle state vector for a sector bending magnet is

399

$$\mathbf{B}(\alpha) = \begin{pmatrix} \cos \alpha & \rho \sin \alpha & 0 & 0 & 0 & \rho(1 - \cos \alpha) \\ -\frac{\sin \alpha}{\rho} & \cos \alpha & 0 & 0 & 0 & \sin \alpha \\ 0 & 0 & 1 & \rho \alpha & 0 & 0 \\ 0 & 0 & 0 & 1 & 0 & 0 \\ -\sin \alpha & -\rho(1 - \cos \alpha) & 0 & 0 & 1 & \rho \left(\frac{\alpha}{\gamma^2} - \alpha + \sin \alpha \right) \\ 0 & 0 & 0 & 0 & 0 & 1 \end{pmatrix}, \quad (61)$$

400 with ρ and α being the bending radius and angle of the bend- 404 sion and dispersion angle at the dipole center where we set to
401 ing magnet, respectively. In a planar uncoupled ring, the 405 be $\alpha = 0$ are given by $\alpha_{x0}, \beta_{x0}, \alpha_{z0}, \beta_{z0}, D_{x0}, D'_{x0}$. From
402 normalized eigenvectors of the one-turn map are given by 406 Eqs. (61) and (50) we have the evolution of \mathcal{H}_x expression in
403 Eq. (50). Assuming the Courant-Snyder functions, disper- 407 the dipole

408

$$\mathcal{H}_x(\alpha) \equiv \beta_{55}^I(\alpha) = 2|\mathbf{E}_{I5}(\alpha)|^2 = 2|(\mathbf{B}(\alpha)\mathbf{E}_I(0))_5|^2 \\ = \left(\sqrt{\beta_{x0}} (\sin \alpha + D'_{x0}) + \frac{\alpha_{x0}}{\sqrt{\beta_{x0}}} [D_{x0} - \rho(1 - \cos \alpha)] \right)^2 + \left(\frac{D_{x0} - \rho(1 - \cos \alpha)}{\sqrt{\beta_{x0}}} \right)^2. \quad (62)$$

409 Similarly, the evolution of β_z in the dipole is given by

410

$$\beta_z(\alpha) \equiv \beta_{55}^{III}(\alpha) = 2|\mathbf{E}_{III5}(\alpha)|^2 = 2|(\mathbf{B}(\alpha)\mathbf{E}_{III}(0))_5|^2 \\ = \left(\sin \alpha \frac{\alpha_{z0}}{\sqrt{\beta_{z0}}} D_{x0} + \rho(1 - \cos \alpha) \frac{\alpha_{z0}}{\sqrt{\beta_{z0}}} D'_{x0} + \sqrt{\beta_{z0}} - \rho(-\alpha + \sin \alpha) \frac{\alpha_{z0}}{\sqrt{\beta_{z0}}} \right)^2 \\ + \left(-\sin \alpha \frac{1}{\sqrt{\beta_{z0}}} D_{x0} - \rho(1 - \cos \alpha) \frac{1}{\sqrt{\beta_{z0}}} D'_{x0} + \rho(-\alpha + \sin \alpha) \frac{1}{\sqrt{\beta_{z0}}} \right)^2. \quad (63)$$

411 For simplicity we have neglected the contribution of $\frac{\rho \alpha}{\gamma^2}$ to 423 with
412 R_{56} of dipole in the above calculation of β_z , since we are 424 interested in the relativistic cases. But we remind the readers
413 that in a quasi-isochronous ring, the contribution of $\frac{C_0}{\gamma^2}$ to the
414 ring R_{56} or phase slippage may not be negligible.

415 With the evolution of \mathcal{H}_x and β_z known, now we derive the
416 theoretical minimum emittances. For simplicity, we assume
417 the ring consists of iso-bending-magnets, with the bending
418 angle induced by each bending magnet being θ , and the op-
419 tical functions are identical in each bending magnets. Then
420 from Eq. (53), we have

422

$$\epsilon_x = C_q \frac{\gamma^2}{J_x} \frac{1}{\rho} f_x(\alpha_{x0}, \beta_{x0}, D_{x0}, D'_{x0}), \quad (64)$$

425 f_x can be interpreted as the average value of \mathcal{H}_x in dipoles.
426 The lengthy explicit expression of $f_x(\alpha_{x0}, \beta_{x0}, D_{x0}, D'_{x0})$ is
427 omitted here. It can be obtained straightforwardly by insert-
428 ing Eq. (62) in Eq. (65). The mathematical problem we are
429 trying to solve is then to minimize f_x , by adjusting $\alpha_{x0}, \beta_{x0},$
430 D_{x0}, D'_{x0} . From Eq. (65) we have

431

$$\frac{\partial f_x}{\partial \alpha_{x0}} = \alpha_{x0} \frac{2D_{x0} \left(D_{x0} - 2\rho + 2\rho \frac{\sin \frac{\theta}{2}}{\frac{\theta}{2}} \right) + \rho^2 \left(3 - 4 \frac{\sin \frac{\theta}{2}}{\frac{\theta}{2}} + \frac{\sin \theta}{\theta} \right)}{\beta_{x0}} + D'_{x0} 2 \left(D_{x0} - \rho + \rho \frac{\sin \frac{\theta}{2}}{\frac{\theta}{2}} \right), \\ \frac{\partial f_x}{\partial D'_{x0}} = \alpha_{x0} 2 \left(D_{x0} - \rho + \rho \frac{\sin \frac{\theta}{2}}{\frac{\theta}{2}} \right) + D'_{x0} 2 \beta_{x0}. \quad (66)$$

432 We notice that the requirement of $\frac{\partial f_x}{\partial \alpha_{x0}} = 0$ and $\frac{\partial f_x}{\partial D'_{x0}} = 0$ 433 leads to $\alpha_{x0} = 0$ and $D'_{x0} = 0$. Under the above conditions,

434 then

$$435 \quad \frac{\partial f_x}{\partial D_{x0}} = \frac{2 \left(D_{x0} - \rho + \rho \frac{\sin \frac{\theta}{2}}{\frac{\theta}{2}} \right)}{\beta_{x0}}.$$

436 The requirement of $\frac{\partial f_x}{\partial D_{x0}} = 0$ leads to

$$437 \quad D_{x0} = \rho \left(1 - \frac{\sin \frac{\theta}{2}}{\frac{\theta}{2}} \right) \approx \frac{\rho \theta^2}{24}.$$

438 Under the above conditions, then

$$439 \quad \frac{\partial f_x}{\partial \beta_{x0}} = \frac{\theta(\theta - \sin \theta) - \frac{\rho^2(\theta^2 + \theta \sin \theta + 4 \cos \theta - 4)}{\beta_{x0}^2}}{2\theta^2}.$$

440 The requirement of $\frac{\partial f_x}{\partial \beta_{x0}} = 0$ leads to

$$441 \quad \beta_{x0} = \rho \sqrt{\frac{(\theta^2 + \theta \sin \theta + 4 \cos \theta - 4)}{\theta(\theta - \sin \theta)}} \approx \frac{\rho \theta}{2\sqrt{15}}.$$

442 Summarizing, the extreme value of f_x is realized when

$$443 \quad \alpha_{x0} = 0, \beta_{x0} \approx \frac{\rho \theta}{2\sqrt{15}}, D_{x0} \approx \frac{\rho \theta^2}{24}, D'_{x0} = 0,$$

444 which means

$$445 \quad \mathcal{H}_{x0} = \rho \frac{\left(1 - \frac{\sin \frac{\theta}{2}}{\frac{\theta}{2}} \right)^2}{\sqrt{\frac{(\theta^2 + \theta \sin \theta + 4 \cos \theta - 4)}{\theta(\theta - \sin \theta)}}} \approx \frac{5\rho\theta^3}{96\sqrt{15}}, \quad (72)$$

446 and

$$447 \quad f_{x,\min} = \rho \left(1 - \frac{\sin \theta}{\theta} \right) \sqrt{\frac{(\theta^2 + \theta \sin \theta + 4 \cos \theta - 4)}{\theta(\theta - \sin \theta)}} \\ \approx \frac{\rho \theta^3}{12\sqrt{15}}. \quad (73)$$

448 One can check that this is the minimum value of f_x . Note that
449 $f_{x,\min} = \frac{8}{5} \mathcal{H}_{x0}$. Under these conditions we get the minimum

450 horizontal emittance

$$451 \quad \epsilon_{x,\min} = C_q \frac{\gamma^2}{J_x} \frac{\theta^3}{12\sqrt{15}}. \quad (74)$$

452 The above results are consistent with the classical results of
453 Teng [29]. For practical use, and considering nominally $J_x \approx$
454 1, the above scaling can be written as

$$455 \quad \epsilon_{x,\min} [\text{nm}] = 31.6 E_0^2 [\text{GeV}] \theta^3 [\text{rad}]. \quad (75)$$

456 For example, if $E_0 = 6$ GeV and $\theta = \frac{2\pi}{300}$ rad, we have
457 $\epsilon_{x,\min} = 10.4$ pm.

458 B. Theoretical Minimum Longitudinal Emittance

459

460 Now we analyze the theoretical minimum longitudinal
461 emittance. Similar to the horizontal direction, we have

$$461 \quad \epsilon_z = C_q \frac{\gamma^2}{J_z} \frac{1}{\rho} f_z(\alpha_{z0}, \beta_{z0}, D_{x0}, D'_{x0}), \quad (76)$$

462 with

$$463 \quad f_z(\alpha_{z0}, \beta_{z0}, D_{x0}, D'_{x0}) = \frac{1}{\theta} \int_{-\frac{\theta}{2}}^{\frac{\theta}{2}} \beta_z(\alpha) d\alpha, \quad (77)$$

464 which can be interpreted as the average value of β_z in dipoles.
465 Then

$$466 \quad \begin{aligned} \frac{\partial f_z}{\partial \alpha_{z0}} &= \alpha_{z0} \mathcal{G}(\rho, \theta, D_{x0}, D'_{x0}, \beta_{z0}) + D'_{x0} 2\rho \left(1 - \frac{\sin \frac{\theta}{2}}{\frac{\theta}{2}} \right), \\ \frac{\partial f_z}{\partial D'_{x0}} &= \alpha_{z0} 2\rho \left(1 - \frac{\sin \frac{\theta}{2}}{\frac{\theta}{2}} \right) \\ &\quad + D'_{x0} \frac{(1 + \alpha_{z0}^2) \rho^2 \left(3 - 4 \frac{\sin \frac{\theta}{2}}{\frac{\theta}{2}} + \frac{\sin \theta}{\theta} \right)}{\beta_{z0}}, \end{aligned} \quad (78)$$

467 where the lengthy explicit expression of
468 $\mathcal{G}(\rho, \theta, D_{x0}, D'_{x0}, \beta_{z0})$ is omitted here. Similar to the
469 analysis of transverse minimum emittance, we notice again
470 that the requirement of $\frac{\partial f_z}{\partial \alpha_{z0}} = 0$ and $\frac{\partial f_z}{\partial D'_{x0}} = 0$ leads to
471 $\alpha_{z0} = 0$ and $D'_{x0} = 0$. Under the above conditions, then

$$472 \quad \frac{\partial f_z}{\partial D_{x0}} = \frac{D_{x0} \left(1 - \frac{\sin \theta}{\theta} \right) - \rho \left(1 - \frac{\sin \theta}{\theta} - 2 \frac{\sin \frac{\theta}{2}}{\frac{\theta}{2}} + 2 \cos \frac{\theta}{2} \right)}{\beta_{z0}}. \quad (79)$$

473 The requirement of $\frac{\partial f_z}{\partial D_{x0}} = 0$ leads to

$$474 \quad D_{x0} = \frac{\rho \left(1 - \frac{\sin \theta}{\theta} - 2 \frac{\sin \frac{\theta}{2}}{\frac{\theta}{2}} + 2 \cos \frac{\theta}{2} \right)}{1 - \frac{\sin \theta}{\theta}} \approx -\frac{\rho \theta^2}{40}. \quad (80)$$

475 Under the above conditions, then

$$476 \quad \frac{\partial f_z}{\partial \beta_{z0}} = 1 - \frac{\rho^2 (\theta^4 - 12\theta^2 - (\theta^2 - 48)\theta \sin \theta - 12(\theta^2 - 4)\cos \theta - 48)}{12\theta(\theta - \sin \theta)\beta_{z0}^2}. \quad (81)$$

477 The requirement of $\frac{\partial f_z}{\partial \beta_{z0}} = 0$ leads to

$$478 \quad \beta_{z0} = \rho \sqrt{\frac{(\theta^4 - 12\theta^2 - (\theta^2 - 48)\theta \sin \theta - 12(\theta^2 - 4)\cos \theta - 48)}{12\theta(\theta - \sin \theta)}} \approx \frac{\rho\theta^3}{120\sqrt{7}}, \quad (82)$$

479 Summarizing, the extreme value of f_z is realized when

$$480 \quad \alpha_{z0} = 0, \beta_{z0} \approx \frac{\rho\theta^3}{120\sqrt{7}}, D_{x0} \approx -\frac{\rho\theta^2}{40}, D'_{x0} = 0, \quad (83)$$

481 and

$$482 \quad f_{z,\min} = \rho \sqrt{\frac{(\theta^4 - 12\theta^2 - (\theta^2 - 48)\theta \sin \theta - 12(\theta^2 - 4)\cos \theta - 48)}{3\theta(\theta - \sin \theta)}} \approx \frac{\rho\theta^3}{60\sqrt{7}}. \quad (84)$$

483 One can check that this is the minimum value of f_z . Note that
484 $f_{z,\min} = 2\beta_{z0}$. Under these conditions we get the minimum
485 longitudinal emittance

$$486 \quad \epsilon_{z,\min} = C_q \frac{\gamma^2}{J_z} \frac{\theta^3}{60\sqrt{7}}. \quad (85)$$

487 The above result has also been given in Ref. [7]. For practical
488 use, and considering nominally $J_z \approx 2$, the above scaling can
489 be written as

$$490 \quad \epsilon_{z,\min} [\text{nm}] = 4.62 E_0^2 [\text{GeV}] \theta^3 [\text{rad}]. \quad (86)$$

491 For example, if $E_0 = 0.6$ GeV and $\theta = \frac{2\pi}{50}$ rad, we have
492 $\epsilon_{z,\min} = 3.3$ pm.

493 Here we remind the readers that in reality it may not be
494 easy to reach the optimal conditions Eq. (83) for all the
495 dipoles in a ring. This is based on the observation that when
496 we realize Eq. (83) at the dipole center, the dipole as a whole
497 will have a nonzero R_{56} or more accurately a nonzero phase
498 slippage. So to make the longitudinal optics identical in dif-
499 ferent dipoles, there should be RF or laser modulator kicks
500 between neighboring dipoles, otherwise the required drift
501 space between each two dipoles will be very long to com-
502 pensate this nonzero phase slippage [7]. It may not be easy
503 to apply too many RF cavities or laser modulators in a ring to
504 manipulate the longitudinal optics, while in the transverse di-
505 mension it is straightforward to implement many quadrupoles
506 to manipulate the transverse optics. Instead, we may choose
507 a more practical strategy to realize small longitudinal emit-
508 tance, which is letting each half of the bending magnet be
509 isochronous, and the longitudinal optics for each dipole can
510 then be identical. This can be realized by requiring

$$511 \quad \alpha_{z0} = 0, \beta_{z0} \approx \frac{\rho\theta^3}{12\sqrt{210}}, D_{x0} \approx -\frac{\rho\theta^2}{24}, D'_{x0} = 0. \quad (87)$$

512 In this case, we still have $f_z = 2\beta_{z0}$. Under such conditions,
513 the minimum longitudinal emittance is [17]

$$514 \quad \epsilon_{z,\min,ISO} = C_q \frac{\gamma^2}{J_z} \frac{\theta^3}{6\sqrt{210}}. \quad (88)$$

515 The emittance given in Eq. (88) is larger than the real theo-
516 retical minimum Eq. (86), but offers a more practical refer-
517 ence. For practical use, and considering nominally $J_z \approx 2$,
518 the above scaling can be written as

$$519 \quad \epsilon_{z,\min,ISO} [\text{nm}] = 8.44 E_0^2 [\text{GeV}] \theta^3 [\text{rad}]. \quad (89)$$

520 Based on this emittance and β_{z0} , we can know the bunch
521 length at the dipole center contributed from the longitudinal
522 emittance. We remind the readers that the bunch length can in
523 principle be even smaller than this value, by pushing β_{z0} to an
524 even smaller value, although the longitudinal emittance will
525 actually grow then since β_z will diverge faster when going
526 away from the dipole center. If the ring works in a longitu-
527 dinal weak focusing regime to be introduced in next section,
528 there is actually a lower limit of bunch length in this pro-
529 cess, which is a factor of $\sqrt{2}$ smaller than the bunch length
530 given by conditions of Eqs. (89) and (87). The energy spread
531 will diverge when we push the bunch length to this limit [30].
532 Putting in the numbers, we have this lower limit of bunch
533 length in a longitudinal weak focusing ring [17]

$$534 \quad \sigma_{z,\min,ISO} [\mu\text{m}] = 4.93 \rho^{\frac{1}{2}} [\text{m}] E_0 [\text{GeV}] \theta^3 [\text{rad}]. \quad (90)$$

535 For example, if $E_0 = 0.6$ GeV, $\theta = \frac{2\pi}{50}$ rad and $\rho = 1.5$ m
536 which corresponds to a bending field strength $B_0 = 1.33$ T,
537 then $\sigma_{z,\min,ISO} = 7.2$ nm.

C. Application of Transverse Gradient Bend

539 The previous analysis assumes that the transverse gradient
540 of the bending field is zero. Now we consider the applica-
541 tion of transverse gradient bending (TGB) magnets to lower
542 the horizontal and longitudinal emittances. For simplicity, we
543 will consider the case of a constant gradient. The transfer
544 matrix of a sector bending magnet with a constant transverse
545 gradient $n = -\frac{\rho}{B_y} \frac{\partial B_y}{\partial x}$ is

$$\mathbf{B}_{\text{TGB}}(\alpha) = \begin{pmatrix}
\cos(\sqrt{1-n}\alpha) & \frac{\rho}{\sqrt{1-n}} \sin(\sqrt{1-n}\alpha) & 0 & 0 \\
-\frac{\sqrt{1-n}}{\rho} \sin(\sqrt{1-n}\alpha) & \cos(\sqrt{1-n}\alpha) & 0 & 0 \\
0 & 0 & \cos(\sqrt{n}\alpha) & \frac{\rho}{\sqrt{n}} \sin(\sqrt{n}\alpha) \\
0 & 0 & -\frac{\sqrt{n}}{\rho} \sin(\sqrt{n}\alpha) & \cos(\sqrt{n}\alpha) \\
-\frac{1}{\sqrt{1-n}} \sin(\sqrt{1-n}\alpha) & -\frac{\rho}{1-n} (1 - \cos(\sqrt{1-n}\alpha)) & 0 & 0 \\
0 & 0 & 0 & 0 \\
0 & \frac{\rho}{1-n} (1 - \cos(\sqrt{1-n}\alpha)) & 1 & 0 \\
0 & \frac{1}{\sqrt{1-n}} \sin(\sqrt{1-n}\alpha) & 0 & 0 \\
0 & 0 & 0 & 0 \\
1 & \frac{\rho\alpha}{\gamma^2} + \frac{\rho}{(1-n)^{\frac{3}{2}}} (-\sqrt{1-n}\alpha + \sin(\sqrt{1-n}\alpha)) & 0 & 0 \\
0 & 1 & 0 & 0
\end{pmatrix}. \quad (91)$$

546

547

1. Horizontal Emittance

548 Following similar steps presented in the above analysis, we
549 find the minimum value of f_x in Eq. (65) is now realized when

$$\begin{aligned}
\alpha_{x0} &= 0, \beta_{x0} \approx \frac{\rho\theta}{2\sqrt{15}} \left[1 + \frac{(1-n)\theta^2}{140} \right] + \mathcal{O}(\theta^6), \\
D_{x0} &\approx \frac{\rho\theta^2}{24} \left[1 - \frac{(1-n)\theta^2}{48} \right] + \mathcal{O}(\theta^6), D'_{x0} = 0,
\end{aligned} \quad (92)$$

550 where $\mathcal{O}(\theta^n)$ means terms of order θ^n and higher, which
551 means

$$\mathcal{H}_{x0} = \frac{D_{x0}^2}{\beta_{x0}} \approx \frac{5\rho\theta^3}{96\sqrt{15}} \left[1 - \frac{9(1-n)\theta^2}{280} \right] + \mathcal{O}(\theta^7), \quad (93)$$

554 and

$$f_{x,\min} \approx \frac{\rho\theta^3}{12\sqrt{15}} \left[1 - \frac{3(1-n)\theta^2}{70} \right] + \mathcal{O}(\theta^7). \quad (94)$$

556 So we have

$$\epsilon_{x,\min,\text{TGB}} = C_q \frac{\gamma^2}{J_x} \frac{\theta^3}{12\sqrt{15}} \left[1 - \frac{3(1-n)\theta^2}{70} \right]. \quad (95)$$

558 Therefore, the impact of the transverse gradient on the theoretical minimum emittance is on the higher order of the bending angle of each magnet. However, we should recognize that 559 n can be a quite large value in practice. So its impact may 560 actually be not small. In addition, a transverse gradient bend 561 can also affect the damping partition, whose details we do not 562 go into here.

565

2. Longitudinal Emittance

566 Similarly, using TGB, the minimum value of f_z in Eq. (77)
567 is realized when

$$\alpha_{z0} = 0, \beta_{z0} \approx \frac{\rho\theta^3}{120\sqrt{7}} \left[1 + \frac{(1-n)\theta^2}{90} \right] + \mathcal{O}(\theta^7),$$

$$D_{x0} \approx -\frac{\rho\theta^2}{40} \left[1 + \frac{19(1-n)\theta^2}{1680} \right] + \mathcal{O}(\theta^6), D'_{x0} = 0, \quad (96)$$

568

569 and

$$f_{z,\min} \approx \frac{\rho\theta^3}{60\sqrt{7}} \left[1 + \frac{(1-n)\theta^2}{90} \right] + \mathcal{O}(\theta^7). \quad (97)$$

570 Note that $f_{z,\min} = 2\beta_{z0}$ still holds here. So we have

$$\epsilon_{z,\min,\text{TGB}} = C_q \frac{\gamma^2}{J_z} \frac{\theta^3}{60\sqrt{7}} \left[1 + \frac{(1-n)\theta^2}{90} \right]. \quad (98)$$

D. Application of Longitudinal Gradient Bend

571 We can also apply longitudinal gradient bends (LGBs) to 572 lower the transverse and longitudinal emittance. For simplicity, we will study the case of a LGB consisting of several 573 sub-dipoles with each a constant bending radius. Further, we 574 will assume each sub-dipole is a sector dipole. The analysis 575 for the case of rectangular dipoles is similar, as long as the 576 impact of edge angles on transfer matrix and damping partition 577 have been properly handled. Now we investigate the case 578 of sector sub-dipoles. For example, we may choose to let the 579 LGB has a symmetric structure

$$(\rho_2, \theta_2), (\rho_1, \theta_1), (\rho_0, 2\theta_0), (\rho_1, \theta_1), (\rho_2, \theta_2) \quad (99)$$

580 The total bending angle of such a LGB is $\theta_T = 2(\theta_0 + \theta_1 +$
581 $\theta_2)$, and the total length is $2(\rho_0\theta_0 + \rho_1\theta_1 + \rho_2\theta_2)$. Note that
582 $\rho_i\theta_i \geq 0$. We use this structure as an example for the analysis.
583 The presented method however applies also to a more general
584 setup.

1. Horizontal Emittance

585 Now we calculate the theoretical minimum horizontal
586 emittance by invoking LGBs with each the structure given
587 in Eq. (99). Still we assume all the LGB setup in the ring and
588 optical functions in each LGB are identical, then

$$\epsilon_x = C_q \frac{\gamma^2}{J_x} I_{5x}(\alpha_{x0}, \beta_{x0}, D_{x0}, D'_{x0}) \quad (100)$$

596 with

597

$$I_{5x}(\alpha_{x0}, \beta_{x0}, D_{x0}, D'_{x0}) = \frac{1}{2 \left(\frac{\theta_0}{\rho_0} + \frac{\theta_1}{\rho_1} + \frac{\theta_2}{\rho_2} \right)} \int_{-(\rho_0\theta_0+\rho_1\theta_1+\rho_2\theta_2)}^{(\rho_0\theta_0+\rho_1\theta_1+\rho_2\theta_2)} \frac{\mathcal{H}_x(s)}{|\rho(s)|^3} ds. \quad (101)$$

598 Note that the dimension of I_{5x} here is equivalent to $\frac{f_x}{\rho}$ given 602 that given in Eq. (62), but note that here for different part
 599 in previous sections. The mathematical problem is then to 603 (sub-dipole) of the LGBs, we should apply the transfer ma-
 600 minimize I_{5x} , by adjusting α_{x0} , β_{x0} , D_{x0} , D'_{x0} . The cal- 604 trix from the middle point of the LGB to the corresponding
 601 culation method of \mathcal{H}_x evolution in a LGB is the same as 605 location. Following similar procedures, we find that to get
 606 the minimum emittance, we still need $\alpha_{x0} = 0$ and $D'_{x0} = 0$.
 607 Then we have $\mathcal{H}_x(-s) = \mathcal{H}_x(s)$, which means

608

$$I_{5x} = \frac{1}{\left(\frac{\theta_0}{\rho_0} + \frac{\theta_1}{\rho_1} + \frac{\theta_2}{\rho_2} \right)} \left(\int_0^{\rho_0\theta_0} \frac{\mathcal{H}_x(s)}{|\rho_0|^3} ds + \int_{\rho_0\theta_0}^{\rho_0\theta_0+\rho_1\theta_1} \frac{\mathcal{H}_x(s)}{|\rho_1|^3} ds + \int_{\rho_0\theta_0+\rho_1\theta_1}^{\rho_0\theta_0+\rho_1\theta_1+\rho_2\theta_2} \frac{\mathcal{H}_x(s)}{|\rho_2|^3} ds \right). \quad (102)$$

609 We find a general analytical discussion of the combination 636 optimization goals are $\frac{\epsilon_{x,LGB}}{\epsilon_{x,UB}}$ and the length of a LGB L_{LGB} ,
 610 of ρ_i and θ_i cumbersome. Here for simplicity and to get a 637 where $\epsilon_{x,UB}$ is the theoretical minimum emittance of applying
 611 concrete feeling, we first consider one specific case: $\rho_i = 638$ bending magnet without longitudinal gradient. We require
 612 $\rho_0 2^i$. The physical consideration behind this choice is that 639 $\rho_i \theta_i > 0$. In the optimization, we keep the total bending an-
 613 \mathcal{H}_x will be smaller in the central part of the bending magnet, 640 gle of a LGB a constant value. The optimization result of one
 614 and larger at the entrance and exit. So we make the bending 641 specific case where $\theta_T = 2(\theta_0 + \theta_1 + \theta_2) = \frac{\pi}{10}$ is presented
 615 field in the center stronger and smaller at the entrance and 642 in Fig. 2, from which we can see that in this case by applying
 616 exit region, such that to minimize the quantum excitation of 643 LGBs, in principle we can lower the horizontal emittance by
 617 horizontal emittance. For example, we may choose 644 a factor of five with a reasonable length of the LGB. Note that
 618

$$\left(4\rho, \frac{\theta}{8}\right), \left(2\rho, \frac{\theta}{8}\right), \left(\rho, \frac{\theta}{4}\right), \left(\rho, \frac{\theta}{4}\right), \left(2\rho, \frac{\theta}{8}\right), \left(4\rho, \frac{\theta}{8}\right). \quad (103)$$

618

619 The total length of such a LGB is $2\rho\theta$. The minimum value of 645 in this optimization and the one in the following section, we
 620 I_{5x} and horizontal emittance ϵ_x in this case is realized when 646 have assumed that $\rho_i > 0$. But the formalism applies also to
 621

$$\alpha_{x0} = 0, \beta_{x0} \approx \frac{\sqrt{\frac{35977}{133755}} \rho \theta}{4}, D_{x0} \approx \frac{127 \rho \theta^2}{7104}, D'_{x0} = 0, \quad (104)$$

621

622 which means

$$\mathcal{H}_{x0} = \frac{D_{x0}^2}{\beta_{x0}} \approx 0.183 \times \frac{5}{96\sqrt{15}} \rho \theta^3, \quad (105)$$

624 and

$$I_{5x,\min} \approx 0.344 \times \frac{\theta^3}{12\sqrt{15}}, \quad (106)$$

626 which compared to Eq. (74) means the theoretical minimum 647 horizontal emittance can now become about one third of the
 627 case with no longitudinal gradient. So application of LGB is 648 quite effective in lowering the transverse emittance.
 628

629 The next question is: what is the optimal combination of 649 $\theta_{0,1,2}$ and $\rho_{0,1,2}$? This questions is not straightforward to
 630 answer by analytical method. Here we refer to numerical 650 method to do the optimization directly. α_{x0} and D'_{x0} are set
 631 to be zero in the optimization. The variables in the numer- 651 ical optimization are $(\theta_0, \theta_1, \theta_2, \rho_0, \rho_1, \rho_2, \beta_{x0}, D_{x0})$. Two
 632

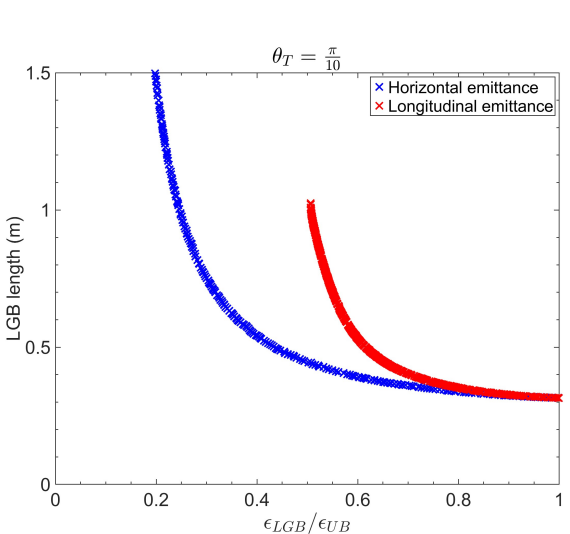


Fig. 2. Application of LGB to minimize horizontal (blue) and longitudinal (red) emittance, respectively. The subscripts “LGB” and “UB” represent longitudinal gradient bend and uniform bend, respectively.

648

2. Longitudinal Emittance

651 with

649

Similarly, for the longitudinal emittance we have

650

$$\epsilon_z = C_q \frac{\gamma^2}{J_z} I_{5z}(\alpha_{z0}, \beta_{z0}, D_{x0}, D'_{x0}) \quad (107)$$

652

$$I_{5z}(\alpha_{z0}, \beta_{z0}, D_{x0}, D'_{x0}) = \frac{1}{2 \left(\frac{\theta_0}{\rho_0} + \frac{\theta_1}{\rho_1} + \frac{\theta_2}{\rho_2} \right)} \oint_{-(\rho_0\theta_0+\rho_1\theta_1+\rho_2\theta_2)}^{(\rho_0\theta_0+\rho_1\theta_1+\rho_2\theta_2)} \frac{\beta_z(s)}{|\rho(s)|^3} ds. \quad (108)$$

653

For example, if we still choose the setup given in Eq. (103),
654 the minimum value of I_{5z} and longitudinal emittance in this
655 case is realized when

656

$$\begin{aligned} \alpha_{z0} &= 0, \beta_{z0} \approx \frac{\sqrt{\frac{36233641}{62419}} \rho \theta^3}{7680}, \\ D_{x0} &\approx -\frac{169 \rho \theta^2}{9640}, D'_{x0} = 0, \end{aligned} \quad (109)$$

657 and

658

$$F_{z,\min} \approx 0.838 \times \frac{\theta^3}{60\sqrt{7}}, \quad (110)$$

659 which compared with Eq. (85) means the theoretical mini-
660 mum longitudinal emittance now can become a bit smaller
661 than the case of applying a constant bending field.662 Similar to what presented just now about lowering trans-
663 verse emittance, we also apply the numerical optimization to
664 choose a better combination of ρ_i and θ_i in lowering longitu-
665 dinal emittance. Presented in Fig. 2 is the result of one spe-
666 cific case where $\theta_T = 2(\theta_0 + \theta_1 + \theta_2) = \frac{\pi}{10}$, from which we
667 can see that in this case by applying LGBs, in principle we
668 can lower the longitudinal emittance by a factor of two with
669 a reasonable length of the LGB. So generally, LGB is more
670 effective in lowering the horizontal emittance, compared to
671 lowering the longitudinal emittance.

672

IV. STEADY-STATE MICRO-BUNCHING STORAGE RINGS

673

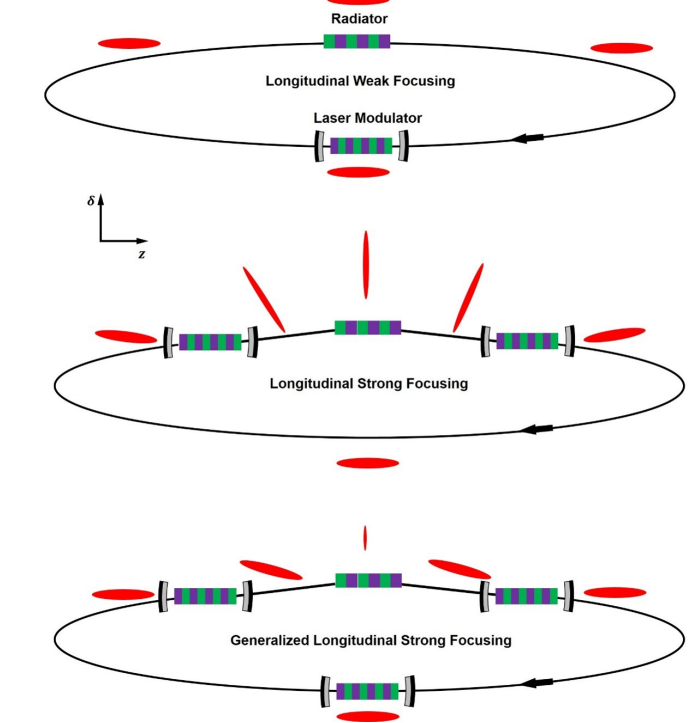
674 In this section, based on the theoretical minimum emittance
675 derived in the last section, we conduct some key analysis of
676 three specific SSMB scenarios along the thinking of realiz-
677 ing nm bunch length and high-average-power EUV radiation,

Fig. 3. Schematic layout of longitudinal weak focusing (LWF), longitudinal strong focusing (LSF), generalized longitudinal strong focusing (GLSF) SSMB storage rings. The red ellipses illustrate the beam distribution in longitudinal phase space. To realize the same bunch length compression ratio, the required energy chirp strength in the GLSF scheme is much smaller than that of LSF.

i.e., longitudinal weak focusing (LWF), longitudinal strong focusing (LSF) and generalized longitudinal strong focusing (GLSF). The analysis aims to answer the question why GLSF is our present choice in realizing high-average-power EUV radiation. Before going into the details, here first we use Table 1 and Fig. 3 to briefly summarize the characteristics of these three scenarios. Note that in Fig. 3, the beam distribution in longitudinal phase space are all of the microbunch, whose length is at the laser wavelength range. We also remind the readers that in the figure, the energy chirp strength in GLSF is much smaller than that of LSF. The physical reason should be clear with the analysis in this section *unfolded*.

TABLE 1. Main characteristics of LWF, LSF and GLSF SSMB storage rings.

LWF	$\nu_s \ll 1$	$\frac{\beta_{z,\max}}{\beta_{z,\min}} \approx 1$	2D phase space dynamics
LSF	$\nu_s \sim 1$	$\frac{\beta_{z,\max}}{\beta_{z,\min}} \gg 1$	2D phase space dynamics
GLSF	-	$\frac{\sigma_{z,\max}}{\sigma_{z,\min}} \gg 1$	4D or 6D phase space dynamics

In all the example calculations to be shown in the following part of this paper, we set the electron energy to be $E_0 = 600$ MeV, and modulation laser wavelength to be $\lambda_L = 1064$ nm. The choice of this beam energy is because it is an appropriate energy for EUV generation using an undulator as radiator. On one hand, it is not too high, otherwise the laser modulation will become more difficult, which means more laser power is needed to imprint a given modulation strength. On the other hand, it is not too low otherwise intra-beam scattering (IBS) could become too severe. Actually as we will see in Sec. VIII, IBS is a fundamental issue in SSMB storage rings which require at least one of the three eigen emittances to be small. The reason for choosing this laser wavelength is due to the fact that it is the common wavelength range for high-power optical enhancement cavity, which is used together with an undulator to form the laser modulator of SSMB.

A. Longitudinal Weak Focusing

Now we start the quantitative analysis. We start from the longitudinal weak focusing (LWF) SSMB ring. In a LWF ring with a single laser modulator (LM) as shown in Fig. 3, the single-particle longitudinal dynamics turn by turn is modeled as

$$\begin{aligned} \delta_{n+1} &= \delta_n + \frac{h}{k_L} \sin(k_L z_n), \\ z_{n+1} &= z_n - \eta C_0 \delta_{n+1}, \end{aligned} \quad (111)$$

where the subscripts $n, n+1$ means the number of revolutions, h is the energy chirp strength around the zero-crossing phase, $k_L = \frac{2\pi}{\lambda_L}$ is the wavenumber of the modulation laser and λ_L is the laser wavelength, C_0 is the ring circumference, and

$$\eta = \frac{\Delta T/T_0}{\Delta E/E_0} = \frac{1}{C_0} \oint \left(\frac{D_x}{\rho} - \frac{1}{\gamma^2} \right) ds \quad (112)$$

is the phase slippage factor of the ring. Note that in the above model, we have assumed that the radiation energy loss in an SSMB storage ring will be compensated by other system instead of the laser modulators, so the microbunching will be formed around the laser zero-crossing phase. The laser in principle can also be used for energy compensation, but is not a cost-effective choice and will also limit the output radiation power. We can use induction linacs or RF cavities to supply the radiation energy loss. Linear stability of Eq. (111) around the zero-crossing phase requires that $0 < h\eta C_0 < 4$. To avoid strong chaotic dynamics which may destroy the regular longitudinal phase space structure, an empirical criterion is

$$0 < h\eta C_0 \lesssim 0.1. \quad (113)$$

In a LWF ring, when the synchrotron tune $|\nu_s| \approx \sqrt{h\eta C_0}/2\pi \ll 1$, the longitudinal beta function at the center of laser modulator is [17]

$$\beta_{zM} \approx \sqrt{\frac{\eta C_0}{h}}. \quad (114)$$

Note that in this paper, we will use subscript ‘M’ to represent modulator, and ‘R’ to represent radiator. From Eq. (113) we then require

$$|\eta C_0| \lesssim \frac{\beta_{zM}}{\sqrt{10}}. \quad (115)$$

Now we can use the previous analysis of theoretical minimum longitudinal emittance, more specifically Eq. (90), and the above result to do some evaluation for a LWF ring. If $E_0 = 600$ MeV, the bending radius of dipoles in the ring $\rho_{ring} = 1.5$ m which corresponds to a bending field strength $B_{ring} = 1.33$ T, and if our desired bunch length is $\sigma_z = 50$ nm ($\sigma_z \lesssim \lambda_L/20$ for microbunches to be safely stored in the optical microbuckets for $\lambda_L = 1064$ nm), then we may need $\sigma_{z,min,ISO} \leq 50/\sqrt{2}$ nm to avoid significant energy widening when we reach the desired bunch length. From Eq. (90) we then need $\theta \leq \frac{2\pi}{30}$ rad. Therefore, we need at least 30 bending magnets in the ring. Assuming the length of each isochronous cell containing a bending magnet is 3 m, then the arc section of such a storage ring has a length of about 90 m. Considering the straight section for beam injection/extraction, radiation energy loss compensation, and insertion device for radiation generation, the circumference of such a ring could be 100 m to 120 m.

To reach the desired bunch length, according to Eq. (87) we need $\beta_{zM} = \beta_{z0} = \rho\theta^3/12\sqrt{210}$. In our present example case, if $\rho = 1.5$ m, $\theta = \frac{2\pi}{30}$, then this value we need is $\beta_{zM} = 79.2$ μ m. Then from Eq. (115) we have

$$|\eta C_0| \lesssim 25 \mu\text{m}. \quad (116)$$

If $C_0 = 100$ m, then it means we need a phase slippage factor $|\eta| \lesssim 2.5 \times 10^{-7}$, which is a quite small value. If we want a bunch length even smaller than 50 nm at a beam energy of 600 MeV, then the required phase slippage will be too demanding to be realized using present technology. More details on the lattice design of an LWF SSMB ring which can store microbunches with a couple of 10 nm bunch length can be found in Ref. [16].

B. Longitudinal Strong Focusing

After discussing the LWF SSMB ring, we now start the analysis of LSF. First we observe that the above analysis of LWF SSMB considers the case with only a single LM. When there are multiple LMs, for the longitudinal dynamics, it is similar to implementing multiple quadrupoles in the transverse dimension, and the beam dynamics can have more possibilities. Longitudinal strong focusing scheme for example can be invoked, not unlike its transverse counterpart which is the foundation of modern high-energy accelerators. Here we use a setup with two LMs for SSMB as an example to show the scheme of manipulating β_z around the ring using the strong focusing regime. The schematic layout of the ring is shown in Fig. 4. The treatment of cases with more LMs is similar.

We divide the ring into five sections from the transfer ma-

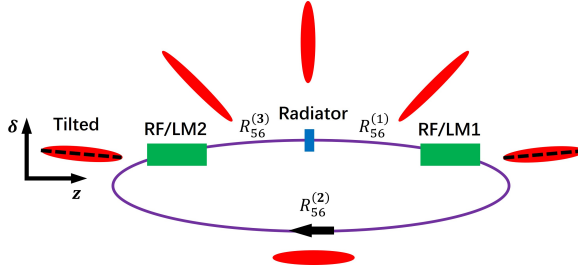


Fig. 4. A schematic layout of a storage ring using two RF systems for longitudinal strong focusing and an example beam distribution evolution in longitudinal phase space. (Figure from Ref. [8])

788 trix viewpoint, i.e., three longitudinal drifts (R_{56}) and two
789 LM kicks (h), with the linear transfer matrices of the state
790 vector in longitudinal (z, δ)^T given by

$$\begin{aligned} \mathbf{T}_{D1} &= \begin{pmatrix} 1 & R_{56}^{(1)} \\ 0 & 1 \end{pmatrix}, \quad \mathbf{T}_{LM1} = \begin{pmatrix} 1 & 0 \\ h_1 & 1 \end{pmatrix}, \\ \mathbf{T}_{D2} &= \begin{pmatrix} 1 & R_{56}^{(2)} \\ 0 & 1 \end{pmatrix}, \quad \mathbf{T}_{LM2} = \begin{pmatrix} 1 & 0 \\ h_2 & 1 \end{pmatrix}, \\ \mathbf{T}_{D3} &= \begin{pmatrix} 1 & R_{56}^{(3)} \\ 0 & 1 \end{pmatrix}. \end{aligned} \quad (117)$$

792 Then the one-turn map at the radiator center is

$$793 \quad \mathbf{M}_R = \mathbf{T}_{D3} \mathbf{T}_{LM2} \mathbf{T}_{D2} \mathbf{T}_{LM1} \mathbf{T}_{D1}.$$

794 For the generation of coherent radiation, we usually want the
795 bunch length to reach its minimum at the radiator, then we
796 need $\alpha_z = 0$ at the radiator.

797 With the primary goal of presenting the principle, instead
798 of a detailed design, here for simplicity we focus on one spe-
799 cial case: $R_{56}^{(1)} = R_{56}^{(3)}$, $h_1 = h_2 = h$. Denote

$$800 \quad \zeta_1 \equiv 1 + R_{56}^{(1)} h, \quad \zeta_2 \equiv 1 + \frac{R_{56}^{(2)}}{2} h,$$

801 we then have

$$802 \quad \mathbf{M}_R = \begin{pmatrix} 2\zeta_1\zeta_2 - 1 & 2\frac{\zeta_1\zeta_2 - \zeta_1}{h} \\ 2h\zeta_2 & 2\zeta_1\zeta_2 - 1 \end{pmatrix}. \quad (120)$$

803 The linear stability requires $|2\zeta_1\zeta_2 - 1| < 1$ which means
804 $0 < \zeta_1\zeta_2 < 1$.

805 We remind the readers that the analysis above in this sub-
806 section about LSF has been presented before in Ref. [17] and
807 is presented here again for completeness. Now we try to go
808 further to gain more insight. The longitudinal beta function at
809 the radiator is

$$810 \quad \beta_{zR} = \frac{2\frac{\zeta_1^2\zeta_2 - \zeta_1}{h}}{\sin \Phi_z} = \frac{1}{|h|} \sqrt{\frac{\zeta_1(1 - \zeta_1\zeta_2)}{\zeta_2}}, \quad (121)$$

811 where $\Phi_z = 2\pi\nu_s$ is the synchrotron phase advance per turn.

812 The longitudinal beta function at the opposite of the radiator,
813 from where to LM2 has an $R_{56}^{(2)} = \frac{R_{56}^{(2)}}{2}$, is

$$814 \quad \beta_{zRO} = \frac{1}{|h|} \sqrt{\frac{\zeta_2(1 - \zeta_1\zeta_2)}{\zeta_1}}, \quad (122)$$

815 which can be obtained by switching ζ_1 and ζ_2 in the expres-
816 sion of β_{zR} in Eq. (121). So we have

$$817 \quad \frac{\beta_{zRO}}{\beta_{zR}} = \frac{\zeta_2}{\zeta_1}. \quad (123)$$

818 The longitudinal beta function at the LM1 and LM2 (here we
819 name them as modulators) is

$$820 \quad \beta_{zM} = \beta_{zR} + \frac{R_{56}^{(1)}}{\beta_{zR}}. \quad (124)$$

821 For efficient bunch compression from the place of modulator
822 to the place of radiator, we have $|\zeta_1| \ll 1$. Then

$$823 \quad \frac{\beta_{zM}}{\beta_{zR}} = \frac{\zeta_1 - 2\zeta_1\zeta_2 + \zeta_2}{\zeta_1(1 - \zeta_1\zeta_2)} \approx \frac{\zeta_2}{\zeta_1(1 - \zeta_1\zeta_2)} = \frac{1}{h^2\beta_{zR}^2}, \quad (125)$$

824 from which we have the required energy chirp strength

$$825 \quad |h| \approx \frac{1}{\sqrt{\beta_{zR}\beta_{zM}}}. \quad (126)$$

826 This relation is similar to the theorems to be presented in
827 Sec. V about transverse-longitudinal coupling-based bunch
828 compression schemes which are the backbone of the GLSF
829 scheme. The relation can also be casted as

$$830 \quad |h| \approx \frac{\sqrt{\epsilon_z/\beta_{zM}}}{\sqrt{\epsilon_z\beta_{zR}}} = \frac{\sqrt{\epsilon_z/\beta_{zM}}}{\sigma_{zR}}, \quad (127)$$

831 with $\sigma_{zR} = \sqrt{\epsilon_z\beta_{zR}}$ being the bunch length at the radiator.

832 We now investigate the required energy chirp strength and
833 modulation laser power based on the analysis. We assume
834 that in a LSF ring, the longitudinal emittance is dominantly
835 from the quantum excitation in ring dipoles. This assumption
836 will be justified later to see if it is really the case. Further,
837 we assume that the average longitudinal beta function at the
838 dipoles equals that at the modulator, i.e., $\langle \beta_z \rangle = \beta_{zM}$. Then
839 the equilibrium longitudinal emittance given by the balance of
840 quantum excitation and radiation damping in a ring consisting
841 of iso-bending-magnets has the scaling

$$842 \quad \epsilon_{z,LSF} = C_q \frac{\gamma^2}{J_z} \frac{I_{5z}}{I_2} = C_q \frac{\gamma^2}{J_z} \frac{\frac{\langle \beta_z \rangle}{\rho_{ring}^3} 2\pi\rho_{ring}}{\frac{1}{\rho_{ring}^2} 2\pi\rho_{ring}} \propto \gamma^2 \frac{\beta_{zM}}{\rho_{ring}}, \quad (128)$$

843 which combining with Eq. (127) gives

$$844 \quad |h| \propto \frac{\gamma}{\sigma_{zR}\sqrt{\rho_{ring}}}. \quad (129)$$

845 Here, σ_{zR} is determined by our desired radiation wavelength.

846 Therefore, given the beam energy and desired bunch length,
847 to lower the required energy chirp strength in LSF, we should
848 use as large ρ_{ring} as possible which means as weak as bending
849 magnet as possible. But note that the total length of the bend-
850 ing magnets should be within a reasonable range. Also note

that when the bending magnets in the ring are very weak, the assumption that the longitudinal emittance in a LSF ring is dominantly from them will fail, since the quantum excitation in the bending magnets will become weaker, while there are other contributions like quantum excitation at the laser modulators.

We have mentioned in the introduction section that a short bunch can generate coherent radiation. The parameter used to quantify the capability of beam for coherent radiation generation is called bunching factor, and in the 1D case is defined as

$$b(\omega) = \int_{-\infty}^{\infty} \psi(z) e^{-i\frac{\omega}{c}z} dz, \quad (130)$$

with ω the radiation frequency, $\psi(z)$ the longitudinal charge density distribution satisfying the normalization $\int_{-\infty}^{\infty} \psi(z) dz = 1$. We will present more indepth discussion of bunching factor in Sec. VI A. The coherent radiation power of a beam with N_p particles at frequency ω is related to the radiation of a single particle according to

$$P_{\text{beam}}(\omega) = N_e^2 b^2(\omega) P_{\text{single}}(\omega). \quad (131)$$

For a Gaussian bunch with an RMS bunch length of σ_z , we have $b(\omega) = \exp\left[-\left(\frac{\omega}{c}\sigma_z\right)^2/2\right]$. For significant 13.5 nm-wavelength coherent EUV radiation generation, we may need $\sigma_{zR} \lesssim 4$ nm which corresponds to $b_{13.5 \text{ nm}} \gtrsim 0.18$. To increase the radiation power, we may need the radiator, which is assumed to be an undulator, has a large period number N_u (for example $N_u \approx 300$). To avoid significant bunch lengthening from the energy spread and the undulator $R_{56} = 2N_u\lambda_R$, we then need $N_u\lambda_R\sigma_\delta \lesssim \sigma_{zR}$, which then requires the energy spread at the radiator $\sigma_{\delta R} \lesssim 1 \times 10^{-3}$. So we need $\epsilon_z = \sigma_{zR}\sigma_{\delta R} \lesssim 4$ pm. Since in a LSF ring, as explained we cannot make the optimal conditions Eq. (83) be satisfied in all the bending magnets, then a reasonable argument is that the real longitudinal emittance should be at least a factor of two larger than the true theoretical minimum, which then requires

$$\epsilon_{z,\min} \lesssim 2 \text{ pm}. \quad (132)$$

Then according to Eq. (86), if $E_0 = 600$ MeV, we need $\theta \lesssim \frac{2\pi}{59}$, which means 59 bending magnets are needed. As suming the length of each isochronous cell containing a bending magnet is 3 m, then the arc section of such a ring has a length of about 177 m. Considering the straight section for beam injection/extraction, radiation energy loss compensation, and longitudinal strong focusing section, the circumference of such a ring is about 200 m.

If $\epsilon_z = 4$ pm, to get $\sigma_{zR} \lesssim 4$ nm, we then need

$$\beta_{zR} = \frac{\sigma_{zR}^2}{\epsilon_z} \lesssim 4 \mu\text{m}. \quad (133)$$

From Eq. (126), given β_{zR} , we should apply as large β_{zM} as possible to decrease the energy chirp strength h . Since $\beta_{z0} \propto \rho$ with θ given, we will choose a reasonable large bending radius for the dipoles in the ring. If $\rho = 10$ m

which corresponds to $B_0 = 0.2$ T and a total bending magnet length of 62.8 m, then the longitudinal beta function at the dipole center required to reach the practical theoretical minimum longitudinal emittance (see Eqs. (89) and (87)) is $\beta_{z0} = \rho\theta^3/12\sqrt{210} = 69.5 \mu\text{m}$. Then we may let

$$\beta_{zM} \approx 2\beta_{z0} \approx 139 \mu\text{m}. \quad (134)$$

Then from Eqs. (126), (133) and (134), the energy chirp strength required in such a LSF SSMB ring is

$$|h| \approx \frac{1}{\sqrt{\beta_{zR}\beta_{zM}}} \gtrsim 4.24 \times 10^4 \text{ m}^{-1}. \quad (135)$$

According to Eq. (221) to be presented later about the laser modulator induced energy chirp strength, if $E_0 = 600$ MeV, and for a modulator undulator with period $\lambda_{uM} = 8$ cm ($B_{0M} = 1.13$ T), length $L_{uM} = 1.6$ m, and for a laser with wavelength $\lambda_L = 1064$ m, to introduce the required energy chirp strength, we need a laser power $P_L \approx 1$ GW. This is a large value and is three orders of magnitude higher than the average stored laser power reachable in an optical enhancement cavity at the moment [31], which is at the level of one megawatt (MW). This makes the optical enhancement cavity can only work in a low duty cycle pulsed mode, thus limiting the filling factor of the microbunched electron beam in the ring, and thus limiting the average output EUV power.

We remind the readers that there is a subtle point in a LSF SSMB ring if we take the nonlinear sinusoidal modulation waveform into account, since the dynamical system is then strongly chaotic and requires careful analysis to ensure a large enough stable region for particle motion in the longitudinal phase space. More details in this respect can be found in Ref. [18].

Now for completeness of discussion, let us evaluate the contribution of modulator undulators to longitudinal emittance in our above example case, since there is also quantum excitation at the modulators. The quantum excitation contributions of two modulators to ϵ_z in a LSF ring are

$$\begin{aligned} \Delta\epsilon_{zM} &= C_q \frac{\gamma^2}{J_z} \frac{\Delta I_{5zM}}{I_2} \\ &= C_q \frac{\gamma^2}{J_z} \frac{1}{I_2} \times 2 \int_{-\frac{L_{uM}}{2}}^{\frac{L_{uM}}{2}} \frac{\beta_{zM}}{|\rho(s)|^3} ds \\ &= C_q \frac{\gamma^2}{J_z} \frac{1}{I_2} \times 2 \frac{\beta_{zM}}{\rho_{0M}^3} \frac{4}{3\pi} L_{uM}, \end{aligned} \quad (136)$$

where ΔI_{5zM} is the contribution of two modulators to I_{5z} defined in Eq. (54), ρ_{0M} is the bending radius at the peak magnetic field of the modulator. Put in the numbers, and taking the approximation $I_2 \approx \frac{2\pi}{\rho_{ring}}$ which means the radiation loss is mainly from dipoles in the ring, $J_z \approx 2$, we have

$$\Delta\epsilon_{zM} [\text{nm}] = 8.9 B_{\text{ring}}^{-1} [\text{T}] B_{0M}^3 [\text{T}] \beta_{zM} [\text{m}] L_{uM} [\text{m}]. \quad (137)$$

In our example case, $B_{\text{ring}} = 0.2$ T, $B_{0M} = 1.13$ T, $\beta_{zM} = 139 \mu\text{m}$, $L_{uM} = 1.6$ m, we have

$$\Delta\epsilon_{zM} = 14.3 \text{ pm}, \quad (138)$$

which is even larger than the desired 4 pm longitudinal emittance, and therefore is unacceptable.

The above evaluation of longitudinal emittance contribution means we need to use a weaker or shorter modulator. Since our desired longitudinal emittance is $\epsilon_z \lesssim 4$ pm, we need to control the contribution from two modulators to be $\Delta\epsilon_{zM} \lesssim 1$ pm since the ring dipoles will also contribute longitudinal emittance with a theoretical minimum about 2 pm. For example, we may choose to weaken the modulator field by more than a factor of two. If $\lambda_{uM} = 0.15$ m and $B_{0M} = 0.435$ T, $L_{uM} = 1.5$ m, then the contribution of two modulators to longitudinal emittance is

$$\Delta\epsilon_{zM} = 0.76 \text{ pm}, \quad (139)$$

which should be acceptable for a target total longitudinal emittance of 4 pm. But then to introduce the desired energy chirp strength, we now need $P_L \approx 2$ GW.

Note that in this updated parameter choice, there is still one issue we need take care. In the evaluation of quantum excitation contribution of modulators to longitudinal emittance, we have implicitly assumed that the longitudinal beta function does not change inside it. This is not true strictly speaking. The undulator itself has an $R_{56} = 2N_u\lambda_0$, with λ_0 the fundamental resonance wavelength of the undulator and in our case is the modulation laser wavelength. And the criterion whether the thin-lens approximation applies is to evaluate whether or not $|hR_{56}| \ll 1$, where R_{56} is that of the undulator. Here in this updated example, we have $hR_{56} = h2N_u\lambda_L = 0.9$ for the modulator, which means that the thin-lens kick approximation actually does not apply here. So more accurately we should use the thick-lens map of the modulator [17] to calculate the evolution of longitudinal beta function in the modulator, and then evaluate the contribution to longitudinal emittance.

With all the subtle points carefully handled, LSF as analyzed above in principle can realize the desired nm bunch length and thus generate coherent EUV radiation. The main issue of such an EUV source is the required modulation laser power (GW level) is too high and makes the optical enhancement cavity can only work in a low duty cycle pulsed mode, thus limiting the average EUV output power.

C. Generalized Longitudinal Strong Focusing

The previous analysis of LWF and LSF leads us to consider the generalized longitudinal strong focusing (GLSF) scheme [9]. The basic idea of GLSF is to take advantage of the ultrasmall natural vertical emittance in a planar electron storage ring. More specifically, we will apply a partial transverse-longitudinal emittance exchange at the optimal laser wavelength range to achieve efficient microbunching generation. As shown in Fig. 3, the schematic setup of a GLSF ring is very similar to that of a LSF ring. But as stressed before, the energy chirp strength required in GLSF is much smaller than that in the LSF scheme, which means the required modulation laser power can also be smaller. A sharp reader may also notice that in Fig. 3, the longitudinal

phase space area of beam is not conserved in the bunch compression or harmonic generation section of a GLSF ring. The fundamental physical law like Liouville's theorem of course cannot be violated in a symplectic system. The reason for this apparent "contradiction" is that GLSF invokes 4D or 6D phase space dynamics as summarized in Tab. 1, and what are conserved are the eigen emittances, instead of the projected emittances. One may also note that in the plot, the phase space rotation direction in the GLSF scheme is reversed after the radiator compared to that before the radiator, while in the LSF scheme this is not the case. In other words, in GLSF, we choose to make the upstream and downstream modulations cancel each other. In this sense, this setup is a special case of the reversible seeding scheme of SSMB [32]. The reason of doing this is that we want to make the system is transverse-longitudinal coupled only in a limited local region in the ring, the so called GLSF section, such that we can maintain $\mathcal{H}_y = 0$ being at the majority places of the ring to minimize the quantum excitation and IBS contribution to vertical emittance, thus keeping the small vertical emittance of a planar uncoupled ring. Further, this cancellation of nonlinear sinusoidal modulation waveforms will make the nonlinear dynamics of the ring easier to handle. To make the modulations perfectly cancel, we need the lattice between the upstream and down stream modulator to be an isochronous achromat. This reversible seeding setup makes the following decoupling of the system straightforward. All we need to do is to make the GLSF section an achromat, as the section from the upstream modulator to downstream modulator is transparent to the longitudinal dynamics. Another advantage of this reversible seeding setup is that it makes the bunch length at the modulator more flexible. It can be a short microbunched beam as shown in Fig. 3. It can also be a conventional RF-bunched beam, or even a coasting beam. A coasting beam in this context means the beam is not pre-microbunched, and its length is much longer than the modulation laser wavelength, or even longer than that of an RF bunch. Actually in our present design to be presented in Sec. VIII, we actually use an RF-bunched beam in the ring. So the third laser modulator of such a GLSF ring is actually an RF system. Having explained the reason why we choose this reversible seeding setup for GLSF, we remind the readers that this however is not the only possible way to realize the GLSF scheme [9]. For example, a symmetric lattice setup with respect to the radiator is also possible, although the nonlinear dynamics might be challenging.

After this general introduction of the GLSF scheme, we now appreciate in a more physical way why GLSF could be favored compared to LSF, in lowering the required modulation laser power. The key is that LSF has contribution of ϵ_z from both the LSF section and the ring dipoles, while GLSF has only contribution of ϵ_y from the GLSF section, since \mathcal{H}_y outside the GLSF section is zero as just explained. This is the key physical argument from the single-particle dynamics perspective that why GLSF may require a smaller energy modulation compared to LSF, to realize the same desired bunch length at the radiator. Actually if the longitudinal emittance in LSF is only from the quantum excitation of LSF modulators,

and the vertical emittance in GLSF is only from the quantum excitation of GLSF modulators, then GLSF and LSF are actually equivalent in essence (only a factor of two difference in damping rates) concerning the requirement on energy modulation strength from the single-particle dynamics perspective.

Now we explain the above argument more clearly using formulas. As we will show in the following section, more specifically Eq. (150), in GLSF at best case we have

$$|h| = \frac{1}{\sqrt{\mathcal{H}_{yR} \mathcal{H}_{yM}}} = \frac{\sqrt{\epsilon_y / \mathcal{H}_{yM}}}{\sqrt{\epsilon_y \mathcal{H}_{yR}}} = \frac{\sqrt{\epsilon_y / \mathcal{H}_{yM}}}{\sigma_{zR}}, \quad (140)$$

where $\mathcal{H}_y = \beta_{55}^{II}$ is defined in Sec. II and quantifies the contribution of vertical emittance to the bunch length. Note that we have used $\sigma_{zR} = \sqrt{\epsilon_y \mathcal{H}_{yR}}$, which means the bunch length at the radiator in GLSF scheme is solely determined by the beam vertical emittance. One can appreciate the similarity of the above formula with Eq. (127) for the case of LSF. Therefore, GLSF will be advantageous to LSF in lowering the required energy modulation strength if

$$\frac{\epsilon_{y, \text{GLSF}}}{\mathcal{H}_{yM, \text{GLSF}}} < \frac{\epsilon_{z, \text{LSF}}}{\beta_{zM, \text{LSF}}}. \quad (141)$$

Now we compare the two schemes in a more quantitative way. We assume that the two schemes work at the same beam energy. As we will show in Sec. VIII C, in a GLSF SSMB ring and if we consider only single-particle dynamics, the dominant contribution of vertical emittance is from the quantum excitation of two modulators in the GLSF section, and we have

$$\epsilon_{y, \text{GLSF}} \approx C_q \frac{\gamma^2}{J_y} \frac{1}{I_2} \times 2 \frac{\mathcal{H}_{yM, \text{GLSF}}}{\rho_{0M}^3} \frac{4}{3\pi} L_{uM, \text{GLSF}}. \quad (142)$$

While in LSF, we assume that the longitudinal emittance is mainly from the quantum excitation in dipoles of the ring, and the average longitudinal beta function around the ring dipoles is the same as that at the modulators $\langle \beta_z \rangle \approx \beta_{zM}$. Taking the approximation $I_2 \approx \frac{2\pi}{\rho_{\text{ring}}}$ which means in both rings the radiation loss is mainly from the dipoles in the ring, $J_z \approx 2$, $J_x \approx 1$, and combining with Eq. (128), Eq. (141) then corresponds to

$$4\rho_{\text{ring}, \text{GLSF}} \frac{\frac{4}{3\pi} L_{uM, \text{GLSF}}}{\rho_{0M, \text{GLSF}}^3} < \rho_{\text{ring}, \text{LSF}} \frac{2\pi \rho_{\text{ring}, \text{LSF}}}{\rho_{\text{ring}, \text{LSF}}^3}. \quad (143)$$

The above condition should be straightforward to fulfill in practice. For example, if the bending magnet strengths are the same in both schemes, i.e., if $\rho_{\text{ring}, \text{GLSF}} = \rho_{\text{ring}, \text{LSF}} = \rho_{\text{ring}}$, the above relation corresponds to

$$L_{uM, \text{GLSF}} < \frac{3\pi^2}{8} \frac{\rho_{0M, \text{GLSF}}^3}{\rho_{\text{ring}}^2}, \quad (144)$$

which is easy to satisfy in practice. So GLSF can be favored compared to LSF in lowering the required modulation laser power.

D. Short Summary

From the analysis in this section our tentative conclusion is: a LWF SSMB ring can be used to generate bunches with a couple of 10 nm bunch length, thus to generate coherent visible and infrared radiation. If we want to push the bunch length to an even shorter range, the required phase slippage factor of the ring will be too small from an engineering view-point. A LSF SSMB ring can create bunches with a bunch length at nm level, thus to generate coherent EUV radiation. However, the required modulation laser power is at GW level, and makes the optical enhancement cavity can only work at a low duty cycle pulsed mode, thus limiting the average output EUV radiation power. At present, a GLSF SSMB ring is the most promising among these three schemes to realize nm bunch length with a smaller modulation laser power compared to LSF SSMB, thus allowing a higher average power EUV radiation generation.

V. TRANSVERSE-LONGITUDINAL COUPLING FOR BUNCH COMPRESSION AND HARMONIC GENERATION

In the following sections, we will go into more details of the GLSF scheme, more specifically we will investigate the backbone of a GLSF SSMB storage ring, the transverse-longitudinal phase space coupling dynamics, in a systematic way. As the first step, in this section we present three theorems or inequalities that dictate such TLC-based bunch compression or harmonic generation schemes. If the initial bunch is longer than the modulation RF or laser wavelength, then compression of bunch or microbunch can just be viewed as a harmonic generation scheme. Therefore, in this paper, we will treat bunch compression and harmonic generation as the same thing in essence. We remind the readers that the theorems presented here are the generalization of that presented in Refs. [17, 33] from 4D phase space to 6D phase space. These formal mathematical relations will be useful in our later more detailed study for a GLSF SSMB light source.

A. Problem Definition

Let us first define the problem we are trying to solve. We assume ϵ_y is the small eigen emittance we want to exploit. The case of using ϵ_x is similar. The schematic layout of a TLC-based bunch compression section is shown in Fig. 5. Suppose the beam at the entrance of the bunch compression section is $x-y-z$ decoupled, with its second moments matrix given by



Fig. 5. A schematic layout of applying TLC dynamics for bunch compression. (Figure adapted from Ref. [33]).

1142

$$\Sigma_i = \langle \mathbf{X} \mathbf{X}^T \rangle_i = \begin{pmatrix} \epsilon_x \beta_{xi} & -\epsilon_x \alpha_{xi} & 0 & 0 & 0 & 0 \\ -\epsilon_x \alpha_{xi} & \epsilon_x \gamma_{xi} & 0 & 0 & 0 & 0 \\ 0 & 0 & \epsilon_y \beta_{yi} & -\epsilon_y \alpha_{yi} & 0 & 0 \\ 0 & 0 & -\epsilon_y \alpha_{yi} & \epsilon_y \gamma_{yi} & 0 & 0 \\ 0 & 0 & 0 & 0 & \epsilon_z \beta_{zi} & -\epsilon_z \alpha_{zi} \\ 0 & 0 & 0 & 0 & -\epsilon_z \alpha_{zi} & \epsilon_z \gamma_{zi} \end{pmatrix}, \quad (145)$$

1143 where α , β and γ are the Courant-Snyder functions, the sub- 1165
 1144 script i means initial, and ϵ_x , ϵ_y and ϵ_z are the eigen emit- 1166
 1145 tances of the beam corresponding to the horizontal, vertical 1167
 1146 and longitudinal mode, respectively. Note that the eigen emit- 1168
 1147 tances are beam invariants with respect to linear symplectic 1169
 1148 transport. For the application of TLC for bunch compression, 1170
 1149 it means that the final bunch length at the exit or radiator σ_{zR} 1171
 1150 depends only on the vertical emittance ϵ_y , and neither on the 1172
 1151 horizontal one ϵ_x and nor on the longitudinal one ϵ_z . 1173

1152 We divide such a bunch compression section into three 1172 parts, with their symplectic transfer matrices given by 1153

$$M_1 = \begin{pmatrix} r_{11} & r_{12} & r_{13} & r_{14} & 0 & r_{16} \\ r_{21} & r_{22} & r_{23} & r_{24} & 0 & r_{26} \\ r_{31} & r_{32} & r_{33} & r_{34} & 0 & r_{36} \\ r_{41} & r_{42} & r_{43} & r_{44} & 0 & r_{46} \\ r_{51} & r_{52} & r_{53} & r_{54} & 1 & r_{56} \\ 0 & 0 & 0 & 0 & 0 & 1 \end{pmatrix}, \quad (146)$$

1154 M_2 = modulation kick map,

$$M_3 = \begin{pmatrix} R_{11} & R_{12} & R_{13} & R_{14} & 0 & R_{16} \\ R_{21} & R_{22} & R_{23} & R_{24} & 0 & R_{26} \\ R_{31} & R_{32} & R_{33} & R_{34} & 0 & R_{36} \\ R_{41} & R_{42} & R_{43} & R_{44} & 0 & R_{46} \\ R_{51} & R_{52} & R_{53} & R_{54} & 1 & R_{56} \\ 0 & 0 & 0 & 0 & 0 & 1 \end{pmatrix}, \quad (147)$$

1155 with M_1 representing “from entrance to modulator”, M_2 rep- 1166
 1156 resenting “modulation kick” and M_3 representing “modula- 1167
 1157 tor to radiator”. Note that M_1 and M_3 are in their general 1168
 1158 thick-lens form, and do not necessarily need to be x - y decou- 1169
 1159 pled. The transfer matrix from the entrance to the radiator is 1170
 1160 then

1161

$$O = M_3 M_2 M_1. \quad (147)$$

1162 From the problem definition, for σ_{zR} to be independent of ϵ_x 1181
 1163 and ϵ_z , we need

$$O_{51} = 0, O_{52} = 0, O_{55} = 0, O_{56} = 0. \quad (148)$$

B. Theorems and Proof

I. Theorems

1164 Given the above problem definition, and assuming the 1165
 1166 modulation kick map M_2 is a thin-lens one, we have three 1167
 1168 theorems which dictate the relation between the modulator 1169
 1170 kick strength with the optical functions at the modulator and 1171
 1172 radiator, respectively.

Theorem one: If

$$M_2 = \begin{pmatrix} 1 & 0 & 0 & 0 & 0 & 0 \\ 0 & 1 & 0 & 0 & 0 & 0 \\ 0 & 0 & 1 & 0 & 0 & 0 \\ 0 & 0 & 0 & 1 & 0 & 0 \\ 0 & 0 & 0 & 0 & 1 & 0 \\ 0 & 0 & 0 & 0 & h & 1 \end{pmatrix}, \quad (149)$$

1173 which corresponds to the case of a normal RF or a TEM00 1174
 1175 mode laser modulator, then

$$h^2 \mathcal{H}_{yM} \mathcal{H}_{yR} \geq 1, \quad (150)$$

1176 where the subscripts M and R represent the place of modula- 1177
 1178 tor and radiator, respectively.

Theorem two: If

$$M_2 = \begin{pmatrix} 1 & 0 & 0 & 0 & 0 & 0 \\ 0 & 1 & 0 & 0 & 0 & 0 \\ 0 & 0 & 1 & 0 & 0 & 0 \\ 0 & 0 & 0 & 1 & g & 0 \\ 0 & 0 & 0 & 0 & 1 & 0 \\ 0 & 0 & g & 0 & 0 & 1 \end{pmatrix}, \quad (151)$$

1180 which corresponds to the case of a transverse deflecting (in 1181
 1182 y -dimension) RF or a TEM01 mode laser modulator or other 1183
 1184 schemes for angular modulation, then

$$g^2 \beta_{yM} \mathcal{H}_{yR} \geq 1. \quad (152)$$

1161

1162 From the problem definition, for σ_{zR} to be independent of ϵ_x 1181
 1163 and ϵ_z , we need

$$O_{51} = 0, O_{52} = 0, O_{55} = 0, O_{56} = 0. \quad (148)$$

1161

1162 From the problem definition, for σ_{zR} to be independent of ϵ_x 1181
 1163 and ϵ_z , we need

$$O_{51} = 0, O_{52} = 0, O_{55} = 0, O_{56} = 0. \quad (148)$$

1161

1162 From the problem definition, for σ_{zR} to be independent of ϵ_x 1181
 1163 and ϵ_z , we need

$$O_{51} = 0, O_{52} = 0, O_{55} = 0, O_{56} = 0. \quad (148)$$

1161

1162 From the problem definition, for σ_{zR} to be independent of ϵ_x 1181
 1163 and ϵ_z , we need

$$O_{51} = 0, O_{52} = 0, O_{55} = 0, O_{56} = 0. \quad (148)$$

1161

1162 From the problem definition, for σ_{zR} to be independent of ϵ_x 1181
 1163 and ϵ_z , we need

$$O_{51} = 0, O_{52} = 0, O_{55} = 0, O_{56} = 0. \quad (148)$$

1161

1162 From the problem definition, for σ_{zR} to be independent of ϵ_x 1181
 1163 and ϵ_z , we need

$$O_{51} = 0, O_{52} = 0, O_{55} = 0, O_{56} = 0. \quad (148)$$

1161

1162 From the problem definition, for σ_{zR} to be independent of ϵ_x 1181
 1163 and ϵ_z , we need

$$O_{51} = 0, O_{52} = 0, O_{55} = 0, O_{56} = 0. \quad (148)$$

1161

1162 From the problem definition, for σ_{zR} to be independent of ϵ_x 1181
 1163 and ϵ_z , we need

$$O_{51} = 0, O_{52} = 0, O_{55} = 0, O_{56} = 0. \quad (148)$$

1161

1162 From the problem definition, for σ_{zR} to be independent of ϵ_x 1181
 1163 and ϵ_z , we need

$$O_{51} = 0, O_{52} = 0, O_{55} = 0, O_{56} = 0. \quad (148)$$

1161

1162 From the problem definition, for σ_{zR} to be independent of ϵ_x 1181
 1163 and ϵ_z , we need

$$O_{51} = 0, O_{52} = 0, O_{55} = 0, O_{56} = 0. \quad (148)$$

1161

1162 From the problem definition, for σ_{zR} to be independent of ϵ_x 1181
 1163 and ϵ_z , we need

$$O_{51} = 0, O_{52} = 0, O_{55} = 0, O_{56} = 0. \quad (148)$$

1161

1162 From the problem definition, for σ_{zR} to be independent of ϵ_x 1181
 1163 and ϵ_z , we need

$$O_{51} = 0, O_{52} = 0, O_{55} = 0, O_{56} = 0. \quad (148)$$

1161

1162 From the problem definition, for σ_{zR} to be independent of ϵ_x 1181
 1163 and ϵ_z , we need

$$O_{51} = 0, O_{52} = 0, O_{55} = 0, O_{56} = 0. \quad (148)$$

1161

1162 From the problem definition, for σ_{zR} to be independent of ϵ_x 1181
 1163 and ϵ_z , we need

$$O_{51} = 0, O_{52} = 0, O_{55} = 0, O_{56} = 0. \quad (148)$$

1161

1162 From the problem definition, for σ_{zR} to be independent of ϵ_x 1181
 1163 and ϵ_z , we need

$$O_{51} = 0, O_{52} = 0, O_{55} = 0, O_{56} = 0. \quad (148)$$

1161

1162 From the problem definition, for σ_{zR} to be independent of ϵ_x 1181
 1163 and ϵ_z , we need

$$O_{51} = 0, O_{52} = 0, O_{55} = 0, O_{56} = 0. \quad (148)$$

1161

1162 From the problem definition, for σ_{zR} to be independent of ϵ_x 1181
 1163 and ϵ_z , we need

$$O_{51} = 0, O_{52} = 0, O_{55} = 0, O_{56} = 0. \quad (148)$$

1161

1162 From the problem definition, for σ_{zR} to be independent of ϵ_x 1181
 1163 and ϵ_z , we need

$$O_{51} = 0, O_{52} = 0, O_{55} = 0, O_{56} = 0. \quad (148)$$

1161

1162 From the problem definition, for σ_{zR} to be independent of ϵ_x 1181
 1163 and ϵ_z , we need

$$O_{51} = 0, O_{52} = 0, O_{55} = 0, O_{56} = 0. \quad (148)$$

1161

1162 From the problem definition, for σ_{zR} to be independent of ϵ_x 1181
 1163 and ϵ_z , we need

$$O_{51} = 0, O_{52} = 0, O_{55} = 0, O_{56} = 0. \quad (148)$$

1161

1162 From the problem definition, for σ_{zR} to be independent of ϵ_x 1181
 1163 and ϵ_z , we need

$$O_{51} = 0, O_{52} = 0, O_{55} = 0, O_{56} = 0. \quad (148)$$

1161

1162 From the problem definition, for σ_{zR} to be independent of ϵ_x 1181
 1163 and ϵ_z , we need

$$O_{51} = 0, O_{52} = 0, O_{55} = 0, O_{56} = 0. \quad (148)$$

1161

1162 From the problem definition, for σ_{zR} to be independent of ϵ_x 1181
 1163 and ϵ_z , we need

$$O_{51} = 0, O_{52} = 0, O_{55} = 0, O_{56} = 0. \quad (148)$$

1161

1162 From the problem definition, for σ_{zR} to be independent of ϵ_x 1181
 1163 and ϵ_z , we need

$$O_{51} = 0, O_{52} = 0, O_{55} = 0, O_{56} = 0. \quad (148)$$

1161

1162 From the problem definition, for σ_{zR} to be independent of ϵ_x 1181
 1163 and ϵ_z , we need

$$O_{51} = 0, O_{52} = 0, O_{55} = 0, O_{56} = 0. \quad (148)$$

1161

1162 From the problem definition, for σ_{zR} to be independent of ϵ_x 1181
 1163 and ϵ_z , we need

$$O_{51} = 0, O_{52} = 0, O_{55} = 0, O_{56} = 0. \quad (148)$$

1161

1162 From the problem definition, for σ_{zR} to be independent of ϵ_x 1181
 1163 and ϵ_z , we need

$$O_{51} = 0, O_{52} = 0, O_{55} = 0, O_{56} = 0. \quad (148)$$

1161

1162 From the problem definition, for σ_{zR} to be independent of ϵ_x 1181
 1163 and ϵ_z , we need

$$O_{51} = 0, O_{52} = 0, O_{55} = 0, O_{56} = 0. \quad (148)$$

1161

1162 From the problem definition, for σ_{zR} to be independent of ϵ_x 1181
 1163 and ϵ_z , we need

$$O_{51} = 0, O_{52} = 0, O_{55} = 0, O_{56} = 0. \quad (148)$$

1161

1162 From the problem definition, for σ_{zR} to be independent of ϵ_x 1181
 1163 and ϵ_z , we need

$$O_{51} = 0, O_{52} = 0, O_{55} = 0, O_{56} = 0. \quad (148)$$

1161

1162 From the problem definition, for σ_{zR} to be independent of ϵ_x 1181
 1163 and ϵ_z , we need

$$O_{51} = 0, O_{52} = 0, O_{55} = 0, O_{56} = 0. \quad (148)$$

1161

1162 From the problem definition, for σ_{zR} to be independent of ϵ_x 1181
 1163 and ϵ_z , we need

$$O_{51} = 0, O_{52} = 0, O_{55} = 0, O_{56} = 0. \quad (148)$$

1161

1162 From the problem definition, for σ_{zR} to be independent of ϵ_x 1181
 1163 and ϵ_z , we need

$$O_{51} = 0, O_{52} = 0, O_{55} = 0, O_{56} = 0. \quad (148)$$

1161

1162 From the problem definition, for σ_{zR} to be independent of ϵ_x 1181
 1163 and ϵ_z , we need

$$O_{51} = 0, O_{52} = 0, O_{55} = 0, O_{56} = 0. \quad (148)$$

1161

1162 From the problem definition, for σ_{zR} to be independent of ϵ_x 1181
 1163 and ϵ_z , we need

$$O_{51} = 0, O_{52} = 0, O_{55} = 0, O_{56} = 0. \quad (148)$$

1161

1162 From the problem definition, for σ_{zR} to be independent of ϵ_x 1181
 1163 and ϵ_z , we need

$$O_{51} = 0, O_{52} = 0, O_{55} = 0, O_{56} = 0. \quad (148)$$

1161

1162 From the problem definition, for σ_{zR} to be independent of ϵ_x 1181
 1163 and ϵ_z , we need

$$O_{51} = 0, O_{52} = 0, O_{55} = 0, O_{56} = 0. \quad (148)$$

1161

1162 From the problem definition, for σ_{zR} to be independent of ϵ_x 1181
 1163 and ϵ_z , we need

$$O_{51} = 0, O_{52} = 0, O_{55} = 0, O_{56} = 0. \quad (148)$$

1161

1162 From the problem definition, for σ_{zR} to be independent of ϵ_x 1181
 1163 and ϵ_z , we need

$$O_{51} = 0, O_{52} = 0, O_{55} = 0, O_{56} = 0$$

¹¹⁸⁷ then

$$\sup_{1188} q^2 \gamma_{yM} \mathcal{H}_{yR} \geq 1. \quad (154)$$

¹¹⁸⁹ There is no commonly used single element realizing the kick

¹¹⁹⁰ map Eq. (153) directly. Instead, it takes the combination of ¹¹⁹⁵ Here we present the details for the proof of Theorem one.
¹¹⁹¹ several elements to realize such a map, making its applica- ¹¹⁹⁶ The proof of the other two is just similar. From the problem
¹¹⁹² tion less straightforward compared to the cases correspond to ¹¹⁹⁷ definition, for σ_{zR} to be independent of ϵ_x and ϵ_z , we need

$$\begin{aligned} O_{51} &= r_{11}R_{51} + r_{21}R_{52} + r_{31}R_{53} + r_{41}R_{54} + r_{51}(hR_{56} + 1) = 0, \\ O_{52} &= r_{12}R_{51} + r_{22}R_{52} + r_{32}R_{53} + r_{42}R_{54} + r_{52}(hR_{56} + 1) = 0, \\ O_{55} &= hR_{56} + 1 = 0, \\ O_{56} &= r_{16}R_{51} + r_{26}R_{52} + r_{36}R_{53} + r_{46}R_{54} + r_{56}(hR_{56} + 1) + R_{56} = 0. \end{aligned} \quad (155)$$

¹¹⁹⁹ Under the above conditions, we have

$$\sup_{1200} \mathbf{O} = \begin{pmatrix} \mathbf{A} & \mathbf{B} & \mathbf{C} \\ \mathbf{D} & \mathbf{E} & \mathbf{F} \\ \mathbf{G} & \mathbf{H} & \mathbf{I} \end{pmatrix}, \quad (156)$$

¹²⁰¹ with $\mathbf{A} \sim \mathbf{I}$ being 2×2 submatrices of \mathbf{T} , and

$$\begin{aligned} \mathbf{G} &= \begin{pmatrix} 0 & 0 \\ r_{51}h & r_{52}h \end{pmatrix}, \\ \mathbf{H} &= \begin{pmatrix} r_{13}R_{51} + r_{23}R_{52} + r_{33}R_{53} + r_{43}R_{54} & r_{14}R_{51} + r_{24}R_{52} + r_{34}R_{53} + r_{44}R_{54} \\ r_{53}h & r_{54}h \end{pmatrix}, \\ \mathbf{I} &= \begin{pmatrix} 0 & 0 \\ h & r_{56}h + 1 \end{pmatrix}. \end{aligned} \quad (157)$$

¹²⁰³ Note that \mathbf{I} in this subsection does not mean the identity matrix. The bunch length squared at the modulator and the radiator are

$$\begin{aligned} \sigma_{zM}^2 &= \epsilon_x \frac{(\beta_{xi}r_{51} - \alpha_{xi}r_{52})^2 + r_{52}^2}{\beta_{xi}} + \epsilon_y \frac{(\beta_{yi}r_{53} - \alpha_{yi}r_{54})^2 + r_{54}^2}{\beta_{yi}} + \epsilon_z (\beta_{zi} - 2\alpha_{zi}r_{56} + \gamma_{zi}r_{56}^2) \\ &= \epsilon_x \mathcal{H}_{xM} + \epsilon_y \mathcal{H}_{yM} + \epsilon_z \beta_{zM}, \\ \sigma_{zR}^2 &= \epsilon_y \frac{(\beta_{yi}O_{53} - \alpha_{yi}O_{54})^2 + O_{54}^2}{\beta_{yi}} = \epsilon_y \mathcal{H}_{yR}. \end{aligned} \quad (158)$$

¹²⁰⁵ According to the Cauchy-Schwarz inequality, we have

$$\begin{aligned} h^2 \mathcal{H}_{yM} \mathcal{H}_{yR} &= h^2 \frac{[(\beta_{yi}r_{53} - \alpha_{yi}r_{54})^2 + r_{54}^2]}{\beta_{yi}} \frac{[(\beta_{yi}O_{53} - \alpha_{yi}O_{54})^2 + O_{54}^2]}{\beta_{yi}} \\ &\geq \frac{h^2}{\beta_{yi}^2} [-(\beta_{yi}r_{53} - \alpha_{yi}r_{54})O_{54} + r_{54}(\beta_{yi}O_{53} - \alpha_{yi}O_{54})]^2 \\ &= (O_{53}r_{54}h - O_{54}r_{53}h)^2 = (O_{53}O_{64} - O_{54}O_{63})^2 = |\text{Det}(\mathbf{H})|^2, \end{aligned} \quad (159)$$

¹²⁰⁷ where $\text{Det}()$ means the determinant of the matrix. The equality holds when $\frac{-(\beta_{yi}r_{53} - \alpha_{yi}r_{54})}{O_{54}} = \frac{r_{54}}{(\beta_{yi}O_{53} - \alpha_{yi}O_{54})}$. The symplecticity of \mathbf{O} requires that $\mathbf{O} \mathbf{S} \mathbf{O}^T = \mathbf{S}$, where $\mathbf{S} = \begin{pmatrix} \mathbf{J} & 0 & 0 \\ 0 & \mathbf{J} & 0 \\ 0 & 0 & \mathbf{J} \end{pmatrix}$ and $\mathbf{J} = \begin{pmatrix} 0 & 1 \\ -1 & 0 \end{pmatrix}$, so we have

$$\begin{pmatrix} \mathbf{AJA}^T + \mathbf{BJB}^T + \mathbf{CJC}^T & \mathbf{AJD}^T + \mathbf{BJE}^T + \mathbf{CJF}^T & \mathbf{AJG}^T + \mathbf{BJH}^T + \mathbf{CJI}^T \\ \mathbf{DJA}^T + \mathbf{EJB}^T + \mathbf{FJC}^T & \mathbf{DJD}^T + \mathbf{EJE}^T + \mathbf{FJF}^T & \mathbf{DJG}^T + \mathbf{EJH}^T + \mathbf{FJI}^T \\ \mathbf{GJA}^T + \mathbf{HJB}^T + \mathbf{IJC}^T & \mathbf{GJD}^T + \mathbf{HJE}^T + \mathbf{IJF}^T & \mathbf{GJG}^T + \mathbf{HJH}^T + \mathbf{IJI}^T \end{pmatrix} = \mathbf{S}. \quad (160)$$

¹²¹⁰ According to Eq. (157), we have

$$\sup_{1211} \mathbf{GJG}^T = \begin{pmatrix} 0 & 0 \\ 0 & 0 \end{pmatrix}, \quad \mathbf{IJI}^T = \begin{pmatrix} 0 & 0 \\ 0 & 0 \end{pmatrix}. \quad (161)$$

1212 Therefore,

$$1213 \quad \mathbf{H} \mathbf{J} \mathbf{H}^T = \mathbf{J}, \quad (162)$$

1214 which means \mathbf{H} is also a symplectic matrix. So we have
1215 $\text{Det}(\mathbf{H}) = 1$. The theorem is thus proven.

1216 C. Dragt's Minimum Emittance Theorem

1217 Theorem one in Eq. (150) can also be expressed as

$$1218 \quad |h| \geq \frac{\epsilon_y}{\sqrt{\epsilon_y \mathcal{H}_{yM}} \sqrt{\epsilon_y \mathcal{H}_{yR}}} = \frac{\epsilon_y}{\sigma_{zyM} \sigma_{zR}}. \quad (163)$$

1219 Note that in the above formula, σ_{zyM} means the bunch length
1220 at the modulator contributed from the vertical emittance ϵ_y .
1221 So given a fixed ϵ_y and desired σ_{zR} , a smaller h , i.e., a
1222 smaller RF acceleration gradient or modulation laser power
1223 ($P_L \propto |h|^2$), means a larger \mathcal{H}_{yM} , thus a larger σ_{zyM} , is
1224 needed. As $|h|\sigma_{zM}$ quantifies the energy spread introduced
1225 by the modulation kick, we thus also have

$$1226 \quad \sigma_{zR} \sigma_{\delta R} \geq \epsilon_y.$$

1227 Similarly for Theorem two and three, we have

$$1228 \quad |g| \geq \frac{\epsilon_y}{\sigma_{yzM} \sigma_{zR}}, \quad (165)$$

1229 and

$$1230 \quad |q| \geq \frac{\epsilon_y}{\sigma_{yzM} \sigma_{zR}}, \quad (166)$$

1231 respectively, and also Eq. (164). Note that in the above for-
1232 mulas, the vertical beam size or divergence at the modulator
1233 contains only the vertical betatron part, i.e., that from the ver-
1234 tical emittance ϵ_y .

1235 Equation (164) is actually a manifestation of the classical
1236 uncertainty principle [34], which states that

$$1237 \quad \begin{aligned} \Sigma_{11} \Sigma_{22} &\geq \epsilon_{\min}^2, \\ \Sigma_{33} \Sigma_{44} &\geq \epsilon_{\min}^2, \\ \Sigma_{55} \Sigma_{66} &\geq \epsilon_{\min}^2, \end{aligned} \quad (167)$$

1238 where ϵ_{\min} is the minimum one among the three eigen emit-
1239 tances $\epsilon_{I,II,III}$. In our bunch compression case, we assume
1240 that ϵ_y is the smaller one compared to ϵ_z .

1241 Actually there is a stronger inequality compared to the clas-
1242 sical uncertainty principle, i.e., the minimum emittance theo-
1243 rem [34], which states that the projected emittance cannot be
1244 smaller than the minimum one among the three eigen emit-
1245 tances,

$$1246 \quad \begin{aligned} \epsilon_{x,\text{pro}}^2 &= \Sigma_{11} \Sigma_{22} - \Sigma_{12}^2 \geq \epsilon_{\min}^2, \\ \epsilon_{y,\text{pro}}^2 &= \Sigma_{33} \Sigma_{44} - \Sigma_{34}^2 \geq \epsilon_{\min}^2, \\ \epsilon_{z,\text{pro}}^2 &= \Sigma_{55} \Sigma_{66} - \Sigma_{56}^2 \geq \epsilon_{\min}^2. \end{aligned} \quad (168)$$

D. Theorems Cast in Another Form

1247

1248 As another way to appreciate the result, here we cast the
1249 theorems in a form using the generalized beta functions as
1250 introduced in Sec. II. According to definition, we have

$$1251 \quad \beta_y \equiv \beta_{33}^{II}, \gamma_y \equiv \beta_{44}^{II}, \mathcal{H}_y \equiv \beta_{55}^{II}. \quad (169)$$

1252 **Theorem one:** If \mathbf{M}_2 is as shown in Eq. (149), then

$$1253 \quad M_{2,65}^2(\text{Mod}) \beta_{55}^{II}(\text{Mod}) \beta_{55}^{II}(\text{Rad}) \geq 1, \quad (170)$$

1254 where $M_{2,65}$ is the $_{65}$ matrix term of \mathbf{M}_2 , i.e., h . **The su-**
1255 **perscript 2 of $M_{2,65}^2$ means the square of $M_{2,65}$.** For better
1256 visualization, in this subsection, we use brackets to denote
1257 the location, with Ent, Mod and Rad meaning entrance, mod-
1258 ulator and radiator, respectively.

1259 **Theorem two:** If \mathbf{M}_2 is as shown in Eq. (151), then

$$1260 \quad M_{2,63}^2(\text{Mod}) \beta_{33}^{II}(\text{Mod}) \beta_{55}^{II}(\text{Rad}) \geq 1. \quad (171)$$

1261 **Theorem three:** If \mathbf{M}_2 is as shown in Eq. (153), then

$$1262 \quad M_{2,64}^2(\text{Mod}) \beta_{44}^{II}(\text{Mod}) \beta_{55}^{II}(\text{Rad}) \geq 1. \quad (172)$$

1263 At the entrance, the generalized Twiss matrix corresponding
1264 to eigen mode I is

$$1265 \quad \mathbf{T}_I(\text{Ent}) = \begin{pmatrix} \beta_{xi} & -\alpha_{xi} & 0 & 0 & 0 & 0 \\ -\alpha_{xi} & \gamma_{xi} & 0 & 0 & 0 & 0 \\ 0 & 0 & 0 & 0 & 0 & 0 \\ 0 & 0 & 0 & 0 & 0 & 0 \\ 0 & 0 & 0 & 0 & 0 & 0 \\ 0 & 0 & 0 & 0 & 0 & 0 \end{pmatrix}, \quad (173)$$

1266 and similar expressions for $\mathbf{T}_{II,III}(\text{Ent})$, with x replaced by
1267 y, z and the location of the 2×2 matrix shifted in the diagonal
1268 direction. Then

$$1269 \quad \beta_{33}^{II}(\text{Mod}) = \frac{(\beta_{yi} r_{33} - \alpha_{yi} r_{34})^2 + r_{34}^2}{\beta_{yi}}, \quad (174)$$

$$1271 \quad \beta_{44}^{II}(\text{Mod}) = \frac{(\beta_{yi} r_{43} - \alpha_{yi} r_{44})^2 + r_{44}^2}{\beta_{yi}}, \quad (175)$$

$$1273 \quad \beta_{55}^{II}(\text{Mod}) = \frac{(\beta_{yi} r_{53} - \alpha_{yi} r_{54})^2 + r_{54}^2}{\beta_{yi}}, \quad (176)$$

$$1275 \quad \beta_{55}^I(\text{Rad}) = \frac{(\beta_{xi} O_{51} - \alpha_{xi} O_{52})^2 + O_{52}^2}{\beta_{xi}}, \quad (177)$$

$$1277 \quad \beta_{55}^{II}(\text{Rad}) = \frac{(\beta_{yi} O_{53} - \alpha_{yi} O_{54})^2 + O_{54}^2}{\beta_{yi}}, \quad (178)$$

$$1279 \quad \beta_{55}^{III}(\text{Rad}) = \frac{(\beta_{zi} O_{55} - \alpha_{zi} O_{56})^2 + O_{56}^2}{\beta_{zi}}. \quad (179)$$

1280 For σ_{zR} to be independent of ϵ_x and ϵ_z , we need $\beta_{55}^I(\text{Rad}) =$
1281 0 and $\beta_{55}^{III}(\text{Rad}) = 0$, which then lead to Eq. (148). And the
1282 following proof procedures are the same as that shown in the
1283 above Sec. V B 2.

1284 VI. ENERGY MODULATION-BASED COUPLING
1285 SCHEMES

$$1325 \quad b(k_z) = \mathcal{F}(0, 0, 0, 0, k_z, 0) = \int_{-\infty}^{\infty} \psi(z) e^{-ik_z z} dz, \quad (185)$$

1286 After introducing the three formal theorems, now we con- 1326 where $\psi(z) = \int_{-\infty}^{\infty} \int_{-\infty}^{\infty} \int_{-\infty}^{\infty} \int_{-\infty}^{\infty} \int_{-\infty}^{\infty} \int_{-\infty}^{\infty} \psi(\mathbf{X}) dx dx' dy dy' d\delta$
1287 duct more detailed analysis of the TLC-based bunch compres- 1327 is the normalized longitudinal distribution of particles. Here
1288 sion or microbunching generation schemes. We group these 1328 in this paper, we will use \mathcal{F} to denote the 6D form function,
1289 schemes into two categories, i.e., energy modulation-based 1329 and b the classical 1D bunching factor.
1290 and angular modulation-based schemes. They corresponds 1330 Now we derive the form function and bunching factor
1291 to the case of Theorem One and Two presented in last sec- 1331 for a single-stage energy modulation-based microbunching
1292 tion. In this section, we focus on energy modulation-based 1332 schemes. A lumped description of the laser-induced energy
1293 schemes, and next section is dedicated to angular modulation- 1333 modulation can be written as:
1294 based schemes. The physical realization corresponding to the 1334 $\delta = \delta + A \sin(k_L z), \quad (186)$
1295 case of Theorem Three is not that straightforward compared 1335 where $k_L = \frac{2\pi}{\lambda_L}$ is the laser wavenumber and A is the modu-
1296 to the cases of Theorem One and Two, and we do not expand 1336 lation strength. After the modulation, the particle state vector
1297 its discussion [it](#) in this paper. 1337 evolves according to:

1298 A. Form Function and Bunching Factor

1299 1. General Formula

1300 For coherent radiation generation, a parameter of vital im-
1301 portant is the bunching factor of the electron beam. Here
1302 first we derive the bunching factor [formula](#) of the energy-
1303 modulation based TLC microbunching schemes. The mathe-
1304 matical model is formulated as follows.

1305 6D particle state vector:

$$1306 \quad \mathbf{X} \equiv (x \ x' \ y \ y' \ z \ \delta)^T. \quad (180)$$

1307 6D spectral vector:

$$1308 \quad \mathbf{K} \equiv (k_x \ k_{x'} \ k_y \ k_{y'} \ k_z \ k_\delta). \quad (181)$$

1309 Normalized particle density distribution in phase space $\psi(\mathbf{X})$:

$$1310 \quad \int \psi(\mathbf{X}) d\mathbf{X} = 1, \quad \psi(\mathbf{X}) \geq 0, \quad (182)$$

1311 where $\int d\mathbf{X}$ means $\int_{-\infty}^{\infty} \int_{-\infty}^{\infty} \int_{-\infty}^{\infty} \int_{-\infty}^{\infty} \int_{-\infty}^{\infty} \int_{-\infty}^{\infty} dx dx' dy$
1312 $dy' dz d\delta$. Here we introduce the form function (FF) of beam
1313 as:

$$1314 \quad \mathcal{F}(\mathbf{K}) \equiv \int \psi(\mathbf{X}) e^{-i\mathbf{K}\mathbf{X}} d\mathbf{X}. \quad (183)$$

1315 $\psi(\mathbf{X})$ and $\mathcal{F}(\mathbf{K})$ then forms a Fourier transform pair

$$1316 \quad \psi(\mathbf{X}) = \frac{1}{2\pi} \int \mathcal{F}(\mathbf{K}) e^{i\mathbf{K}\mathbf{X}} d\mathbf{K}, \quad (184)$$

1317 where $\int d\mathbf{K}$ means $\int_{-\infty}^{\infty} \int_{-\infty}^{\infty} \int_{-\infty}^{\infty} \int_{-\infty}^{\infty} \int_{-\infty}^{\infty} dk_x dk_{x'}$
1318 $dk_y dk_{y'} dk_z dk_\delta$. This form function is another complete de-
1319 scription of beam distribution and can offer complementary
1320 insight for beam dynamics study. More details on this respect
1321 will be reported elsewhere.

1322 The classical 1D bunching factor or form factor used in
1323 literature is a specific point in our defined FF, i.e., with $\mathbf{K} =$
1324 $(0, 0, 0, 0, k_z, 0)$,

1326 where $\psi(z) = \int_{-\infty}^{\infty} \int_{-\infty}^{\infty} \int_{-\infty}^{\infty} \int_{-\infty}^{\infty} \int_{-\infty}^{\infty} \int_{-\infty}^{\infty} \psi(\mathbf{X}) dx dx' dy dy' d\delta$
1327 is the normalized longitudinal distribution of particles. Here
1328 in this paper, we will use \mathcal{F} to denote the 6D form function,
1329 and b the classical 1D bunching factor.
1330 Now we derive the form function and bunching factor
1331 for a single-stage energy modulation-based microbunching
1332 schemes. A lumped description of the laser-induced energy
1333 modulation can be written as:
1334 $\delta = \delta + A \sin(k_L z), \quad (186)$
1335 where $k_L = \frac{2\pi}{\lambda_L}$ is the laser wavenumber and A is the modu-
1336 lation strength. After the modulation, the particle state vector
1337 evolves according to:

$$1338 \quad \mathbf{X}_f = \mathbf{R} \mathbf{X}_i, \quad (187)$$

1339 where \mathbf{R} is the linear 6×6 symplectic transfer matrix of the
1340 magnet lattice, which could be a single-pass one like a linear
1341 accelerator or a multi-pass one like a storage ring. In this pa-
1342 per we only consider the case that the magnet lattice is linear.
1343 Denote:

$$1344 \quad \begin{aligned} \mathbf{A} &\equiv (0, 0, 0, 0, 0, A)^T, \\ \mathbf{U}_p &\equiv (0 \ 0 \ 0 \ pk_L \ 0), \\ \mathbf{M}_p &\equiv \mathbf{K} \mathbf{R} - \mathbf{U}_p, \end{aligned} \quad (188)$$

1345 with p being an integer. Then the final FF is

$$\begin{aligned} 1346 \quad \mathcal{F}(\mathbf{K}) &= \int \psi_f(\mathbf{X}) e^{-i\mathbf{K}\mathbf{X}} d\mathbf{X} \\ &= \int \psi_{m+}(\mathbf{X}) e^{-i\mathbf{K}\mathbf{R}\mathbf{X}} d\mathbf{X} \\ &= \int \psi_0(\mathbf{X}) e^{-i(\mathbf{K}\mathbf{R}\mathbf{X} + \mathbf{K}\mathbf{R}\mathbf{A} \sin(k_L z))} d\mathbf{X} \\ &= \sum_{p=-\infty}^{\infty} J_p(-\mathbf{K}\mathbf{R}\mathbf{A}) \int \psi_0(\mathbf{X}) e^{-i(\mathbf{K}\mathbf{R}\mathbf{X} - pk_L z)} d\mathbf{X} \\ &= \sum_{p=-\infty}^{\infty} J_p(-\mathbf{K}\mathbf{R}\mathbf{A}) \int \psi_0(\mathbf{X}) e^{-i\mathbf{M}_p \mathbf{X}} d\mathbf{X} \\ &= \sum_{p=-\infty}^{\infty} J_p(-\mathbf{K}\mathbf{R}\mathbf{A}) \mathcal{F}_0(\mathbf{M}_p), \end{aligned} \quad (189)$$

1347 where $\psi_0(\mathbf{X})$, $\psi_{m+}(\mathbf{X})$, and $\psi_f(\mathbf{X})$ mean the beam distri-
1348 bution at the beginning, right after the energy modulation
1349 and the final point, respectively. J_p is the p -th order Bessel
1350 function of the first kind. Jacobi-Anger identity $e^{ix \sin y} =$
1351 $\sum_{n=-\infty}^{\infty} e^{iny} J_n[x]$ has been used in the above derivation.
1352 Note that we have also used the fact that for a symplectic
1353 matrix \mathbf{R} we have $\text{Det}(\mathbf{R}) = 1$. $\mathcal{F}_0(\mathbf{K})$ is the initial FF.

1354 The above formula is general and applies for arbitrary ini-
1355 tial beam distribution. If the initial beam distribution is Gaus-
1356 sian in 6D phase space:

$$\psi_0(\mathbf{X}) = \frac{1}{(2\pi)^3 \sqrt{\text{Det}(\Sigma_0)}} \exp\left(-\frac{1}{2} \mathbf{X}^T \Sigma_0^{-1} \mathbf{X}\right) \quad (190)$$

with Σ_0 being the initial second moments of the beam, the initial FF is then

$$\mathcal{F}_0(\mathbf{K}) = \exp\left(-\frac{\mathbf{K} \Sigma_0 \mathbf{K}^T}{2}\right). \quad (191)$$

The final FF is then

$$\mathcal{F}(\mathbf{K}) = \sum_{p=-\infty}^{\infty} J_p(-\mathbf{KRA}) \exp\left(-\frac{\mathbf{M}_p \Sigma_0 \mathbf{M}_p^T}{2}\right), \quad (192)$$

1362

2. HGHG

In many applications, the classical 1D bunching factor suffices. With $\mathbf{K} = (0 \ 0 \ 0 \ 0 \ k_z \ 0)$, then

$$\mathbf{KRA} = k_z R_{56} A,$$

$$\mathbf{M}_p = k_z \left(R_{51} \ R_{52} \ R_{53} \ R_{54} \ R_{55} - \frac{p k_L}{k_z} \ R_{56} \right). \quad (193)$$

If further $R_{51} = 0$, $R_{52} = 0$, $R_{53} = 0$, $R_{54} = 0$ and $R_{55} = 1$, and the initial beam is transverse-longitudinal decoupled and upright in the longitudinal phase space, which corresponds to the case of high-gain harmonic-generation (HGHG) [35], then

$$b(k_z) = \sum_{p=-\infty}^{\infty} J_p(-k_z R_{56} A) \exp\left(-\frac{k_z^2}{2} \left[\left(1 - \frac{p k_L}{k_z}\right)^2 \sigma_{z0}^2 + (R_{56} \sigma_{\delta0})^2 \right]\right), \quad (194)$$

1372

where σ_{z0} and $\sigma_{\delta0}$ are the initial RMS bunch length and energy spread, respectively. If the initial bunch length is much longer than the laser wavelength, i.e., $k_L \sigma_{z0} \gg 1$, the above exponential terms will be non-zero only when $k_z = p k_L$, which means there is only bunching at the laser harmonics.

In this case, we have the bunching factor at the n -th (n being integer) laser harmonic

$$b_n = b(k_z = n k_L)$$

$$= J_n(-n k_L R_{56} A) \exp\left[-\frac{(n k_L R_{56} \sigma_{\delta0})^2}{2}\right]. \quad (195)$$

1380
1381 For $n > 4$, the maximal value of the Bessel function J_n is about $0.67/n^{1/3}$ and is achieved when its argument is equal to $n + 0.81n^{1/3}$. For large n , this argument corresponds to $k_L R_{56} A \sim 1$. Then to make sure the exponential term in Eq. (195) not too small, we need $A \sim n \sigma_{\delta0}$. So generally if we want to realize n -th harmonic bunching in HGHG, we need an energy modulation strength a factor of n larger than the initial energy spread.

1389

3. TLC-based Microbunching

1390 Now let us consider the case of nonzero $R_{51,52,53,54}$, which corresponds to transverse-longitudinal coupling (TLC)-based 1391 microbunching. Below we use y - z coupling as an example 1392 for the analysis and ignore the x -dimension. The analysis for 1393 x - z coupling is similar. If $\mathbf{K} \equiv (0 \ 0 \ 0 \ 0 \ k_z \ 0)$, $R_{51} = 0$, 1394 $R_{52} = 0$, $R_{55} = 1$, $R_{66} = 1$, then 1395

$$\mathbf{KRA} = k_z R_{56} A,$$

$$\mathbf{M}_p = k_z \left(0 \ 0 \ R_{53} \ R_{54} \ 1 - \frac{p k_L}{k_z} \ R_{56} \right). \quad (196)$$

1396
1397 Using the real and imaginary generalized beta functions and 1398 Twiss matrices introduced in Sec. II, the bunching factor at 1399 the n -th laser harmonic can be expressed as

$$b_n = \sum_{p=-\infty}^{\infty} J_p(-n k_L R_{56} A) \exp\left[-\frac{(\epsilon_{II} \mathbf{M}_p \mathbf{T}_{II} \mathbf{M}_p^T + \epsilon_{III} \mathbf{M}_p \mathbf{T}_{III} \mathbf{M}_p^T)}{2}\right], \quad (197)$$

1401 where $\mathbf{T}_{II,III}$ are the real generalized Twiss matrices right before the modulation. We then require

$$\mathbf{M}_p \mathbf{T}_{III} \mathbf{M}_p^T \Big|_{p=n} = (n k_L)^2 (\mathbf{R} \mathbf{T}_{III} \mathbf{R}^T - 2 \mathbf{R} \mathbf{T}_{III} + \mathbf{T}_{III})_{55} = 0. \quad (198)$$

1403 The physical reason of this requirement is that for $p = n$, we want the longitudinal emittance does not contribute to the bunching 1404 factor. By doing this, the bunching factor will be mainly determined by the vertical emittance, which is assumed to be a small 1405 value. Therefore, we can realize high harmonic bunching with a shallow energy modulation strength A . The above relation can 1406 be written more specifically using the generalized beta functions and the matrix terms of \mathbf{R} as

$$R_{53}^2 \beta_{33}^{III} + R_{54}^2 \beta_{44}^{III} + R_{56}^2 \beta_{66}^{III} + 2 R_{53} R_{54} \beta_{34}^{III} + 2 R_{53} R_{56} \beta_{36}^{III} + 2 R_{54} R_{56} \beta_{46}^{III} = 0. \quad (199)$$

1408 If the generalized Twiss matrices of the eigenmode II and III right before the modulation are given by Eq. (51), and further 1409 assuming that at the modulation point we have $D_x = 0$ and $D'_x = 0$, then Eq. (199) can be casted into

$$R_{53} D_y + R_{54} D'_y + R_{56} = 0. \quad (200)$$

1410

¹⁴¹¹ This relation means that the final coordinate z does not depend on the initial energy deviation δ in linear approximation. Under
¹⁴¹² the above condition, we have

$$\mathbf{M}_p \mathbf{T}_{III} \mathbf{M}_p^T = (nk_L)^2 \left(1 - \frac{p}{n}\right)^2 \beta_{z\mathbf{M}}, \quad (201)$$

¹⁴¹⁴ and

$$\mathbf{M}_p \mathbf{T}_{II} \mathbf{M}_p^T = (nk_L)^2 \left[\mathcal{H}_{yR} + \left(1 - \frac{p}{n}\right)^2 \mathcal{H}_{yM} + 2 \left(1 - \frac{p}{n}\right) (\gamma_y R_{54} D_y - \alpha_y R_{53} D_y + \alpha_y R_{54} D'_y - \beta_y R_{53} D'_y) \right]. \quad (202)$$

¹⁴¹⁵ Then the bunching factor at the n -th laser harmonic at the final point which in our context means the radiator is
¹⁴¹⁶

$$\begin{aligned} b_n &= \sum_{p=-\infty}^{\infty} J_p (-nk_L R_{56} A) \exp \left[-\frac{(nk_L)^2}{2} \epsilon_y \mathcal{H}_{yR} \right] \exp \left[-\frac{k_L^2}{2} (n-p)^2 (\epsilon_y \mathcal{H}_{yM} + \epsilon_z \beta_{z\mathbf{M}}) \right] \\ &\quad \exp \left[-\frac{k_L^2}{2} 2n(n-p) \epsilon_y (\gamma_y R_{54} D_y - \alpha_y R_{53} D_y + \alpha_y R_{54} D'_y - \beta_y R_{53} D'_y) \right]. \end{aligned} \quad (203)$$

¹⁴¹⁸ Here we remind the readers that there is an extra factor in ¹⁴⁴³ wavelength, then there is only one term non-vanishing in the
¹⁴¹⁹ Eq. (203) compared to the result in our previous publications ¹⁴⁴⁴ above summation, i.e., the term with $p = n$. Then
¹⁴²⁰ in Refs. [17, 33], i.e.,

$$\begin{aligned} b_n &= \sum_{p=-\infty}^{\infty} J_p (-nk_L R_{56} A) \exp \left[-\frac{(nk_L)^2}{2} \epsilon_y \mathcal{H}_{yR} \right] \quad (204) \quad \begin{aligned} & \quad b_n = J_n (-nk_L R_{56} A) \exp \left[-\frac{(nk_L)^2}{2} \epsilon_y \mathcal{H}_{yR} \right]. \quad (206) \\ & \quad \text{Here we make a short comment that our derivation of} \\ & \quad \text{bunching factor } \text{here}, \text{ and also most of that found in literature,} \\ & \quad \text{neglects the collective interactions between the electron beam} \\ & \quad \text{and the co-propagation electromagnetic field. Such a collec-} \\ & \quad \text{tive interaction may disturb the modulation performance. Al-} \\ & \quad \text{though not much work on this subject, the interested readers} \\ & \quad \text{may refer to a recent relevant work [40].} \end{aligned} \\ &\quad \exp \left[-\frac{k_L^2}{2} (n-p)^2 (\epsilon_y \mathcal{H}_{yM} + \epsilon_z \beta_{z\mathbf{M}}) \right]. \end{aligned}$$

¹⁴²² We conclude that the Eq. (203) here is rigorously more accu-
¹⁴²³ rate.

¹⁴²⁴ If the modulation waveform is linear, according to
¹⁴²⁵ Eq. (158), the RMS bunch length at the modulator and ra-
¹⁴²⁶ diator are given by

$$\begin{aligned} \sigma_{z\mathbf{M}}^2 &= \epsilon_z \beta_{z\mathbf{M}} + \epsilon_y \mathcal{H}_{yM}, \\ \sigma_{zR}^2 &= \epsilon_y \mathcal{H}_{yR}. \end{aligned} \quad (205)$$

¹⁴²⁷ So in this paper, we call $\sigma_{zR} = \sqrt{\epsilon_y \mathcal{H}_{yR}}$ the linear bunch

¹⁴²⁹ length at the radiator. We have proven in last section there is

¹⁴³⁰ a fundamental inequality dictating the energy chirp strength

¹⁴³¹ h and \mathcal{H}_y at the modulator and radiator, respectively, i.e.,
¹⁴³² $h^2 \mathcal{H}_{yM} \mathcal{H}_{yR} \geq 1$. Basically, given the vertical emittance and

¹⁴³³ desired σ_{zR} , to lower the energy chirp strength, we need to
¹⁴³⁴ lengthen the bunch at the modulator. If the initial bunch is
¹⁴³⁵ shorter than the modulation laser wavelength, considering the
¹⁴³⁶ actual laser modulation waveform is sinusoidal, then accord-
¹⁴³⁷ ing to Eq. (203), a bunch lengthening at the modulator means
¹⁴³⁸ a bunching factor drop at the radiator as can be seen from the
¹⁴³⁹ second exponential term. For more discussions on this point,
¹⁴⁴⁰ the readers are referred to Refs. [17, 33].

¹⁴⁴¹ When $k_L^2 (\epsilon_y \mathcal{H}_{yM} + \epsilon_z \beta_{z\mathbf{M}}) \gg 1$ which means the bunch
¹⁴⁴² length at the modulation point is much longer than the laser

B. Modulation Strength

¹⁴⁴⁵ After deriving the bunching factor, now we derive the for-
¹⁴⁴⁶ mula of modulation strength, given the laser, electron and un-
¹⁴⁴⁷ dulator parameters. This is a necessary work for quantitative

I. A Normally Incident Laser

¹⁴⁴⁸ The most common method of imprinting energy modula-
¹⁴⁴⁹ tion on an electron beam at the laser wavelength is to use a
¹⁴⁵⁰ TEM00 mode laser to resonate with the electrons in an undu-
¹⁴⁵¹ lator. Below we use a planar undulator as the modulator. A
¹⁴⁵² helical undulator can also be applied for energy modulation,
¹⁴⁵³ but since we want to preserve the ultrasmall vertical emit-
¹⁴⁵⁴ tance, we need to avoid $x-y$ coupling as much as possible,
¹⁴⁵⁵ and thus a planar undulator might be preferred. The electro-
¹⁴⁵⁶ magnetic field of a TEM00 mode Gaussian laser polarized in
¹⁴⁵⁷ the horizontal plane is [36]

1469

$$\begin{pmatrix} E_x \\ E_y \\ E_z \\ cB_x \\ cB_y \\ cB_z \end{pmatrix} = E_{x0} e^{ik_L s - i\omega_L t + i\phi_0} (-iZ_R Q) \exp \left[i \frac{k_L Q}{2} (x^2 + y^2) \right] \begin{pmatrix} 1 \\ 0 \\ -Qx \\ -Q^2 xy \\ Q^2 x^2 - \frac{iQ}{k_L} + 1 \\ -Qy \end{pmatrix}, \quad (207)$$

1470 where $E_{x,y,z}$ and $B_{x,y,z}$ are the horizontal, vertical and longitudinal electric and magnetic field, respectively, s is the longitudinal global path length variable, t is the time variable, c is the speed of light in free space, $\omega_L = k_L c$, $Z_R = \pi w_0^2 / \lambda_L$ is the Rayleigh length, w_0 the beam waist radius, and

1475

$$Q = \frac{i}{Z_R \left(1 + i \frac{s}{Z_R} \right)} \quad (208)$$

1476 with i here being the imaginary unit. We remind the readers
1477 that it has been implicitly assumed that all the fields will take
1478 the real part of their complex expressions.

1479 The relationship between the peak electric field E_{x0} and
1480 the laser peak power P_L is given by

1481

$$P_L = \frac{E_{x0}^2 Z_R \lambda_L}{4 Z_0}, \quad (209)$$

1482 in which $Z_0 = 376.73 \Omega$ is the impedance of free space. The
1483 prescribed wiggling motion of electron in a planar undulator
1484 is

1485

$$x(s) = \frac{K}{\gamma k_u} \sin(k_u s),$$

1486 with γ being the Lorentz factor,

1487

$$K = \frac{e B_0 \lambda_u}{2 \pi m_e c} = 0.934 \cdot B_0 [\text{T}] \cdot \lambda_u [\text{cm}] \quad (211)$$

1488 being the dimensionless undulator parameter, where B_0 is the peak magnetic field, λ_u is the undulator period, and $k_u = 2\pi/\lambda_u$ being the undulator wavenumber. The resonant condition of laser-electron interaction inside a planar undulator is

1493

$$\lambda_L = \frac{1 + \frac{K^2}{2}}{2\gamma^2} \lambda_u. \quad (212)$$

1494 From the prescribed motion we can calculate the electron horizontal and longitudinal velocity

1496

$$v_x(s) \approx \frac{\beta c K}{\gamma} \cos(k_u s),$$

$$v_z(s) = \sqrt{v^2 - v_x^2} \approx \bar{v}_z - \frac{c K^2}{4\gamma^2} \cos(2k_u s), \quad (213)$$

1497 with $\beta = \sqrt{1 - \frac{1}{\gamma^2}}$, and
1498 the average longitudinal velocity of electron in the undulator.
1499 Therefore, we have the longitudinal path length of electron as
1500 a function of time given by

$$\bar{v}_z = c \left(1 - \frac{1 + K^2/2}{2\gamma^2} \right) \quad (214)$$

1501 Then
1502

$$s(t) \approx \bar{v}_z t - \frac{K^2}{8\gamma^2 k_u} \sin(2k_u \bar{v}_z t). \quad (215)$$

$$k_L s - \omega_L t \approx -k_u s - \chi \sin(2k_u s), \quad (216)$$

1503 where
1504

$$\chi = \frac{K^2 k_L}{8\gamma^2 k_u} = \frac{K^2}{4 + 2K^2}. \quad (217)$$

1505 Note that since the longitudinal coordinate of electron will
1506 affect the laser phase observed, so we need to calculate its
1507 precision to the order of $\frac{1}{\gamma^2}$, while for the horizontal coordinate
1508 x , we only need to calculate it to the order of $\frac{1}{\gamma}$. In the
1509 following, we will adopt the approximation $\beta \approx 1$ since we
1510 are interested in relativistic cases.

1511 Given the electron prescribed motion and laser electric
1512 field, the laser and electron exchange energy according to
1513
1514

$$\frac{d\mathcal{W}}{dt} = -(ev_x E_x + ev_z E_z), \quad (218)$$

1515 where \mathcal{W} is the work done on the electron by the laser, or
1516 the energy transfer from the laser to the electron. Note that
1517 in this manuscript e represents the elementary charge and is
1518 assumed to be positive. Assuming that the laser beam waist is
1519 in the middle of the undulator, whose length is L_u , and when
1520 the electron transverse coordinates are much smaller than the
1521 laser beam waist $x, y \ll w_0$, which is true in most of the cases
1522 under consideration, we drop the factor $\exp[i \frac{k_L Q}{2} (x^2 + y^2)]$
1523 in the laser electric field. Further, when the transverse displacement
1524 of electron is much smaller than the Rayleigh length $x \ll Z_R$ which is also usually the case,
1525 we can also drop the contribution from E_z on the energy modulation. As
1526 suming the relative phase of laser field to the electron horizontal velocity
1527 v_x at the undulator center is ϕ_0 , the integrated
1528 modulation voltage induced by the laser on the electron beam
1529 in a planar undulator is then
1530

1532 $V_L \approx \text{Re} \left[\int_{-\frac{L_u}{2}}^{\frac{L_u}{2}} v_x E_x \frac{ds}{c} \right] \approx E_{x0} \frac{K}{\gamma} \text{Re} \left[e^{i\phi_0} \int_{-\frac{L_u}{2}}^{\frac{L_u}{2}} \frac{1}{1 + i \frac{s}{Z_R}} \sum_{n=-\infty}^{\infty} J_n(-\chi) e^{in2k_u s} \frac{1 + e^{-i2k_u s}}{2} ds \right], \quad (219)$

1533 where $\text{Re}()$ means taking the real component of the complex 1539 0.8 m ($N_u = 10$), $Z_R = 0.359L_u$, then the induced energy 1540 number. When $L_u \gg \lambda_u$, which means the undulator period 1541 chirp strength with $P_L = 1$ MW is $h = 955 \text{ m}^{-1}$. 1542 number $N_u \gg 1$, in the above integration, only the term with 1543 $n = 0$ and $n = 1$ will give notable non-vanishing value. 1544

1537 Denote $[JJ] \equiv J_0(\chi) - J_1(\chi)$, we then have 1541

1541

2. Dual-Tilted-Laser for Energy Modulation

1538
$$V_L = E_{x0} \frac{K}{\gamma} \frac{[JJ]}{2} \text{Re} \left[e^{i\phi_0} \int_{-\frac{L_u}{2}}^{\frac{L_u}{2}} \frac{1 - i \frac{s}{Z_R}}{1 + \left(\frac{s}{Z_R} \right)^2} ds \right] \quad (220)$$

$$= E_{x0} \frac{K}{\gamma} [JJ] Z_R \tan^{-1} \left(\frac{L_u}{2Z_R} \right) \cos \phi_0.$$

1539 We want the energy modulation strength as large as possible, 1540 so we choose $\phi_0 = 0$. Put in the expression of peak electric 1541 field from Eq. (209), the linear energy chirp strength around 1542 the zero-crossing phase is therefore

1543
$$h = \frac{eV_L}{E_0} k_L$$

$$= \frac{ek_L K [JJ]}{\gamma^2 m_e c^2} \sqrt{\frac{2P_L Z_0}{\lambda_L}} \frac{\tan^{-1} \left(\frac{L_u}{2Z_R} \right)}{\sqrt{\frac{L_u}{2Z_R}}} \sqrt{L_u}. \quad (221)$$

1544 Once the modulator length is given, we can optimize the laser 1545 Rayleigh length to maximize the energy modulation. Figure 6 1546 is a plot of $f(x) = \frac{\tan^{-1}(x)}{\sqrt{x}}$ as a function of x . The 1547 maximum value of $f(x)$ is 0.8034 and is realized when $x = 1.392$. 1548 So when $Z_R = \frac{L_u}{2 \times 1.392} = 0.359L_u$, the energy modulation 1549 reaches the maximum value. Note that when Z_R is within a 1550 small range close to the optimal value, the impact of Rayleigh 1551 length on the energy modulation strength is not very sensitive. 1552 Therefore, for easy of remembering, the optimal condition 1553 can be expressed as

1546

1554

1554

$$Z_R \approx \frac{L_u}{3}.$$

1555

1556

1557

1558

1559

1560

1561

1562

1563

1564

1565

1566

1567

1568

1569

1570

1571

1572

1573

1574

1575

1576

1577

1578

1579

1580

Now with a hope to increase the energy modulation strength with a given laser power, we may use a configuration of crossing two lasers for energy modulation. The basic idea is that if two crossing lasers can double the energy modulation strength of that of a single laser, then the effect is like that

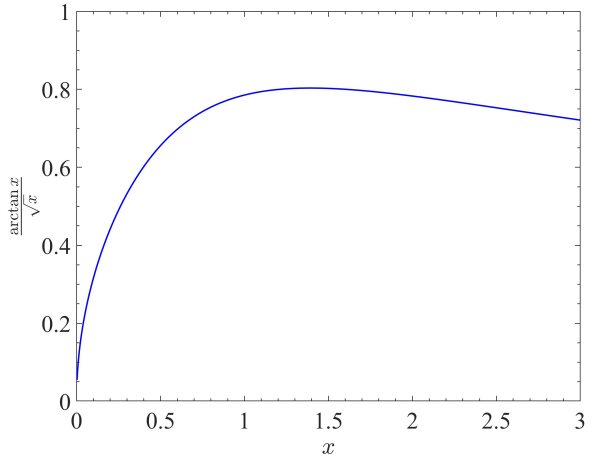


Fig. 6. $f(x) = \frac{\tan^{-1}(x)}{\sqrt{x}}$ vs. x . This curve describes the laser induced energy modulation strength as a function of the laser Rayleigh length, with the laser power and modulator length given.

Now we present the analysis. First we consider the case of two lasers crossing in the y - z plane. The laser field of an oblique TEM00 laser is given by first replacing the physical coordinate with the rotated coordinates

$$x \rightarrow x, y \rightarrow y_1 = y \cos \theta + s \sin \theta, s \rightarrow s_1 = -y \sin \theta + s \cos \theta, t \rightarrow t, \quad (223)$$

with θ in this section and below being the tilted angle of the incident laser instead of the dipole bending angle in Sec. III. We hope their difference is clear from context. The resulting field expression according to Eq. (207) is

1584

$$\begin{pmatrix} E_x \\ E_y \\ E_z \\ cB_x \\ cB_y \\ cB_z \end{pmatrix}_{\text{rot}} = E_{x0} e^{ik_L s_1 - i\omega_L t} \frac{\exp \left[-\frac{k_L(x^2 + y_1^2)}{2(Z_R + is_1)} \right]}{1 + i \frac{s_1}{Z_R}} \begin{pmatrix} 1 \\ 0 \\ -i \frac{x}{Z_R + is_1} \\ \frac{x y_1}{(Z_R + is_1)^2} \\ -\frac{x^2}{(Z_R + is_1)^2} - \frac{1}{k_L(Z_R + is_1)} + 1 \\ -i \frac{y_1}{Z_R + is_1} \end{pmatrix}. \quad (224)$$

1585 Note however, in the above expression, x, y, s of the electromagnetic fields are defined according to the oblique laser propagating direction. To get the expression back in the original coordinate system, i.e., undulator axis as the z axis, we need to rotate 1586 the laser field as,

1588

$$E_x \rightarrow E_{x\text{rot}}, E_y \rightarrow E_y = E_{y\text{rot}} \cos \theta - E_{z\text{rot}} \sin \theta, E_z \rightarrow E_z = E_{y\text{rot}} \sin \theta + E_{z\text{rot}} \cos \theta, t \rightarrow t, \quad (225)$$

1589 and for the electric field the result is

1590

$$\begin{pmatrix} E_x \\ E_y \\ E_z \end{pmatrix}_{\text{unrot}} = E_{x0} e^{ik_L s_1 - i\omega_L t} \frac{\exp \left[-\frac{k_L(x^2 + y_1^2)}{2(Z_R + is_1)} \right]}{1 + i \frac{s_1}{Z_R}} \begin{pmatrix} 1 \\ -i \frac{x}{Z_R + is_1} \sin \theta \\ -i \frac{x}{Z_R + is_1} \cos \theta \end{pmatrix}. \quad (226)$$

1591 Assuming that the two crossing lasers are in-phase and have the same amplitude. In addition, we assume that $\theta_2 = -\theta_1 = -\theta$, 1592 and the two lasers have the same Rayleigh length. Then the superimposed field is

1593

$$\begin{pmatrix} E_x \\ E_y \\ E_z \end{pmatrix}_{\text{unrot}} = E_{x0} e^{ik_L(-y \sin \theta + s \cos \theta) - i\omega_L t} \frac{\exp \left[-\frac{k_L(x^2 + (y \cos \theta + s \sin \theta)^2)}{2(Z_R + i(-y \sin \theta + s \cos \theta))} \right]}{1 + i \frac{(-y \sin \theta + s \cos \theta)}{Z_R}} \begin{pmatrix} 1 \\ -i \frac{x}{Z_R + i(-y \sin \theta + s \cos \theta)} \sin \theta \\ -i \frac{x}{Z_R + i(-y \sin \theta + s \cos \theta)} \cos \theta \end{pmatrix} + E_{x0} e^{ik_L(y \sin \theta + s \cos \theta) - i\omega_L t} \frac{\exp \left[-\frac{k_L(x^2 + (y \cos \theta - s \sin \theta)^2)}{2(Z_R + i(y \sin \theta + s \cos \theta))} \right]}{1 + i \frac{(y \sin \theta + s \cos \theta)}{Z_R}} \begin{pmatrix} 1 \\ i \frac{x}{Z_R + i(y \sin \theta + s \cos \theta)} \sin \theta \\ -i \frac{x}{Z_R + i(y \sin \theta + s \cos \theta)} \cos \theta \end{pmatrix}. \quad (227)$$

]

1594 As before here we focus on the impact of E_x on laser-electron 1610 or
1595 interaction, and ignore the contribution from E_z . When θ is
1596 very small, the superimposed E_x can be approximated as

1611

$$E_x = 2E_{x0} \frac{\exp \left[ik_L s \cos \theta - i\omega t - \frac{k_L(x^2 + s^2 \sin^2 \theta)}{2(Z_R + is \cos \theta)} \right]}{1 + i \frac{is \cos \theta}{Z_R}} \approx 2E_{x0} e^{ik_L s \cos \theta - i\omega_L t} \frac{\exp \left[-\frac{k_L s^2 \theta^2}{2(Z_R + is)} \right]}{1 + i \frac{s}{Z_R}}. \quad (228)$$

1597

1598 Note that in the final approximated expression, we have kept 1614 Note that χ now depends on θ , more specifically,

1599 $s \cos \theta$ in the laser phase term. The reason is that the laser

1600 phase is of key importance in laser-electron interaction and

1601 the accuracy requirement is high. In addition, we have also

1602 kept the $s^2 \theta^2$ in the intensity decay term, this is because $L_u \theta$

1603 may not be small compared to the laser beam waist radius w_0 .

1604 Assume that the laser beam waists are in the middle of the

1605 The expression of E_x for the case of crossing in x - z plane

1606 is similar. So the difference of crossing in x - z plane and y - z

1607 plane is not much in inducing energy modulation.

1608 For effective laser-electron interaction, the off-axis reso-

1609 nance condition now is

1610

$$c \frac{\lambda_u}{v_z} - \lambda_u \cos \theta = \lambda_L, \quad (229)$$

1611 the integrated modulation voltage induced by the DTL in a
1612 planar undulator is then

1613

$$\chi = \frac{K^2 k_L}{8\gamma^2 k_u} \approx \frac{K^2}{4 + 2K^2 + 4\gamma^2 \theta^2}. \quad (232)$$

1614

$$v \equiv \frac{k_L Z_R \theta^2}{2} = \left(\frac{Z_R \theta}{w_0} \right)^2, \quad (233)$$

1615

1616

1617

1618

1619

1620

$$\begin{aligned}
V_L &\approx \operatorname{Re} \left[\int_{-\frac{L_u}{2}}^{\frac{L_u}{2}} v_x E_x \frac{ds}{c} \right] \\
&\approx E_{x0} \frac{K[JJ]}{\gamma} Z_R \int_{-\frac{L_u}{2Z_R}}^{\frac{L_u}{2Z_R}} \frac{\exp \left(-v \frac{u^2}{1+u^2} \right)}{1+u^2} \left[\cos \left(v \frac{u^3}{1+u^2} \right) + u \sin \left(v \frac{u^3}{1+u^2} \right) \right] du \cos \phi_0.
\end{aligned} \tag{234}$$

To maximize the energy modulation, we choose $\phi_0 = 0$. Put in the expression of E_{x0} from Eq. (209), the linear energy chirp strength around the zero-crossing phase is therefore

$$h = \frac{eV_L}{E_0} k_L = \frac{ek_L K[JJ]}{\gamma^2 m_e c^2} \sqrt{\frac{2P_L Z_0}{\lambda_L}} F_{\text{DTL-E}} \left(\frac{L_u}{2Z_R}, \frac{k_L Z_R \theta^2}{2} \right) \sqrt{L_u}, \tag{235}$$

where

$$F_{\text{DTL-E}}(x, v) = \frac{1}{\sqrt{x}} \int_{-x}^x \frac{\exp \left(-v \frac{u^2}{1+u^2} \right)}{1+u^2} \left[\cos \left(v \frac{u^3}{1+u^2} \right) + u \sin \left(v \frac{u^3}{1+u^2} \right) \right] du. \tag{236}$$

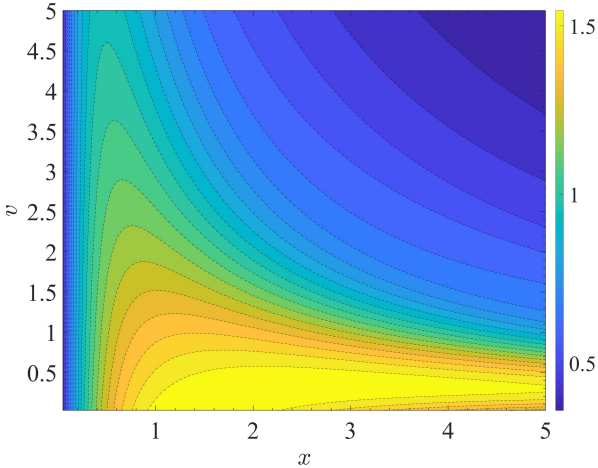


Fig. 7. Contour plot of $F_{\text{DTL-E}}(x, v)$ given by Eq. (236).

A flat contour plot of $F_{\text{DTL-E}}(x, v)$ is given in Fig. 7.

Now we can use the derived formula to calculate the energy chirp strength induced by DTL. First we consider the case of keeping λ_u fixed when changing θ , then the off-axis resonant condition leads to the undulator parameter as a function of θ given by

$$K_\theta = \sqrt{2} \sqrt{2\gamma^2 \left(1 - \frac{1}{\frac{\lambda_L}{\lambda_u} + \cos \theta} \right) - 1}. \tag{237}$$

With the increase of θ , K_θ will decrease. Note that in this case $K_\theta \propto B_{0\theta}$, so the magnetic field strength $B_{0\theta}$ also decreases with the increase of θ . An example calculation of K_θ vs. θ is given in Fig. 8. And The corresponding contour plot of the energy chirp strength normalized by the largest energy chirp induced by a single normally incident laser, vs. θ and Z_R/L_u , is given in Fig. 9.

The previous calculation assumes λ_u is kept unchanged

when we adjust the incident angle θ . This will result in a limited region of θ to fulfill the resonant condition as shown in Fig. 8. Now we conduct the calculation by assuming the peak magnetic field B_0 unchanged when we adjust θ . Put the expression of undulator parameter Eq. (211) in the off-axis resonant condition Eq. (230), we have

$$\frac{1}{2} \left(\frac{eB_0}{2\pi m_e c} \right)^2 \lambda_u^3 + (1 + \gamma^2 \theta^2) \lambda_u - 2\gamma^2 \lambda_L = 0, \tag{238}$$

from which we get

$$\lambda_u = \frac{2\pi^{2/3} \sqrt[3]{\mathcal{D}}}{3^{2/3} B_0^2 e^2} - \frac{4\pi^{4/3} c^2 (\gamma^2 \theta^2 + 1) m_e^2}{\sqrt[3]{3} \sqrt[3]{\mathcal{D}}}, \tag{239}$$

with

$$\begin{aligned}
\mathcal{D} = & \sqrt{3B_0^6 c^4 e^6 m_e^4 \left(27B_0^2 \gamma^4 e^2 \lambda_L^2 + 8\pi^2 c^2 (\gamma^2 \theta^2 + 1)^3 m_e^2 \right)} \\
& + 9B_0^4 c^2 \gamma^2 e^4 m_e^2 \lambda_L.
\end{aligned} \tag{240}$$

For example, if $\lambda_L = 1064$ nm and $B_0 = 1.2$ T, then λ_u as a function of θ for the case of $E_0 = 600$ MeV is shown in Fig. 10. Note that in this case $K_\theta \propto \lambda_u$ which depends on θ , so the undulator parameter also decreases with the increase of θ . But the decrease is not that fast compared to that presented in Fig. 8. And The corresponding contour plot of the energy chirp strength induced by DTL normalized by the largest energy chirp induced by a single normally incident laser, vs. θ and Z_R/L_u , is given in Fig. 11.

As can be seen from the calculation results in Figs. 9 and 11, DTL indeed can induce a larger energy modulation compared to a single normally incident laser. But the required crossing angle (less than 2 mrad) is too small for engineering. So the usual setup of a single normally incident TEM00 mode laser is still the preferred choice in practical application.

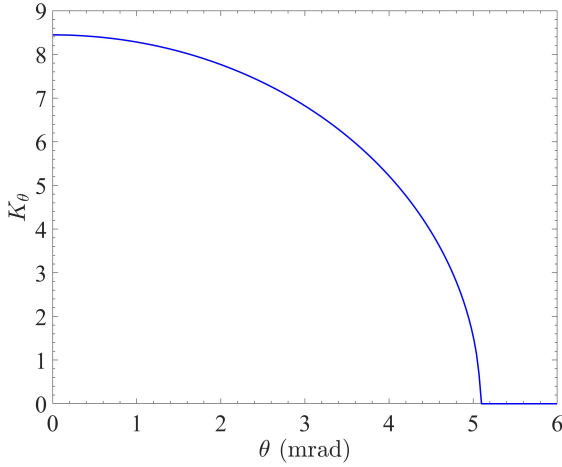


Fig. 8. Undulator parameter K_θ vs. θ with λ_u kept fixed. Parameters used: $E_0 = 600$ MeV, $\lambda_L = 1064$ nm, $\lambda_u = 8$ cm.

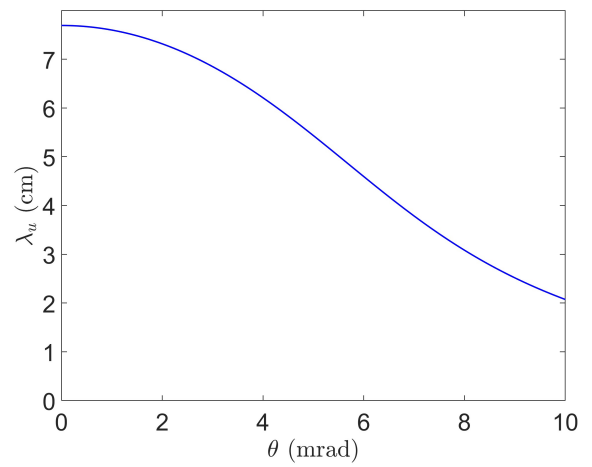


Fig. 10. λ_u vs. θ , with B_0 kept fixed. Parameters used: $E_0 = 600$ MeV, $\lambda_L = 1064$ nm, $B_0 = 1.2$ T.

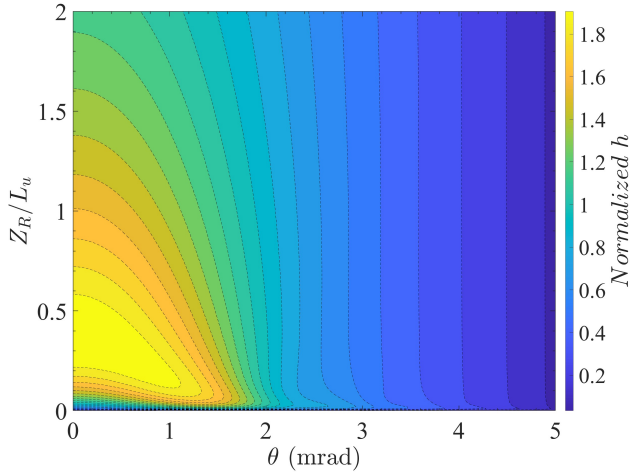


Fig. 9. Energy chirp strength h normalized by the largest energy chirp induced by a single normally incident laser, vs. θ and Z_R/L_u . Keep λ_u fixed when changing θ . Parameters used: $E_0 = 600$ MeV, $\lambda_L = 1064$ nm, $\lambda_u = 0.08$ m, $N_u = 10$, $L_u = 0.8$ m.

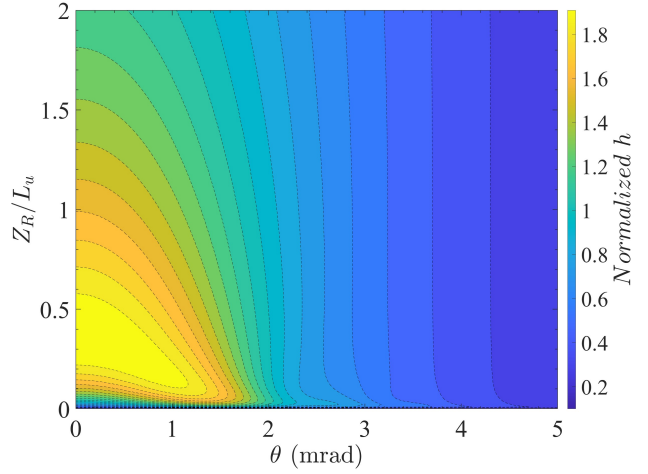


Fig. 11. Energy chirp strength h normalized by the largest energy chirp induced by a single normally incident laser, vs. θ and Z_R/L_u . Keep B_0 fixed when changing θ . Parameters used: $E_0 = 600$ MeV, $\lambda_L = 1064$ nm, $B_0 = 1.2$ T, $L_u = 0.8$ m.

1668

C. Realization Examples

1669 After the derivation of bunching factor and laser-induced
1670 modulation strengths, finally in this section we give some re-
1671 alization examples of microbunching schemes belonging to
1672 what we have analyzed. FEL seeding technique like phase-
1673 merging enhanced harmonic generation (PEHG) [37, 38], and
1674 angular dispersion-induced microbunching (ADM) [39] can
1675 be viewed as specific examples of our general definition of
1676 TLC-based microbunching schemes in Theorem One. More
1677 detailed discussion in this respect has been presented before
1678 in Ref. [33].

1679 Here we make a short comment about the relation between
1680 FEL seeding techniques like HGHG, PEHG, ADM and the
1681 storage ring schemes like LSF, GLSF discussed in this pa-
1682
1683
1684
1685
1686
1687
1688
1689
1690

per. One is single-pass, and the other is multi-pass. One in-
volves matrix multiplication or nonlinear transfer map once,
and the other invokes eigen analysis or normal form analy-
sis of the one-turn map. What they share is the bunch com-
pression or harmonic generation mechanism. The relation
between HGHG and LSF is similar to the relation between
PEHG/ADM and GLSF.

VII. ANGULAR MODULATION-BASED COUPLING SCHEMES

A. Bunching Factor

After investigating the energy modulation-based TLC mi-

1693 crobunching schemes, now in this section we discuss angular modulation-based ones. The problem definition is similar to that in the energy modulation-based schemes, only replacing the energy modulation by angular modulation. We use y' modulation as an example, since we will take advantage of the ultrasmall vertical emittance in a planar ring as explained before. The lumped laser-induced angular modulation is modelled as:

$$y' = y' + A \sin(k_L z), \\ \delta = \delta + Ak_L y \cos(k_L z).$$

$$\frac{\partial \Delta y'}{\partial z} = \frac{\partial \Delta \delta}{\partial y}. \quad (242)$$

1701 Following the derivations in the section of energy 1702 Note that we need to add the second equation above to make 1703 the above modulation symplectic. Such an angular modulation process also satisfies the Panofsky-Wenzel theorem [41] 1704 to that in the energy modulation-based schemes, the final form function in 1705 this case is

$$1709 \begin{aligned} \mathcal{F}(\mathbf{K}) &= \int \psi_f(\mathbf{X}) e^{-i\mathbf{K}\mathbf{X}} d\mathbf{X} \\ &= \int \psi_{m+}(\mathbf{X}) e^{-i\mathbf{K}\mathbf{R}\mathbf{X}} d\mathbf{X} \\ &= \int \psi_0(\mathbf{X}) e^{-i(\mathbf{K}\mathbf{R}\mathbf{X} + \mathbf{K}\mathbf{R}_{i4}A \sin(k_L z) + \mathbf{K}\mathbf{R}_{i6}Ak_L y \cos(k_L z))} d\mathbf{X} \\ &= \sum_{p_1=-\infty}^{\infty} J_{p_1}(-\mathbf{K}\mathbf{R}_{i4}A) \int \psi_0(\mathbf{X}) e^{-i(\mathbf{K}\mathbf{R}\mathbf{X} - p_1 k_L z + \mathbf{K}\mathbf{R}_{i6}Ak_L y \cos(k_L z))} d\mathbf{X} \\ &= \sum_{p_1=-\infty}^{\infty} J_{p_1}(-\mathbf{K}\mathbf{R}_{i4}A) \int \psi_0(\mathbf{X}) \sum_{p_2=-\infty}^{\infty} i^{p_2} J_{p_2}(-\mathbf{K}\mathbf{R}_{i6}Ak_L y) e^{-i[\mathbf{K}\mathbf{R}\mathbf{X} - (p_1 + p_2)k_L z]} d\mathbf{X}. \end{aligned} \quad (243)$$

1710 The integration of the above result is given by generalized hypergeometric function. If $\mathbf{K} = (0 \ 0 \ 0 \ 0 \ k_z \ 0)$ and $R_{56} = 0$, 1711 then $\mathbf{K}\mathbf{R}_{i6} = 0$, and the initial beam distribution is Gaussian as given in Eq. (190), then the 1D bunching factor is

$$1712 \begin{aligned} b(k_z) &= \sum_{p=-\infty}^{\infty} J_p(-\mathbf{K}\mathbf{R}_{i4}A) \int \psi_0(\mathbf{X}) e^{-i(\mathbf{K}\mathbf{R}\mathbf{X} - pk_L z)} d\mathbf{X} \\ &= \sum_{p=-\infty}^{\infty} J_p(-k_z R_{54} A) \exp\left(-\frac{\mathbf{M}_p \Sigma_0 \mathbf{M}_p^T}{2}\right), \end{aligned} \quad (244)$$

1713 with \mathbf{M}_p given by Eq. (188).

1714 To appreciate the physical principle, instead of a general mathematical analysis, we use one specific case as an example. If 1715 $R_{51} = 0$, $R_{52} = 0$, $R_{55} = 1$, $R_{56} = 0$, and the initial beam is transverse-longitudinal decoupled and has an upright distribution 1716 in the longitudinal phase space, then

$$1717 b(k_z) = \sum_{p=-\infty}^{\infty} J_p(-k_z R_{54} A) \exp\left(-\frac{k_z^2}{2} \left[\epsilon_y (R_{53}^2 \beta_y - 2R_{53} R_{54} \alpha_y + R_{54}^2 \gamma_y) + \left(1 - \frac{pk_L}{k_z}\right)^2 \sigma_{z0}^2 \right]\right), \quad (245)$$

1718 with $\alpha_y, \beta_y, \gamma_y$ being the Courant-Snyder functions before 1726 where $\mathcal{H}_{yR} = R_{53}^2 \beta_y - 2R_{53} R_{54} \alpha_y + R_{54}^2 \gamma_y$. One can apply the modulation, and $\sigma_{\delta 0}$ being the initial RMS energy spread. 1727 preciate the similarity of the above result with the bunching 1728 factor of the energy modulation-based TLC microbunching 1729 length, the above exponential terms will be non-zero only 1730 schemes, i.e., Eq. (206). The R_{54} here plays the role of R_{56} 1731 when $1 - \frac{pk_L}{k_z} = 0$, which means there is only bunching at 1732 there. If further $R_{53} = 0$, then Eq. (246) reduces to 1733 the laser harmonics. In this case, we have the bunching factor 1734 at the n -th laser harmonic to be

$$1731 b_n = J_n(-nk_L R_{54} A) \exp\left[-\frac{(nk_L R_{54} \sigma_{y'})^2}{2}\right], \quad (247)$$

$$1725 \begin{aligned} b_n &= b(k_z = nk_L) \\ &= J_n(-nk_L R_{54} A) \exp\left[-\frac{(nk_L)^2}{2} \epsilon_y \mathcal{H}_{yR}\right], \end{aligned} \quad (246)$$

1732 where $\sigma_{y'}$ is the initial RMS beam angular divergence. So 1733 R_{54} and $\sigma_{y'}$ in this scheme play the role of R_{56} and σ_{δ} in 1734 HGHG as shown in Eq. (195), respectively. In a planar un-

coupled ring, the natural vertical emittance is quite small, thus also $\sigma_{y'}$. Therefore, using this scheme we can realize a high harmonic bunching in a storage ring, for example to generate ultrashort soft X-ray pulse.

As can be seen from our analysis, both the energy modulation-based and the angular modulation-based TLC microbunching schemes share the same spirit, i.e., to take advantage of the small transverse emittance, the vertical emittance in our case, to generate microbunching with a shallow modulation strength. These TLC-based microbunching schemes can be viewed as partial transverse-longitudinal emittance exchanges at the optical laser wavelength range. They do not necessarily need to be a complete emittance exchanges since for microbunching, the most important coordinate is z , and δ is relatively less important. As we will show soon, although the spirit is the same, given the same level of modulation laser power, the physical realization of energy modulation-based

TLC microbunching schemes turn out to be more effective for our SSMB application compared to the angular modulation-based schemes.

B. Modulation Strength

I. TEM01 Mode Laser-Induced Angular Modulation

After deriving the bunching factor, now we derive the laser-induced angular modulation strength for quantitative evaluation. We start with the usual angular modulation proposal by applying a TEM01 mode laser in an undulator [42]. The electric field of a Hermite-Gaussian TEM01 mode laser polarized in the horizontal plane is [36]

$$\begin{pmatrix} E_x \\ E_y \\ E_z \\ cB_x \\ cB_y \\ cB_z \end{pmatrix} = E_{x0} e^{ik_L s - i\omega_L t} (-iZ_R Q)^2 \exp \left[i \frac{k_L Q}{2} (x^2 + y^2) \right] \left(\frac{2\sqrt{2}}{w_0} \right) \begin{pmatrix} y \\ 0 \\ -Qxy \\ i \frac{Qx}{k_L} - Q^2 xy^2 \\ \left(Q^2 x^2 - \frac{iQ}{k_L} + 1 \right) y \\ \frac{i}{k_L} - Qy^2 \end{pmatrix}. \quad (248)$$

The relation between E_{x0} and the laser peak power for a TEM01 mode laser is given by

$$P_L = \frac{E_{x0}^2 Z_R \lambda_L}{2 Z_0}. \quad (249)$$

Note there is a factor of two difference in the above laser power formula compared to the case of a TEM00 mode laser. The electron wiggles in a horizontal planar undulator according to Eq. (210), and the laser-electron exchanges energy according to Eq. (218). Making the same assumption and following similar procedures as before, we can get the integrated modulation voltage induced by a TEM01 mode laser in the undulator

$$\begin{aligned} V_L &= \operatorname{Re} \left[E_{x0} \frac{K}{\gamma} e^{i\phi_0} \frac{[JJ]}{2} \frac{2\sqrt{2}}{w_0} y \int_{-\frac{L_u}{2}}^{\frac{L_u}{2}} \frac{1}{\left(1 + i \frac{s}{Z_R} \right)^2} ds \right] \\ &= E_{x0} \frac{K [JJ]}{\gamma} \frac{2\sqrt{2}}{w_0} y Z_R \frac{\frac{L_u}{2Z_R}}{1 + \left(\frac{L_u}{2Z_R} \right)^2} \cos \phi_0. \end{aligned} \quad (250)$$

We will choose $\phi_0 = 0$ to maximize the modulation voltage. Put in the expression of E_{x0} from Eq. (249) and $w_0 = \sqrt{\frac{Z_R \lambda_L}{\pi}}$ we have

$$V_L = \frac{4K [JJ]}{\gamma} \frac{\sqrt{\pi P_L Z_0}}{\lambda_L} \frac{\frac{L_u}{2Z_R}}{1 + \left(\frac{L_u}{2Z_R} \right)^2} y. \quad (251)$$

The induced energy modulation strength with respect to y around the zero-crossing phase is then

$$g = \frac{\partial \left(\frac{eV_L}{E_0} \right)}{\partial y} = \frac{2ek_L K [JJ]}{\gamma^2 m_e c^2} \sqrt{\frac{P_L Z_0}{\pi}} \frac{\frac{L_u}{2Z_R}}{1 + \left(\frac{L_u}{2Z_R} \right)^2}. \quad (252)$$

The symplecticity of the dynamical system will require that this formula also gives the linear angular chirp strength around the zero-crossing phase. It is interesting to note that, given the laser power, the modulation kick strength depends on the ratio between Z_R and L_u , instead of their absolute values.

One may wonder that when $\frac{L_u}{2Z_R}$ is fixed, the induced angular chirp strength is independent of the modulator length L_u . While in a TEM00 mode laser modulator, as given in Eq. (221), we have the energy modulation strength proportional to $\sqrt{L_u}$. Mathematically this is because in the expression of a TEM01 mode laser field, there is a term $(-iZ_R Q)^2$, while in a TEM00 mode laser, this term is $(-iZ_R Q)$. Physically it means the on-axis power density of a TEM01 mode laser decays faster, compared to that of a TEM00 mode laser, when we go away from the laser waist. This may not be surprising if we keep in mind that the intensity peaks of a TEM01 mode laser are not on-axis. But we recognize there is a lower limit of the modulator length, below which the laser waist size is too small and our approximation of ignoring particle transverse coordinate and wiggle motion on the modulation breaks down.

According to Eq. (252), the maximal modulation is realized when $Z_R = \frac{L_u}{2}$ and the value is

$$g_{\max} = \frac{\partial \left(\frac{eV_L}{E_0} \right)}{\partial y} = \frac{ek_L K[JJ]}{\gamma^2 m_e c^2} \sqrt{\frac{P_L Z_0}{\pi}}.$$

For example, if $E_0 = 600$ MeV, $\lambda_L = 1064$ nm, $\lambda_u = 8$ cm ($B_0 = 1.13$ T), $L_u = 0.8$ m ($N_u = 10$), $Z_R = \frac{L_u}{2}$, then for $P_L = 1$ MW the induced angular chirp strength is $g = 0.55$ m $^{-1}$. As a comparison, the energy chirp strength induced by such a 1 MW TEM00 laser modulator as evaluated before is $h = 955$ m $^{-1}$. So generally, a TEM01 mode laser is not effective in imprinting angular modulation. Actually we will see in the next section, even a dual-tilted-laser setup is still not effective enough for our application.

2. Dual-Titled-Laser-Induced Angular Modulation

Another way to imprint angular modulation on the electron beam is using a titled incident TEM00 mode laser to modulate the beam in an undulator. To further lower the required laser power, we can apply dual-tilted-laser (DTL) with a crossing configuration [43, 44]. Here in this paper, we focus on the angular modulation scheme based on the DTL setup. Note that if we want to use a DTL for energy modulation, the two lasers should be in phase to make the two laser induced energy modulations add. While for angular modulation, they should be π -phase shifted with respect to each other. This is because for angular modulation, the particle on the reference orbit should get zero energy kick. Only when the particle transverse coordinate is nonzero will it get an energy kick. So the energy modulations induced by the two lasers should cancel on axis. To induce vertical angular modulation, we let the two lasers cross in y - z plane and be polarized in the horizontal plane. The laser field of a normal incident TEM00 laser is given by Eq. (207). Assuming that the two lasers are π -phase-shifted with respect to each other and have the same amplitude. In addition, we assume that $\theta_2 = -\theta_1 = -\theta$, and the two lasers have the same Rayleigh length. Then the superimposed field is

$$\begin{pmatrix} E_x \\ E_y \\ E_z \end{pmatrix}_{\text{unrot}} = E_{x0} e^{ik_L(-y \sin \theta + s \cos \theta) - i\omega_L t} \frac{\exp \left[-\frac{k_L(x^2 + (y \cos \theta + s \sin \theta)^2)}{2(Z_R + i(-y \sin \theta + s \cos \theta))} \right]}{1 + i \frac{(-y \sin \theta + s \cos \theta)}{Z_R}} \begin{pmatrix} 1 \\ -i \frac{x}{Z_R + i(-y \sin \theta + s \cos \theta)} \sin \theta \\ -i \frac{x}{Z_R + i(-y \sin \theta + s \cos \theta)} \cos \theta \end{pmatrix} - E_{x0} e^{ik_L(y \sin \theta + s \cos \theta) - i\omega_L t} \frac{\exp \left[-\frac{k_L(x^2 + (y \cos \theta - s \sin \theta)^2)}{2(Z_R + i(y \sin \theta + s \cos \theta))} \right]}{1 + i \frac{(y \sin \theta + s \cos \theta)}{Z_R}} \begin{pmatrix} 1 \\ i \frac{x}{Z_R + i(y \sin \theta + s \cos \theta)} \sin \theta \\ -i \frac{x}{Z_R + i(y \sin \theta + s \cos \theta)} \cos \theta \end{pmatrix}. \quad (254)$$

As before, we will focus on the impact of E_x on the laser-electron interaction, and ignore the contribution from E_z . Note that if $y = 0$, then $E_x = 0$. We want to know $\frac{\partial E_x}{\partial y}$ when y is close to zero. For this purpose, we do Taylor expansion of the above horizontal electric field with respect to θ when θ is small,

$$E_x = E_{x0} \frac{Z_R (2isk_L Z_R + 2k_L Z_R^2 + x^2 k_L + y^2 k_L - 2Z_R - 2is) \exp \left[-\frac{k_L(x^2 + y^2)}{2(Z_R + iz)} + ik_L s - i\omega_L t \right]}{(s - iZ_R)^3} \theta y. \quad (255)$$

When $x, y \ll Z_R, \lambda_L \ll Z_R$, we have

$$E_x \approx -i2k_L E_{x0} \frac{\exp \left[-\frac{(x^2 + y^2)}{w_0^2 (1 + i \frac{s}{Z_R})} + ik_L s - i\omega_L t \right]}{\left(1 + i \frac{s}{Z_R} \right)^2} \theta y. \quad (256)$$

But note that when $L_u \theta$ is comparable to w_0 , the term $s \sin \theta$ should be kept in the exponential term. Also for the laser phase, we should use the more accurate $s \cos \theta$. These arguments have been explained before also when we analyze the application of a DTL for energy modulation. So the more correct approximate expression of E_x is

$$E_x \approx -i2k_L E_{x0} \frac{\exp \left(-\frac{s^2 \theta^2}{w_0^2 (1 + i \frac{s}{Z_R})} + ik_L s \cos \theta - i\omega_L t \right)}{\left(1 + i \frac{s}{Z_R} \right)^2} \theta y. \quad (257)$$

Again taking the same notation as given in Eq. (233), the integrated modulation voltage induced by a DTL (two lasers π -phase-

shifted with respect to each other) in a planar horizontal undulator can be calculated to be

$$V_L \approx \operatorname{Re} \left[\int_{-\frac{L_u}{2}}^{\frac{L_u}{2}} v_x E_x \frac{ds}{c} \right] \\ \approx k_L E_{x0} \frac{K[JJ]}{\gamma} \theta y Z_R \left[\int_{-\frac{L_u}{2Z_R}}^{\frac{L_u}{2Z_R}} \frac{\exp\left(-v \frac{u^2}{(1+u^2)}\right)}{(1+u^2)^2} \left[(1-u^2) \cos\left(v \frac{u^3}{(1+u^2)}\right) + 2u \sin\left(v \frac{u^3}{(1+u^2)}\right) \right] du \right] \sin \phi_0. \quad (258)$$

We choose $\phi_0 = \frac{\pi}{2}$ to maximize V_L . Therefore, we get the maximum linear angular chirp strength as

$$g = \frac{\partial \left(\frac{eV_L}{E_0} \right)}{\partial y} = \frac{ek_L K[JJ]}{\gamma^2 m_e c^2} \sqrt{\frac{2P_L Z_0}{\lambda_L}} F_{\text{DTL-A}} \left(\frac{L_u}{2Z_R}, \frac{k_L Z_R \theta^2}{2} \right) \sqrt{L_u} \theta, \quad (259)$$

where

$$F_{\text{DTL-A}}(x, v) = \frac{1}{\sqrt{x}} \int_{-x}^x \frac{\exp\left(-v \frac{u^2}{(1+u^2)}\right)}{(1+u^2)^2} \left[(1-u^2) \cos\left(v \frac{u^3}{(1+u^2)}\right) + 2u \sin\left(v \frac{u^3}{(1+u^2)}\right) \right] du. \quad (260)$$

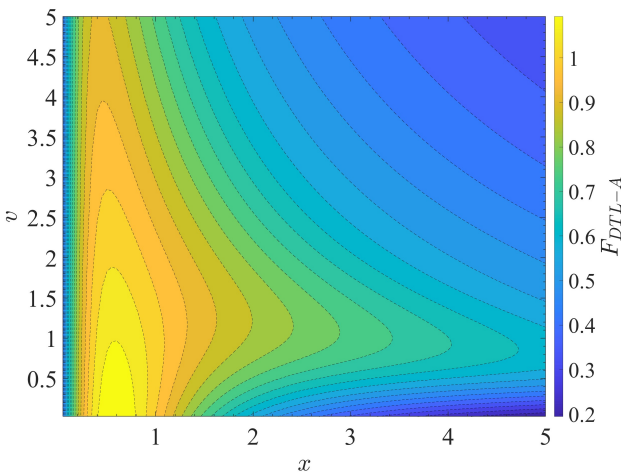


Fig. 12. Contour plot of $F_{\text{DTL-A}}(x, v)$ given by Eq. (260).

A contour plot of $F_{\text{DTL-A}}(x, v)$ is shown in Fig. 12.

Then the angular chirp strength introduced by a DTL compared to the energy chirp strength introduced by a single TEM00 laser modulator, i.e., that given in Eq. (221), with the same laser parameters and undulator length can be expressed as

$$\frac{g}{h} = \xi \theta. \quad (261)$$

with

$$\xi = \frac{F_{\text{DTL-A}} \left(\frac{L_u}{2Z_R}, \frac{k_L Z_R \theta^2}{2} \right)}{\tan^{-1} \left(\frac{L_u}{2Z_R} \right)} \frac{K[JJ]}{K[JJ]|_{\theta=0}}. \quad (262)$$

Note that $K[JJ]$ in the numerator is a function of θ according to the off-axis resonance condition given in Eq. (230).

Since $\xi \sim 1$, and θ is usually in mrad level, given the same laser power, the DTL-induced angular chirp strength will be much smaller than the energy modulation strength induced by a TEM00 mode laser. This observation has been supported by more quantitative calculation of the angular chirp strength induced by a DTL as shown in Figs. 13 and 14. As before, we have considered the case of keeping λ_u or B_0 unchanged when we change the crossing angle θ , respectively. In both cases, the maximal angular chirp strength induced with $P_L = 1$ MW is about $g \approx 1.7 \text{ m}^{-1}$. While from the evaluation in Sec. VIB 1, at the same power level, a TEM00 mode laser modulation can induce an energy chirp strength of $h \sim 955 \text{ m}^{-1}$. This as explained is because θ is only 1 to 2 mrad.

So we can see that the DTL-induced angular chirp strength, although a factor of three larger than that induced by a single normally incident TEM01 mode laser with the same laser power, is still generally quite small. There are two reasons why a DTL is not effective in imprinting angular modulation:

- The crossing angle between the laser and the electron propagating directions results in that they have a rather limited effective interaction region. For example, if the crossing angle is $\theta = 5 \text{ mrad}$, and the undulator length is $L_u = 0.8 \text{ m}$. Then the center of electron beam and center of laser beam at the undulator entrance and exit depart from each other with a distance of $\frac{L_u}{2} \theta = 2 \text{ mm}$, which is a large value compared to the laser beam waist $w_0 = \sqrt{\frac{Z_R \lambda_L}{\pi}} \approx \sqrt{\frac{L_u \lambda_L}{2\pi}} = 368 \mu\text{m}$ and results in a very weak laser electric field felt by the electron there.
- The decrease of undulator parameter K with the increase of θ to meet the off-axis resonance condition, as can be seen in Figs. 8 and 10.

Since the angular chirp strength is small, then according to Theorem Two, the required vertical beta function at the

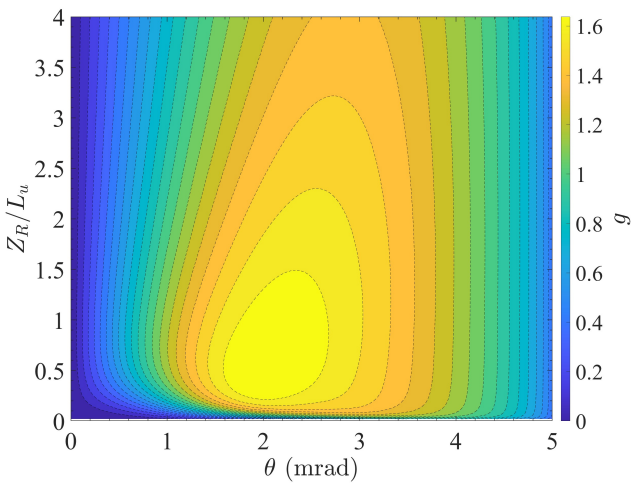


Fig. 13. Angular chirp strength g vs. θ and Z_R/L_u , keep λ_u fixed when changing θ . Parameters used: $E_0 = 600$ MeV, $\lambda_L = 1064$ nm, $P_L = 1$ MW, $\lambda_u = 0.08$ m, $N_u = 10$, $L_u = 0.8$ m.

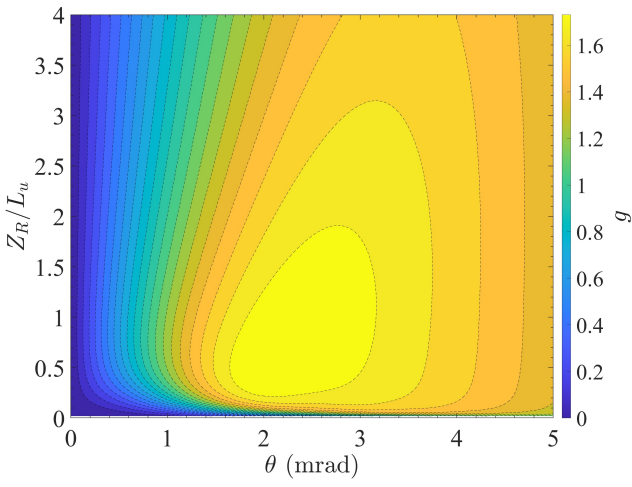


Fig. 14. Angular chirp strength g vs. θ and Z_R/L_u , keep B_0 fixed when changing θ . Parameters used: $E_0 = 600$ MeV, $\lambda_L = 1064$ nm, $P_L = 1$ MW, $B_0 = 1.2$ T, $L_u = 0.8$ m.

1918 Eqs. (150) and (152), for the same modulation laser wave-
1919 length λ_L and power P_L , vertical emittance ϵ_y and target lin-
1920 ear bunch length at the radiator $\sigma_{zR} = \sqrt{\epsilon_y \mathcal{H}_{yR}}$, we have

$$\beta_{yM}(\text{Angular modulation}) \sim \frac{\mathcal{H}_{yM}(\text{Energy modulation})}{\theta^2}. \quad (263)$$

C. Realization Examples

1923 Similar to the section on energy modulation-based
1924 schemes, here we also introduce some realization examples
1925 of angular modulation-based microbunching. The first pro-
1926 posal of applying the angular modulated beam for harmonic
1927 generation to our knowledge is from Ref. [42]. Later an emit-
1928 tance exchange-based harmonic generation scheme is pro-
1929 posed in Ref. [45]. These two schemes apply the TEM01
1930 mode laser to induce angular modulation. Following these
1931 development, there are proposals to realize angular modula-
1932 tion using TEM00 mode lasers, with Ref. [46] using an off-
1933 resonance laser, and Ref. [47] using an tilted incident laser.
1934 And later a dual-tilted-laser (DTL) modulation scheme is ap-
1935 plied in emittance exchange at the optical laser wavelength
1936 range [43]. And most recently, the DTL scheme is proposed
1937 to compress the bunch length in SSMB and lower the require-
1938 ment on the laser power by a factor of four compared to a
1939 single-tilted laser scheme [44]. Note that for these angular
1940 modulation-based harmonic or bunch compression schemes,
1941 we have the inequality given in Eq. (152), i.e., our Theorem
1942 Two.

VIII. 1 KW GLSF SSMB EUV SOURCE

1943 Our goal in this paper as stated is to find a solution for high-
1944 power EUV source based on SSMB, using parameters within
1945 the reach of present technology. According to our analysis,
1946 generalized longitudinal strong focusing (GLSF) turns out to
1947 be the most promising scenario, compared to the longitudinal
1948 weak focusing and longitudinal strong focusing. The key of
1949 a GLSF SSMB ring is the precision transverse-longitudinal
1950 coupling dynamics to utilize the ultrasmall natural vertical
1951 emittance in a planar electron storage ring for efficient mi-
1952 crobunching formation. For our purpose we find energy
1953 modulation-based coupling schemes are preferred than angu-
1954 lar modulation-based coupling ones, in lowering the required
1955 modulation laser power. So the conclusion is that we will use
1956 a TEM00 laser induced energy modulation-based coupling
1957 scheme in a GLSF SSMB storage ring. In this section, we

1958 first present a solution of 1 kW-average-power EUV source
1959 based on GLSF SSMB. More detailed analyses to support our
1960 solution are then developed.

1904 modulator β_{yM} will be large. For example, if $\epsilon_y = 4$ pm,
1905 $\sigma_{zR} = \sqrt{\epsilon_y \mathcal{H}_{yR}} = 2$ nm, and $g = 2 \text{ m}^{-1}$, then we need
1906 $\beta_{yM} = 2.5 \times 10^5$ m, which is too large to be used in prac-
1907 tice in a storage ring. If we want to lower β_{yM} , it then means
1908 a higher modulation laser power is needed. This is the rea-
1909 son why we tend to use energy modulation-based coupling
1910 schemes for bunch compression or microbunching genera-
1911 tion in GLSF SSMB. Our analysis and conclusion here is
1912 consistent with what reported in Ref. [48] when comparing
1913 energy and angular modulation microbunching schemes for
1914 laser plasma accelerator based light source.

1915 Generally, when we compare the energy modulation-based
1916 and DTL-induced angular modulation-based bunch com-
1917 pression schemes, from the Theorem One and Two, i.e.,

TABLE 2. An example parameter set of a GLSF SSMB ring for 1 kW-average-power EUV radiation generation.

Parameter	Value	Description
E_0	600 MeV	Beam energy
C_0	~ 200 m	Circumference
η	$\sim 5 \times 10^{-3}$	Phase slippage factor
I_P	40 A	Peak current
f_e	0.5%	Electron beam filling factor
I_A	200 mA	Average current
B_{ring}	1.33 T	Bending magnet field in the ring
ρ_{ring}	1.5 m	Bending radius in the ring
$U_{0\text{dipoles}}$	7.7 keV	Radiation loss per particle per turn from ring dipoles
B_{0w}	6 T	Bending field of damping wiggler
L_w	40 m	Total length of N_{wc} identical damping wigglers
N_{wc}	20	Number of identical damping wigglers
λ_w	< 0.168 m	Wiggler period length
U_{0w}	328 keV	Radiation loss per particle per turn from damping wiggler
$P_{R\text{beam}}$	68.3 kW	Total radiation loss power of the electron beam
P_{RF}	100 \sim 200 kW	Total power consumption of the RF system
$\sigma_{\delta 0}$	4.2×10^{-4}	Natural energy spread (without damping wiggler)
$\sigma_{\delta w}$	8.2×10^{-4}	Natural energy spread (with damping wiggler)
$\sigma_{\delta\text{IBS}}$	8.5×10^{-4}	Energy spread with IBS (with damping wiggler)
ϵ_x	2 nm	Horizontal emittance
ϵ_y	40 pm	Vertical emittance
$\tau_{y\text{RD}}$	2.38 ms	Vertical radiation damping time with damping wiggler
$\tau_{y\text{IBS}}$	7.11 ms	Vertical IBS diffusion time
λ_L	1064 nm	Modulation laser wavelength
σ_{zR}	2 nm	Linear bunch length at the radiator
\mathcal{H}_{yR}	0.1 μ m	\mathcal{H}_y at the radiator
\mathcal{H}_{yM}	0.056 m	\mathcal{H}_y at the modulator
h	1.33×10^4 m $^{-1}$	Modulator induced linear energy chirp strength
λ_{uM}	0.1 m	Modulator undulator period
B_{0M}	0.806 T	Modulator peak magnetic flux density
K_{uM}	7.53	K of modulator undulator
N_{uM}	15	N_u of modulator undulator
L_{uM}	1.5 m	Modulator length
$\Delta\epsilon_{yM}$	13.4 pm	Modulators' quantum excitation to vertical emittance
Z_R	$\sim \frac{L_{uM}}{3}$	Laser Rayleigh length
P_{LP}	130 MW	Peak modulation laser power
f_L	0.5%	Laser beam filling factor
P_{LA}	651 kW	Average modulation laser power
$\lambda_R = \frac{\lambda_L}{79}$	13.5 nm	Radiation wavelength
b_{79}	0.0675	Bunching factor
$\sigma_{\perp R}$	20 μ m	Effective transverse electron beam size at the radiator
λ_{uR}	1.8 cm	Radiator undulator period
B_{0R}	0.867 T	Radiator peak magnetic flux density
N_{uR}	79 \times 4	Number of undulator periods
L_{uR}	5.69 m	Radiator length
P_{RP}	224 kW	Peak radiation power
P_{RA}	1.12 kW	Average radiation power

1962

A. A Solution of 1 kW EUV Source

1970

B. Some Basic Considerations

1963 Based on what we have studied in previous sections and the 1971 Now we present the detailed considerations and calcu-
 1964 various important physical effects to be discussed in this sec- 1972 tions to support our solution. First are some basic considera-
 1965 tion, here we present an example parameter set of an 1 kW- 1973 tions on the parameter choice. As explained in the beginning
 1966 average-power EUV light source based on GLSF SSMB as 1974 of Sec. IV, we will use a beam energy of $E_0 = 600$ MeV
 1967 shown in Tab. 2. All the parameter list should be doable from 1975 and a modulation laser wavelength of $\lambda_L = 1064$ nm. In the
 1968 an engineering viewpoint. Such a table summarizes our in- 1976 GLSF scheme, a small vertical emittance is crucial. We as-
 1969 vestigations presented in this paper. 1977 sume that the vertical emittance used to accomplish our goal
 1978 stated above is $\epsilon_y = 40$ pm. One may notice that the ver-

tical emittance we use is actually not extremely small. This conservative choice is mainly a refection of consideration for intra-beam scattering (IBS) to be introduced soon. To realize significant coherent EUV generation, and considering that we may generate microbunching based on a coasting beam or RF bunched beam in the ring, which is much longer than the linear bunch length $\sigma_{zR} = \sqrt{\epsilon_y \mathcal{H}_{yR}}$ to be as short as 2 nm. The bunching factor at 13.5 nm according to Eq. (206) is then 0.0675.

With $\epsilon_y = 40$ pm, to get the desired linear bunch length 2 nm at the radiator, we need $\mathcal{H}_{yR} = 0.1$ μm . If β_y at the radiator is around 1 m, then the required control precision of dispersion and dispersion angle at the radiator is at the level of 0.3 mm and 0.3 mrad. Such a precise control of \mathcal{H}_{yR} is challenging but realizable using present technology. We remind the readers that the dispersion function is actually not well defined when the system is transverse-longitudinal coupled, and \mathcal{H}_y here should be replaced by the our defined generalized beta function β_{55}^{II} . But here we still use the classical definition of \mathcal{H}_y in getting the numbers for the above D_x and D'_x control

precision to give the readers a more concrete feeling. Following similar line of thought, we also need a precision control of \mathcal{H}_x or β_{55}^I at the radiator, since the horizontal emittance is even larger than the vertical one. Generally, we require a precision control of both $D_{x,y}$ and $D'_{x,y}$. Besides, we also need to ensure the coupling of horizontal emittance ϵ_x to the vertical plane to be less than 1% since our applied $\epsilon_x = 2$ nm is about two orders of magnitude larger than $\epsilon_y = 40$ pm.

Another important parameter is the beam current, both the average and peak ones. First we observe that given the same average beam current, the average radiation power will be higher with the decreasing of the beam filling factor f_e . This is because the peak power of the coherent radiation is proportional to the peak current squared $P_{RP} \propto I_P^2 \propto I_A^2 f_e^{-2}$, where I_P and I_A are the peak and average current, respectively, and f_e is the electron beam filling factor. The average radiation power is then $P_{RA} = P_{RP} f_e \propto I_A^2 f_e^{-1}$. So we tend to choose as high average current and as small filling factor as we can, as long as collective effects like IBS and coherent synchrotron radiation to be analyzed soon do not degrade the beam properties. We have applied a 40 A peak current and a 200 mA average current in our solution. Note that in the calculation of filling factor, for simplicity we have assumed the beam current is like square waves. The real beam distribution is more like a smooth curve, for example a Gaussian profile if there is only a single RF cavity in the ring. But this observation only results in some numerical factor adjustment and does not affect the core part of our analysis. So in Tab. 2 and below, we take this simplification of a square wave current distribution.

C. Quantum Excitation Contribution to Vertical Emittance

After the general considerations, let us now take a closer look at the critical parameter ϵ_y . It turns out the first contribution of vertical emittance is the quantum excitation in

the GLSF section itself, since \mathcal{H}_y there is nonzero. More clearly, according to our Theorem One, i.e., Eq. (150), the modulator should be placed at a dispersive location if we use energy modulation-based coupling for bunch compression or harmonic generation. Therefore, the quantum excitation of all bend-like elements, like dipoles, modulators and radiator in the GLSF section, will contribute to the vertical emittance. Like the calculation in Eq. (136), the quantum excitation contribution of a radiator to ϵ_y is

$$\Delta\epsilon_{yR} = C_q \frac{\gamma^2}{J_y} \frac{1}{I_2} \times \frac{\mathcal{H}_{yR}}{\rho_{0R}^3} \frac{4}{3\pi} L_{uR}, \quad (264)$$

where L_{uR} is the radiator undulator length, ρ_{0R} is the bending radius corresponds to the peak magnetic field of the radiator B_{0R} . Assuming that the radiation energy loss in the GLSF section is much less than that induced by the bending magnets in the ring, then we have $I_2 \approx \frac{2\pi}{\rho_{ring}}$. Taking the the approximation $J_y \approx 1$, in an easy-to-use form we have

$$\Delta\epsilon_{yR}[\text{nm}] = 8.9 B_{\text{ring}}^{-1}[\text{T}] B_{0R}^3[\text{T}] \mathcal{H}_{yR}[\text{m}] L_{uR}[\text{m}]. \quad (265)$$

For the parameters given in Tab. 2, $B_{\text{ring}} = 1.33$ T, $\lambda_{uR} = 1.8$ cm ($B_{0R} = 0.867$ T), $\mathcal{H}_{yR} = 0.1$ μm , $L_{uR} = 5.69$ m ($N_{uR} = 4 \times 79$), then $\Delta\epsilon_{yR} = 2.5$ fm, which is much less than ϵ_y . Generally, since \mathcal{H}_y at the radiator is quite small, the contribution of radiator to the vertical emittance is not the dominant one, compared to that from modulators and dipoles to be introduced.

Similar to the analysis for radiator, the contribution of two GLSF modulators to ϵ_y is

$$\Delta\epsilon_{yM}[\text{nm}] = 17.8 B_{\text{ring}}^{-1}[\text{T}] B_{0M}^3[\text{T}] \mathcal{H}_{yM}[\text{m}] L_{uM}[\text{m}], \quad (266)$$

where B_{0M} and L_{uM} are the peak magnetic field and length of the modulator undulators, respectively. For the parameters given in Tab. 2, $B_{\text{ring}} = 1.33$ T, $B_{0M} = 0.806$ T, $\mathcal{H}_{yM} = 0.056$ m, $L_{uM} = 1.5$ m, then $\Delta\epsilon_{yM} = 592$ pm, which is a quite large value compared to that contributed from the radiator. This is mainly due to the fact that $\mathcal{H}_{yM} \gg \mathcal{H}_{yR}$. As we will introduce soon, we can apply a horizontal planar damping wiggler to control this contribution by increasing the radiation damping rate.

In the above analysis, we have assumed \mathcal{H}_y is a constant value throughout an undulator. This strictly speaking is not true, since there will be intrinsic dispersion generated inside an undulator. We can refer to the transfer matrix of an undulator or laser modulator to study the evolution of \mathcal{H}_y in an undulator radiator and modulator, to get a more accurate evaluation of their quantum excitation contribution, as to be shown in Sec. VIII D 2. Our calculation shows that this will result in a significant difference for radiator's contribution to ϵ_y , but not much difference for the modulators. However, since the radiator's contribution to ϵ_y is negligible small compared to that of modulators, here we still use the simplified formula Eq. (266) in our following discussion.

There are also vertical bending magnets in the GLSF section for optics manipulation to fulfill the bunch compression or harmonic generation condition. But in principle we can use

weak dipoles to minimize their quantum excitation contribution to vertical emittance, and satisfy the symplectic optics requirement at the same time. Of course, the total length of these dipoles should not be too long. Therefore, in our present evaluation, we will assume that the quantum excitation contribution from the two modulators are the dominant source of ϵ_y if we consider single-particle dynamics alone.

D. Application of Damping Wigglers

1. To Speed Up Damping

It is desired that $\Delta\epsilon_{yM}$ is only a small portion of our desired ϵ_y , since then it provides room for other contributions of vertical emittance, like IBS and that from x - y coupling. In principle, we can also use a weaker modulator field to weaken the quantum excitation, but this then means the laser-electron interaction will be less efficient, and a larger laser power is needed if we want to imprint the same energy modulation strength. Instead, the solution we choose is to increase the radiation damping rate per turn. To speed up damping, which is helpful in controlling the vertical emittance growth from both the quantum excitation and IBS, we may invoke one or multiple damping wigglers. We can put horizontal planar wigglers at dispersion-free locations. In such a way, the damping wiggler will contribute only damping and no excitation to the vertical emittance. Assuming that

$$U_{0w} = R_w U_{0\text{dipoles}}, \quad (267)$$

with $U_{0\text{dipoles}} = C_\gamma E_0^4 / \rho_{\text{ring}}$ the radiation energy loss per particle per turn from the bending magnets in the ring, U_{0w} the radiation loss from all the damping wigglers in the ring, and

$$R_w = \frac{U_{0w}}{U_{0\text{dipoles}}} = \frac{1}{2} \left(\frac{B_{0w}}{B_{\text{ring}}} \right)^2 \frac{L_w}{2\pi\rho_{\text{ring}}}, \quad (268)$$

where B_{0w} and L_w are the peak magnetic field and total length of the damping wigglers, respectively. Since the damping rate is proportional to the radiation energy loss per turn, then the damping constant will be a factor of R_w larger by applying the damping wiggler

$$\alpha_V = (1 + R_w)\alpha_{V0}, \quad (269)$$

with α_{V0} the natural vertical damping rate without the damping wigglers. Then the above evaluated emittance growth from radioastron, modulators and dipoles will become $\frac{1}{1+R_w}$ of the original value. For example for the modulators, we have

$$\Delta\epsilon_{yM}[\text{nm}] = \frac{17.8 B_{\text{ring}}^{-1} [\text{T}] B_{0M}^3 [\text{T}] \mathcal{H}_{yM} [\mu\text{m}] L_{uM} [\text{m}]}{1 + R_w}. \quad (270)$$

Put the above relation in another way

$$L_{uM} [\text{m}] \approx 56.2 (1 + R_w) \frac{B_{\text{ring}} [\text{T}] \Delta\epsilon_{yM} [\text{pm}]}{\mathcal{H}_{yM} [\mu\text{m}] B_{0M}^3 [\text{T}]} \quad (271)$$

We will use a rather strong superconducting damping wig-

gler or damping wiggler to speed up damping to fight against the IBS diffusion and quantum excitation to maintain requirement at the same time. For the parameters given in Tab. 2, $B_{0\text{ring}} = 1.33 \text{ T}$, $U_{0\text{dipoles}} = 7.7 \text{ keV}$, $B_{0w} = 6 \text{ T}$ and $L_w = 40 \text{ m}$, then $U_{0w} = 328 \text{ keV}$ and $R_w = 42.9$. By applying such strong damping wigglers, we now have $\Delta\epsilon_{yM} = 13.4 \text{ pm}$, which is a factor of three smaller than the desired $\epsilon_y = 40 \text{ pm}$ and should be acceptable. Assuming the circumference of the ring is $C_0 = 200 \text{ m}$, the longitudinal and vertical radiation damping time are correspondingly

$$\tau_{\delta RD} = 1.19 \text{ ms}, \quad \tau_{yRD} = 2.38 \text{ ms}. \quad (272)$$

We will compare this radiation damping speed with that of IBS diffusion later.

2. Impact of Damping Wigglers on Energy Spread, Horizontal Emittance and Phase Slippage

Our primary goal of applying damping wiggler is to speed up radiation damping, but the damping wiggler also contributes to quantum excitation, thus may affect the energy spread and horizontal emittance. Let us investigate the energy spread first. Considering both the ring dipoles and damping wiggler, the new equilibrium energy spread is

$$\sigma_{\delta w} = \sigma_{\delta0} \sqrt{\frac{1 + \frac{4}{3\pi} \left(\frac{B_{0w}}{B_{\text{ring}}} \right)^3 \frac{L_w}{2\pi\rho_{\text{ring}}}}{1 + \frac{1}{2} \left(\frac{B_{0w}}{B_{\text{ring}}} \right)^2 \frac{L_w}{2\pi\rho_{\text{ring}}}}}, \quad (273)$$

$$\sigma_{\delta0} = \sqrt{\frac{C_q}{J_z} \frac{\gamma^2}{\rho_{\text{ring}}}} \quad (274)$$

is the natural energy spread if there is no damping wiggler. Nominally, we have the longitudinal damping partition $J_z \approx 2$. So

$$\sigma_{\delta0} \approx 4.69 \times 10^{-4} B_{\text{ring}}^{\frac{1}{2}} [\text{T}] E_0^{\frac{1}{2}} [\text{GeV}]. \quad (275)$$

For example, if $B_{0w} = 1.33 \text{ T}$, and $E_0 = 600 \text{ MeV}$, then $\sigma_{\delta0} = 4.2 \times 10^{-4}$. When $\frac{1}{2} \left(\frac{B_{0w}}{B_{\text{ring}}} \right)^2 \frac{L_w}{2\pi\rho_{\text{ring}}} \gg 1$ and $\frac{4}{3\pi} \left(\frac{B_{0w}}{B_{\text{ring}}} \right)^3 \frac{L_w}{2\pi\rho_{\text{ring}}} \gg 1$, which means the energy spread is dominant by the damping wigglers, we have

$$\sigma_{\delta w} \approx \sigma_{\delta0} \sqrt{\frac{8}{3\pi} \frac{B_{0w}}{B_{\text{ring}}}} \approx 4.32 \times 10^{-4} B_{0w}^{\frac{1}{2}} [\text{T}] E_0^{\frac{1}{2}} [\text{GeV}]. \quad (276)$$

So given the beam energy, the new equilibrium energy spread will depends solely on the peak magnetic field of the damping wiggler B_{0w} . For example, if $E_0 = 600 \text{ MeV}$ and $B_{0w} = 6 \text{ T}$, then the asymptotic energy spread is $\sigma_{\delta w} = 8.2 \times 10^{-4}$.

2166 This energy spread can affect coherent EUV radiation power 2178 Usually the central part of the wiggler has a sinusoidal field
2167 in a long radiator as will be studied in Sec. VIII I. 2179 strength pattern along the longitudinal axis. We set the origin
2180 of the global path length coordinate $s = 0$ to be the location
2181 of the peak magnetic field closest to the wiggler center. Note

2168 Now let us look at the impact on horizontal emittance. We 2182 that this choice of origin location has a correspondence to the
2169 just said that we can place the damping wigglers at horizon- 2183 transfer matrix of wiggler to be given soon. Then the vertical
2170 tally dispersion-free locations to minimize their quantum ex- 2184 magnetic field of a horizontal planar wiggler is
2171 citation on ϵ_x . But there will be some intrinsic horizontal dis-

2172 persion and dispersion angle and thus \mathcal{H}_x generated inside the 2185 with B_{0w} the peak magnetic field and $k_w = 2\pi/\lambda_w$ the
2173 wigglers and the strong field strength raises the concern that 2186 wavenumber of wiggler, and $k_x^2 + k_y^2 = k_w^2$. The linear trans-
2174 the quantum excitation of the damping wigglers may result in 2187 evaluation of this. Part of the content in this section can also 2188 fer matrix of \mathbf{X} from $s = 0$ to $s \in [-\frac{L_w}{2}, \frac{L_w}{2}]$ with L_w the
2177 be found in Ref. [49] 2189 wiggler length is then [50]

$$B_y = B_{0w} \cosh(k_x x) \cosh(k_y y) \cos(k_w s), \quad (277)$$

2190

$$\mathbf{W}(s|0) = \begin{pmatrix} 1 & s & 0 & 0 & 0 & -\frac{K}{\gamma k_w} [1 - \cos(k_w s)] \\ 0 & 1 & 0 & 0 & 0 & -\frac{K}{\gamma} \sin(k_w s) \\ 0 & 0 & \cos(k_y s) & \frac{\sin(k_y s)}{k_y} & 0 & 0 \\ 0 & 0 & -k_y \sin(k_y s) & \cos(k_y s) & 0 & 0 \\ W_{51} & W_{52} & 0 & 0 & 1 & W_{56} \\ 0 & 0 & 0 & 0 & 0 & 1 \end{pmatrix}, \quad (278)$$

2191 where $W_{51} = -W_{26}$, $W_{52} = -sW_{26} + W_{16}$ and

2192

$$W_{56} = \frac{2\lambda_0}{\lambda_w} s + \frac{K^2}{\gamma^2} \left[\frac{\sin(2k_w s) - 4\sin(k_w s)}{4k_w} \right], \quad (279)$$

2193 with $\lambda_0 = \frac{1+K^2/2}{2\gamma^2} \lambda_w$ being the fundamental on-axis reso-
2194 nant wavelength.

2195 In a planar uncoupled ring, the normalized eigenvector of
2196 the storage ring one-turn map corresponding to the horizontal
2197 eigenmode at $s = 0$ can be expressed as the first vector in
2198 Eq. (50). We assume α_{x0}, β_{x0} are the Courant-Snyder func-

2199 tions and D_{x0}, D'_{x0} are the dispersion and dispersion angle
2200 corresponding to the horizontal plane at $s = 0$, respectively.

2201 Then the horizontal chromatic function \mathcal{H}_{x0} at $s = 0$ is

$$\begin{aligned} \mathcal{H}_{x0} &\equiv \beta_{55}^I(0) = 2|E_{I5}(0)|^2 \\ &= \frac{D_{x0}^2 + (\alpha_{x0}D_{x0} + \beta_{x0}D'_{x0})^2}{\beta_{x0}}. \end{aligned} \quad (280)$$

2202 The evolution of \mathcal{H}_x from $s = 0$ to $s \in [-\frac{L_w}{2}, \frac{L_w}{2}]$ is

2204

$$\begin{aligned} \mathcal{H}_x(s) &\equiv \beta_{55}^I(s) = 2|E_{I5}(s)|^2 = 2|(\mathbf{W}(s|0)\mathbf{E}_I(0))_5|^2 \\ &= \frac{(D_{x0} + W_{16} - W_{26}s)^2 + [\alpha_{x0}(D_{x0} + W_{16} - W_{26}s) + \beta_{x0}(D'_{x0} + W_{26})]^2}{\beta_{x0}}, \end{aligned} \quad (281)$$

2205 where W_{ij} means the i -th row and j -th column matrix term of $\mathbf{W}(s|0)$. Put in the explicit expression of the wiggler matrix
2206 terms, we have

2207

$$\begin{aligned} \mathcal{H}_x(s) &= \frac{1}{\rho_w^2 k_w^4 \beta_{x0}} \{ [D_{x0} \rho_w k_w^2 + \sin(k_w s) k_w s + \cos(k_w s) - 1]^2 \\ &\quad + [\beta_{x0} k_w (\rho_w k_w D'_{x0} - \sin(k_w s)) + \alpha_{x0} (D_{x0} \rho_w k_w^2 + \sin(k_w s) k_w s + \cos(k_w s) - 1)]^2 \}. \end{aligned} \quad (282)$$

2208 We assume that the quantum excitation contribution from 2212 Then the quantum excitation of a wiggler to the horizontal
2209 the entrance and exit region of the wiggler, where the field 2213 beam emittance can be evaluated by the integral
2210 strength in reality deviates from the ideal sinusoidal pattern,
2211 is much smaller than that of the central sinusoidal field region.

$$I_{5w} = \int_{-\frac{L_w}{2}}^{\frac{L_w}{2}} \frac{\mathcal{H}_x(s)}{|\rho(s)|^3} ds = \frac{1}{\rho_w^3} \int_{-\frac{L_w}{2}}^{\frac{L_w}{2}} \mathcal{H}_x(s) |\cos(k_w s)|^3 ds, \quad (283)$$

where $\rho_w = \frac{\gamma m_e \beta c}{e B_{0w}}$ corresponds to the bending radius at the location of peak magnetic field B_{0w} , with $\beta = \sqrt{1 - \frac{1}{\gamma^2}}$. Put Eq. (282) in, we have

$$I_{5w} = \frac{4}{15\pi} \frac{L_w}{\rho_w^5 k_w^2} \left[\beta_{x0} + \gamma_{x0} L_w^2 \mathcal{R} + 5\rho_w^2 k_w^2 \mathcal{H}_{x0} - \left(10 + \frac{15\pi}{8} \right) \frac{\rho_w (D_{x0} + \alpha_{x0} D_{x0} + \beta_{x0} D'_{x0})}{\beta_{x0}} \right], \quad (284)$$

where $\gamma_{x0} = \frac{1+\alpha_{x0}^2}{\beta_{x0}}$ and

$$\mathcal{R} = \frac{15}{32\pi^2} \frac{1}{N_w^3} \int_{-N_w\pi}^{N_w\pi} [\sin(x)x + \cos(x) - 1]^2 |\cos(x)|^3 dx, \quad (285)$$

with $N_w = L_w/\lambda_w$ being the number of wiggler period which is assumed to be an integer. Equation (284) above is the exact formula for wiggler's contribution to the radiation integral I_{5x} in an electron storage ring.

Given a specific N_w , \mathcal{R} can be straightforwardly obtained by integration in Eq. (285). When $N_w \gg 1$, we have $\mathcal{R} \approx \frac{1}{12}$, and

$$I_{5w} \approx \frac{4}{15\pi} \frac{L_w}{\rho_w^5 k_w^2} \left[\langle \beta_x \rangle_w + 5\rho_w^2 k_w^2 \mathcal{H}_{x0} - \left(10 + \frac{15\pi}{8} \right) \frac{\rho_w (D_{x0} + \alpha_{x0} D_{x0} + \beta_{x0} D'_{x0})}{\beta_{x0}} \right], \quad (286)$$

where $\langle \beta_x \rangle_w$ is the average value of β_x along the wiggler

$$\langle \beta_x \rangle_w = \frac{1}{L_w} \int_{-\frac{L_w}{2}}^{\frac{L_w}{2}} \beta_x(s) ds = \beta_{x0} + \frac{\gamma_{x0} L_w^2}{12}. \quad (287)$$

Denote $\chi_{x0} = \text{Arg}\left(\frac{E_{I5}(0)}{E_{I1}(0)}\right)$, where $E_{I5}(0)$ and $E_{I1}(0)$

represent the fifth and first term of the first eigenvector in Eq. (50) and $\text{Arg}()$ means the angle of a complex number, then Eq. (286) can be written as

$$I_{5w} \approx \frac{4}{15\pi} \frac{L_w}{\rho_w^5 k_w^2} \left[\langle \beta_x \rangle_w + 5\rho_w^2 k_w^2 \mathcal{H}_{x0} - \left(10 + \frac{15\pi}{8} \right) \rho_w \sqrt{\frac{2\mathcal{H}_{x0}}{\beta_{x0}}} \sin\left(\chi_{x0} - \frac{\pi}{4}\right) \right]. \quad (288)$$

The first term in the above bracket corresponds to the approximated formula found in literature

$$I_{5w,\text{intrinsic}} \approx \frac{4}{15\pi} \frac{L_w \langle \beta_x \rangle_w}{\rho_w^5 k_w^2}. \quad (289)$$

$$I_{5w} \approx \frac{4}{15\pi} \frac{L_w \langle \beta_x \rangle_w}{\rho_w^5 k_w^2} + \frac{4}{3\pi} \frac{L_w \mathcal{H}_{x0}}{\rho_w^3}, \quad (290)$$

It can be viewed as the intrinsic contribution of a wiggler to the radiation integral I_{5x} , since there will be intrinsic dispersion and dispersion angle generated inside the wiggler even if $D_{x0} = 0$ and $D'_{x0} = 0$ as can be seen from the matrix term W_{16} and W_{26} of the wiggler. The second and third terms in the bracket arise from a nonzero \mathcal{H}_{x0} . When D'_{x0} or $\frac{D_{x0}}{\beta_{x0}}$ is of the order $\frac{K}{\gamma} = \frac{1}{\rho_w k_w}$, which can easily be the case in a real lattice, the contribution from this nonzero \mathcal{H}_{x0} in the bracket could be comparable or even larger than the first term and cannot be neglected. The more accurate formula derived here should then be invoked to calculate the wiggler's quantum excitation of beam emittance. When the third term is much smaller than the second term, i.e., roughly

when $\mathcal{H}_{x0} \beta_{x0} \gg \left(\frac{K}{\gamma} \lambda_w\right)^2$, Eq. (288) can be further approx-

where the first term accounts for the intrinsic contribution, and the second term for the nonzero \mathcal{H}_{x0} .

From the above analysis, we can see that the minimum I_{5w} is realized when

$$\alpha_{x0} = 0, \beta_{x0} = \frac{L_w}{2\sqrt{3}}, D_{x0} = 0, D'_{x0} = 0, (\mathcal{H}_{x0} = 0), \quad (291)$$

and the minimal value is

$$I_{5w,\text{min}} \approx \frac{4}{15\sqrt{3}\pi} \frac{L_w^2}{\rho_w^5 k_w^2}. \quad (292)$$

Now we can evaluate the impact of the damping wigglers on the equilibrium horizontal emittance to make sure the desired $\epsilon_x = 2 \text{ nm}$ can be realized. From Eq. (53), the equilib-

rium emittance with the damping wiggler is given by

$$\epsilon_{xw} = C_q \frac{\gamma^2}{J_x} \frac{I_{50} + I_{5w}}{I_{20} + I_{2w}}, \quad (293)$$

where I_{20} and I_{50} are the radiation integrals of the ring without the damping wiggler. Note that the natural emittance without the damping wiggler is given by

$$\epsilon_{x0} = C_q \frac{\gamma^2}{J_x} \frac{I_{50}}{I_{20}}. \quad (294)$$

If we want $\epsilon_{xw} \leq \epsilon_{x0}$, then we need $C_q \frac{\gamma^2}{J_x} \frac{I_{5w}}{I_{2w}} \leq \epsilon_{x0}$. Using $I_{2w} \approx \frac{L_w}{2\rho_w^2}$ and Eq. (292), we then have

$$\lambda_w \leq 2\pi \sqrt{\frac{15\sqrt{3}\pi J_x \epsilon_{x0} \rho_w^3}{8C_q \gamma^2 L_w}}. \quad (295)$$

According to the above scaling, a longer wiggler length requires a shorter wiggler period to control the quantum excitation contribution to the horizontal emittance. This is because the average values of β_x and \mathcal{H}_x in the wiggler are linearly proportional to L_w . But note that the above analysis assumes there is only a single wiggler. If we split the wiggler into N_{wc} identical cells with the total length fixed, we can make the contribution of the wiggler to I_{5w} and thus quantum excitation to horizontal emittance becomes a factor of N_{wc} smaller, while the contribution to I_{2w} and thus the effect on radiation damping is unchanged. Then the tolerance of λ_w can be a factor of $\sqrt{N_{wc}}$ larger. Put in the numerical numbers, we have a more useful scaling

$$\lambda_w [\text{m}] \leq 3.19 \sqrt{\frac{N_{wc} J_x E_0 [\text{GeV}] \epsilon_{x0} [\text{nm}]}{B_{0w}^3 [\text{T}] L_w [\text{m}]}}. \quad (296)$$

Nominally $J_x \approx 1$. For our example parameters given in Tab. 2, $E_0 = 600 \text{ MeV}$, $\epsilon_{x0} = 2 \text{ nm}$, $B_{0w} = 6 \text{ T}$, $L_w = 40 \text{ m}$, $N_{wc} = 20$ which means each small wiggler has a length of 2 m, we then to realize $\epsilon_{xw} \leq \epsilon_{x0}$ we need

$$\lambda_w \leq 0.168 \text{ m}. \quad (297)$$

A wiggler with a period length of 10 to 15 cm and a peak field of 6 T is doable using superconducting magnet technology. We recognize the impact of such a long (total length) damping wiggler on beam dynamics, single-particle nonlinear dynamics and collective instabilities need further in-depth study, especially considering the fact the gap of such a wiggler is small to realize such a strong field strength. Actually another practical reason to split the wiggler into shorter sections is to avoid the synchrotron radiation generated by itself heating the magnet poles. We also recognize it may take some efforts in the lattice design to make the optimal conditions given by Eq. (291) fulfilled in practice.

Apart from the quantum excitation, the damping wiggler also contributes to the phase slippage. If $B_w = 6 \text{ T}$, $\lambda_w = 0.1 \text{ m}$, $L_w = 40 \text{ m}$ which means a total wiggler period number $N_w = 400$, then the wiggler undulator parameter is $K_w = 0.934 \times 6 \times 10 = 56.04$, then the fundamental resonance wavelength of the wiggler is $\lambda_{rw} = 2338$

$\frac{1+K_w^2/2}{2\gamma^2} \lambda_w = 57 \mu\text{m}$. The R_{56} of the whole damping wiggler is twice the fundamental frequency radiation slippage length $R_{w,56} = 2N_w \lambda_{rw} = 45.6 \text{ mm}$ [17]. Since the total R_{56} of the ring used in Tab. 2 is about 1 m, then the contribution of the damping wiggler to R_{56} is acceptable.

E. Intra-beam Scattering

We mentioned that our conservative choice of $\epsilon_y = 40 \text{ pm}$ is mainly out of the consideration for IBS. Now this can be understood with more quantitative calculations. We will see that IBS turns out to be the most fundamental obstacle in obtaining the ultrasmall vertical emittance in GLSF SSMB. This is partially because our choice of beam energy is not too high. In addition, to realize high EUV power, we need a high peak current which means a high charge density in phase space.

We use Bane's high-energy approximation [51] to calculate the IBS diffusion rate

$$\begin{aligned} \frac{1}{T_\delta} &\approx \frac{r_e^2 c N L_c}{16\gamma^3 \epsilon_x^{\frac{3}{4}} \epsilon_y^{\frac{3}{4}} \sigma_z \sigma_\delta^3} \left\langle \sigma_H g_{\text{Bane}} \left(\frac{a}{b} \right) (\beta_x \beta_y)^{-\frac{1}{4}} \right\rangle, \\ \frac{1}{T_{x,y}} &= \frac{\sigma_\delta^2 \langle \mathcal{H}_{x,y} \rangle}{\epsilon_{x,y}} \frac{1}{T_\delta}, \\ \frac{1}{\sigma_H^2} &= \frac{1}{\sigma_\delta^2} + \frac{\mathcal{H}_x}{\epsilon_x} + \frac{\mathcal{H}_y}{\epsilon_y}, \\ g_{\text{Bane}}(\alpha) &= \frac{2\sqrt{\alpha}}{\pi} \int_0^\infty \frac{du}{\sqrt{1+u^2\sqrt{\alpha^2+u^2}}}, \\ a &= \frac{\sigma_H}{\gamma} \sqrt{\frac{\beta_x}{\epsilon_x}}, b = \frac{\sigma_H}{\gamma} \sqrt{\frac{\beta_y}{\epsilon_y}}. \end{aligned} \quad (298)$$

where $r_e = 2.818 \times 10^{-15} \text{ m}$ is the classical electron radius and $L_c = \ln \left(\frac{b_{\max}}{b_{\min}} \right)$ is the Coulomb Log factor, with b_{\max} and b_{\min} being the maximum and minimal impact factor for the scattering process, respectively. Typically L_c is in the range of 10 to 20. N is the number of electrons in the bunch. For a coasting beam, we need to replace $\sigma_z \rightarrow L/(2\sqrt{\pi})$ where L is the bunch length. Note that $\frac{eN}{L/c} = I_P$ according to our definition, where I_P is the peak current.

Now we put in some example numbers to do an estimation for the IBS diffusion rate in a GLSF EUV SSMB ring:

$$\begin{aligned} E_0 &= 600 \text{ MeV}, I_P = 40 \text{ A}, \sigma_\delta = 8.5 \times 10^{-4}, \\ \epsilon_x &= 2 \text{ nm}, \epsilon_y = 40 \text{ pm}, \langle \sigma_H \rangle = 4 \times 10^{-5}, \\ \frac{a}{b} &= \frac{1}{10}, g_{\text{Bane}} \left(\frac{1}{10} \right) = 0.744, \langle (\beta_x \beta_y)^{-\frac{1}{4}} \rangle = 0.32, \\ \langle \mathcal{H}_y \rangle &= \frac{2 \times 1.6 \times 0.056 \text{ m}}{200} = 0.9 \text{ mm}, L_c = 10. \end{aligned} \quad (299)$$

Note that in Tab. 2 we have $\mathcal{H}_y = 0.056 \text{ m}$ at the two modulators, whose length are both 1.6 m. In evaluating $\langle \mathcal{H}_y \rangle$ we have only considered the contribution from the two modulators, where \mathcal{H}_y reach its maximum value. This is a

2339 simplification, but should give a correct order of magnitude 2349
 2340 estimation. Putting in the example numbers, we then have

$$2341 \quad \tau_{\delta\text{IBS}} = 113 \text{ ms}, \tau_{y\text{IBS}} = 7.11 \text{ ms}.$$

2350 Now we want to evaluate if the peak current of 40 A we ap-
 2351 pply in the above example is doable. One of the main limitation

2352 of peak current is the microwave instability induced by coher-
 2353 ent synchrotron radiation (CSR). According to Ref. [52], the

2354 CSR-induced microwave instability threshold is

$$2355 \quad (S_{\text{CSR}})_{\text{th}} = 0.5 + 0.12\Pi, \quad (301)$$

2342 Compared with the radiation damping times given in 2356 with

2343 Eq. (272), we can see that even for the vertical dimension, the
 2344 IBS diffusion is more than three times slower than the radia-
 2345 tion damping. Therefore, the IBS diffusion can now be con-
 2346 trolled by the strong damping induced by the damping wig-
 2347 glers. This calculation also justifies the necessity or benefit of
 2348 applying the damping wiggles.

$$2357 \quad S_{\text{CSR}} = \frac{I\rho^{1/3}}{\sigma_{z0}^{4/3}}, \quad I = \frac{r_e N_b}{2\pi\nu_{s0}\gamma\sigma_{\delta0}}, \quad \Pi = \frac{\sigma_{z0}\rho^{1/2}}{g^{3/2}}, \quad (302)$$

2358 and $2g$ is the separation between the two plates. So the thresh-
 2359 old peak current is

$$2360 \quad I_{\text{th,peak}} = \frac{eN_b}{\sqrt{2\pi}\sigma_{z0}/c} = \frac{1}{2\sqrt{2\pi}} I_{\text{Alf}} \gamma \left(1 + 0.24 \frac{\sigma_{\delta0}|R_{56}|^{1/2}\rho^{1/2}}{|h_{RF}|^{1/2}g^{3/2}} \right) \frac{\sigma_{\delta0}^{4/3}|R_{56}|^{2/3}|h_{RF}|^{1/3}}{\rho^{1/3}}, \quad (303)$$

2361 with $I_{\text{Alf}} = \frac{ec}{r_e} = 17 \text{ kA}$ being the Alven current. The $R_{56} = 2393 \text{ EUV radiation}$ [17, 54]. What we need is $|R_{56}| \sim 1 \text{ m}$, and
 2362 $-\eta C_0$ is that of the whole ring. $h_{RF} = \frac{eV_{RF} \cos \phi_s}{E_0} k_{RF}$ is the 2394 at the same time $\epsilon_x \lesssim 2 \text{ nm}$, and some optimization may be
 2363 linear energy chirp strength around the synchronous RF phase 2395 required realize such a goal.

2364 Putting in some typical parameters for the EUV SSMB: 2396 $E_0 = 600 \text{ MeV}$, $B_0 = 1.33 \text{ T}$, $\rho = 1.5 \text{ m}$, $|R_{56}| = 1 \text{ m}$, 2397

2366 $\sigma_{\delta0} = 8.5 \times 10^{-4}$, $g = 4 \text{ cm}$, $h_{RF} = 0.01 \text{ m}^{-1}$, then 2398

2367 $I_{\text{th,peak}} = 60.3 \times (1 + 0.31) \text{ A} = 79 \text{ A}.$ 2399 Now we check if the required RF system in the above ex-
 2368 So our application of a peak current of 40 A should be safe 2400 ample calculation is feasible. The longitudinal beta function
 2369 from microwave instability. 2401 at the RF cavity is $\beta_z \approx \sqrt{\eta C_0/h_{RF}} = 10 \text{ m}$, then the RMS
 2370 The astute readers may notice that one of the main reasons 2402 bunch length is $\sigma_z = \sigma_{\delta0}\beta_z = 8.5 \text{ mm}$. To get a beam filling
 2371 we have a large threshold current here is the large phase slip- 2403 factor of 0.5%, roughly we need an RF wavelength of 1.7 m,
 2372 page or R_{56} that we applied for the ring. To avoid confusion, 2404 which means an RF frequency of 176.5 MHz. Then the re-
 2373 first we need to make clear that in this example GLSF SSMB 2405 quired energy chirp strength of $h_{RF} = 0.01 \text{ m}^{-1}$ means the
 2374 EUV source, the electron bunch in the ring can be a coasting 2406 required RF voltage is 1.62 MV. Such an RF voltage should
 2375 beam or an RF-bunched beam, and microbunching appears 2407 be doable at this frequency range. Multiple cavities can be
 2376 only at the radiator, due to the phase space manipulation of 2408 invoked if it is too demanding for a single cavity to reach the
 2377 electron beam in the GLSF section. Actually in our setup, we 2409 desired voltage.
 2378 have used an RF-bunched beam in the ring. Therefore, the 2410 We remind the readers again that in this evaluation, we ac-
 2379 phase slippage factor of the ring does not need to be small, 2411 tually assumed that the beam is RF bunched. While in our
 2380 while this is required in a LWF SSMB ring. Then the question 2412 evaluation of IBS, we have assumed that the beam is a coast-
 2381 becomes whether the required large phase slippage is doable 2413 ing beam. These evaluations here mainly serve as an order of
 2382 and what beam dynamics effects it may have. As a reference, 2414 magnitude estimation that support the general feasibility of
 2383 the Metrology Light Source storage ring [53] in standard user 2415 our parameter choice. A more detailed analysis of collective
 2384 mode has an $|R_{56}| \approx 1.6 \text{ m}$, which means a phase slippage 2416 effects will be necessary in the future development of such a
 2385 factor of 3.3×10^{-2} given a circumference of 48 m. Therefore 2417 GLSF SSMB light source.

2386 we believe our application of $|R_{56}| = 1 \text{ m}$ is realizable. But 2416 The large radiation loss of the electron beam in the ring,
 2387 we recognize that such a large R_{56} requires large horizontal 2417 especially that induced by the strong damping wiggles, need
 2388 dispersion D_x at the dipoles, since $-R_{56} = \eta C_0 \approx 2\pi\langle D_x \rangle_\rho$ 2418 to be compensated. Here we present some preliminary anal-
 2389 where $\langle \rangle_\rho$ means average around the dipoles in the ring. A 2419 ysis on the requirement of the energy compensation system
 2390 large D_x may result in a large \mathcal{H}_x , and then the quantum ex- 2420 of such an GLSF SSMB EUV light source. From Tab. 2,
 2391 citation of dipoles to the horizontal emittance ϵ_x should be 2421 total radiation loss per particle per turn is $U_0 = U_{0\text{dipoles}} +$
 2392 carefully evaluated. A too large ϵ_x will degrade the coherent 2422 $U_{0w} + U_{0R} = 341.3 \text{ keV}$, where the three terms on the right

G. Energy Compensation System

2393 The large radiation loss of the electron beam in the ring,
 2394 especially that induced by the strong damping wiggles, need
 2395 to be compensated. Here we present some preliminary anal-
 2396 ysis on the requirement of the energy compensation system
 2397 of such an GLSF SSMB EUV light source. From Tab. 2,
 2398 total radiation loss per particle per turn is $U_0 = U_{0\text{dipoles}} +$
 2399 $U_{0w} + U_{0R} = 341.3 \text{ keV}$, where the three terms on the right

hand side represent the radiation loss in dipoles, damping with the power consumption of the other systems like electric wiggler and radiator, respectively. So the synchronous acceleration phase corresponds to an acceleration voltage of $V_{\text{acc}} = 341.3$ kV. Such a high voltage is not easy to be realized using an induction linac, considering the required repetition rate is at the MHz level. So we use conventional RF cavities to supply the radiation loss. Following the discussion of last section, and assuming we have used an RF frequency of 166.6 MHz (RF wavelength 1.8 m), then we need an RF voltage of 1.72 MV to realize an energy chirp strength of $h_{RF} = 0.01 \text{ m}^{-1}$. Under this parameter set, and consider $V_{RF} \gg V_{\text{acc}}$, the RF bucket half-height is [17]

$$\hat{\delta}_{\frac{1}{2}} = \frac{2}{\beta_z k_{RF}} = \frac{\lambda_{RF}}{\pi} \sqrt{\frac{h}{\eta C_0}} = 5.73 \times 10^{-2}, \quad (305)$$

which is $67.4\sigma_{\delta 0}$ with the energy spread $\sigma_{\delta 0} = 8.5 \times 10^{-4}$. So the bucket half-height should be large enough to ensure the beam quantum lifetime and Touschek lifetime.

To relieve the burden on the RF cavities, we may use three RF cavities to achieve the total RF voltage, with each cavity having a voltage of 573 kV. To minimize the power dissipated on the cavity, we need a large shunt impedance of each cavity which here we assume to be $R_s = 20 \text{ M}\Omega$, then the total power dissipated on the three cavity walls is

$$P_{\text{diss}} = \frac{1}{3} \frac{V_{RF}^2}{R_s} = 49.2 \text{ kW}. \quad (306)$$

The power delivered to the 200 mA-average current beam is

$$P_b = I_A \frac{U_0}{e} = 68.3 \text{ kW}. \quad (307)$$

So the power dissipated on the cavity walls is at the same level as that delivered to the beam. We recognize the large shunt impedance may take efforts to realize in practice. If the shunt impedance is lower than the assumed value, then the power consumption on the wall will be correspondingly larger. Superconducting RF cavities can be used to lower the power dissipation on the wall.

Generally, the total power consumption of the RF system of an SSMB ring is at 100 kW to 200 kW level. Together

tromagnets, superconducting damping wiggler, vacuum and water cooling system, the overall power consumption of such an SSMB storage ring is at the level of several hundred kW.

The output EUV power per radiator is about 1 kW. In principle, an SSMB ring can accommodate multiple GLSF insertions and therefore multiple radiators, but here we consider the case of only one radiator in the ring. So for such an GLSF SSMB storage ring, it takes a couple of 100 kW electricity power to generate 1 kW EUV light. Such a large power consumption may raise the question on the advantage of such an SSMB-EUV source compared to the superconducting RF-based high-repetition rate FEL-EUV source, in particular, the energy recovery linac-based FEL-EUV source. As a comparison, according to Ref. [55], it takes 7 MW overall power consumption to generate 10 kW EUV light in an ERL-

FEL EUV source, which means 700 kW electricity power per 1 kW EUV light. So the overall power efficiency from electricity to EUV light for an SSMB-EUV source and an ERL-FEL EUV source is comparable. But we remind the readers that these numbers are only rough estimation, and it requires more indepth study to reach a concrete conclusion. Another side comment is that the radiation emitted by the damping wiggler may also be useful.

H. Modulation Laser Power

Now we evaluate the modulation laser power required. Given the laser wavelength, modulator undulator parameters and the required energy chirp strength, we can use Eq. (221) to calculate the required laser power

$$P_L = \frac{\lambda_L}{4Z_0 Z_R} \left(h \frac{1}{\frac{eK[JJ]}{\gamma^2 m_e c^2} \tan^{-1} \left(\frac{L_u}{2Z_R} \right) k_L} \right)^2. \quad (308)$$

$$P_L \approx \frac{1}{1 + R_w} \frac{\epsilon_y}{\Delta \epsilon_{yM}} \frac{1}{(K[JJ])^2} \frac{\lambda_L^3}{3\pi^3 Z_0} \frac{55}{48\sqrt{3}} \frac{\alpha_F c^2 \lambda_e^2 \gamma^7 B_{0M}^3}{C_\gamma E_0^3 B_{\text{ring}}} \frac{1}{\sigma_{zR}^2} \frac{\frac{L_u}{2Z_R}}{\left[\tan^{-1} \left(\frac{L_u}{2Z_R} \right) \right]^2}, \quad (309)$$

where $\alpha_F = \frac{1}{137}$ is the fine structure constant, and R_w is given by Eq. (268). In the above derivation we have used the

electron momentum $P_0 = \gamma m_e c$ and approximation $E_0 \approx P_0 c$. Now we try to derive more useful scaling laws to offer guidance in our parameter choice for a GLSF SSMB storage ring. As shown in Fig. 6, to maximize the energy modulation, we need $\frac{Z_R}{L_u} = 0.359 \approx \frac{1}{3}$. When $K > \sqrt{2}$, we approximate

$\frac{L_u}{2Z_R} \approx 0.7$. Then we have

$$\lambda_L = \frac{1 + \frac{K^2}{2}}{2\gamma^2} \lambda_u \approx \frac{K^2}{4\gamma^2} \lambda_u, \quad (310)$$

$$P_L \propto \frac{1}{1 + R_w} \frac{\epsilon_y}{\Delta\epsilon_{yM}} \frac{\lambda_L^3}{K^2} \frac{\gamma^4 B_{0M}^3}{B_{ring}} \frac{1}{\sigma_{zR}^2}$$

$$\propto \frac{1}{1 + R_w} \frac{\epsilon_y}{\Delta\epsilon_{yM}} \frac{\lambda_L^{\frac{7}{3}} \gamma^{\frac{8}{3}} B_{0M}^{\frac{7}{3}}}{B_{ring}} \frac{1}{\sigma_{zR}^2}.$$

Putting in the numbers for the constants, we obtain the quantitative expressions of the above scalings for practical use

$$P_L[\text{kW}] \approx 5.7 \frac{1}{1 + R_w} \frac{\epsilon_y}{\Delta\epsilon_{yM}} \frac{\lambda_L^{\frac{7}{3}} [\text{nm}] E_0^{\frac{8}{3}} [\text{GeV}] B_{0M}^{\frac{7}{3}} [\text{T}]}{\sigma_{zR}^2 [\text{nm}] B_{ring} [\text{T}]}.$$

The above scaling laws are accurate when $K > \sqrt{2}$, and it should be noted that the calculated power refers to the peak power of the laser. For completeness, here we give also the modulator length scaling

$$L_{uM}[\text{m}] \approx 56.2 (1 + R_w) \frac{B_{ring} [\text{T}] \Delta\epsilon_{yM} [\text{pm}]}{\mathcal{H}_{yM} [\mu\text{m}] B_{0M}^3 [\text{T}]}.$$

Therefore, to lower the required modulation laser power, we can apply a large R_w , which means strong damping wigglers. A low beam energy and short laser wavelength are also preferred. But their choices should take more factors into account, for example IBS and engineering experience of optical enhancement cavity as explained in Sec. IV. A strong bending magnet field in the ring is also desired. Concerning the modulator field strength, a weaker one is favored to lower the required laser power. But note that the required modulator length may be longer, if we keep the quantum excitation contribution of modulators to vertical emittance $\Delta\epsilon_{yM}$ unchanged in this process.

I. Radiation Power

Having formed the microbunching, now comes the radiation generation. We will use a planar undulator as the radiator. Coherent undulator radiation power at the odd- H -th harmonic from a transversely-round electron beam is [17, 54]

$$P_{H,\text{peak}}[\text{kW}] = 1.183 N_u H \chi [JJ]_H^2 F F_\perp(S) |b_{z,H}|^2 I_P^2 [\text{A}],$$

where N_u is the number of undulator periods,

$$[JJ]_H^2 = \left[J_{\frac{H-1}{2}}(H\chi) - J_{\frac{H+1}{2}}(H\chi) \right]^2,$$

with $\chi = \frac{K^2}{4+2K^2}$, and the transverse form factor is

$$F F_\perp(S) = \frac{2}{\pi} \left[\tan^{-1} \left(\frac{1}{2S} \right) + S \ln \left(\frac{(2S)^2}{(2S)^2 + 1} \right) \right],$$

with $S = \frac{\sigma_\perp^2 \omega}{L_u}$ and σ_\perp the RMS transverse electron beam size, $b_{z,H}$ is the bunching factor at the H -th harmonic determined by the longitudinal current distribution, and I_P is the peak current.

The above formula is derived by assuming that the longitudinal and transverse distribution of the electron beam do

not change much in the radiator. Actually the energy spread of electron beam can lead to current distribution change inside the undulator, considering that the undulator has an $R_{56} = 2N_u \lambda_0$, where λ_0 is the fundamental on-axis resonant wavelength of the undulator. If we consider the impact of the energy spread on coherent radiation, and assuming that the microbunching length reach its minimum at the radiator center, there will be a correction or reduction factor multiplied to the radiation power given by Eq. (314)

$$\mathcal{C} = \frac{\sqrt{\pi}}{2} \frac{\text{erf}(\frac{\omega}{c} \sigma_\delta N_u \lambda_0)}{\frac{\omega}{c} \sigma_\delta N_u \lambda_0}.$$

Here we remind the readers that in our case of GLSF SSMB, the beam is actually not transversely round at the radiator. Therefore, we have used an effective round beam size in evaluating the radiation power using the above formula. This effective transverse beam size σ_\perp is in between σ_x and σ_y . For a more accurate calculation of radiation power, we can use the real beam distribution and invoke numerical method [17]. With all the beam physics issues properly handled, we have finally obtained a solution of a 1 kW EUV source based on GLSF SSMB as shown in Tab. 2.

IX. SUMMARY

This paper is about our efforts in obtaining a solution for 1 kW EUV light source based on SSMB. Here we give a short summary of this endeavor. We start by presenting the generalized Courant-Snyder formalism to build the theoretical framework for the following investigations. Based on the formalism we conducted theoretical minimum emittance analysis in an electron storage ring, from which we know that to get small longitudinal emittance, we need to decrease the bending angle of each bending magnet which means increasing the number of bending magnets in the ring. In principle we can get as small longitudinal emittance and as short bunch length as we want along this line. But there is actually practical limitation. To get short bunch length, we need not only to increase the bending magnet number, but also to lower the phase slippage factor of the ring. Using present realizable phase slippage, which at minimum is in the order of 1×10^{-6} , a bunch length of a couple of 10 nm is the lower limit if we apply the longitudinal weak focusing regime. To compress the bunch length further, longitudinal strong focusing regime can be invoked, not unlike its transverse counterpart in the final focus of a collider, to compress the longitudinal beta function thus the bunch length at the radiator significantly. This scheme can realize a bunch length of nm level, thus allowing coherent EUV radiation generation.

However, since the compression of longitudinal beta function requires a strong energy chirp of the electron beam, which is similar to a strong quadrupole focusing strength in the transverse dimension, the modulation laser power required is at GW level, making the optical enhancement cavity of SSMB can only work in a low duty cycle pulsed mode, and thus limits the filling factor of the microbunched beam in the ring,

and thus the average output EUV power. This then leads us to the generalized longitudinal strong focusing (GLSF) regime, which is the focus of this paper. The basic idea of GLSF is to exploit the ultrasmall natural vertical emittance in a planar section to the vertical emittance, the application of damping electron storage ring and apply partial transverse-longitudinal wiggler to speed up damping and its impact on the transverse emittance exchange to compress the bunch length or generate high-harmonic bunching with a shallow energy modulation strength, thus lowering the requirement on the modulation laser power. The backbone of such a scheme is the transverse-longitudinal phase space coupling. To find a solution based on the GLSF scheme, we first conduct some formal mathematical analysis of transverse-longitudinal coupling (TLC)-based bunch compression and harmonic generation schemes and prove three related theorems which are useful in the later choice of parameters and evaluation of laser power. We then go into the details of different specific coupling schemes, grouping them into two categories, i.e., energy modulation-based coupling schemes and angular modulation-based coupling schemes. We derive the formulas of bunching factor and laser-induced modulation strength in each case, and use them for quantitative calculations and comparisons. Our conclusion from these analyses is that the commonly used TEM00 mode laser-induced energy modulation-based schemes are favored for our application in SSMB, as its requirement on the modulation laser power is lower than that in the angular

lar modulation-based schemes. There are also other various important physical issues to be taken into account in finding a solution, like the quantum excitation contribution of GLSF to the transverse emittance exchange, the intra-beam scattering and coherent synchrotron radiation-induced microwave instability, and the energy compensation system. The motivation of these studies is to make our choice of parameters as self-consistent as possible from a beam physics perspective. Finally, based on all the analyses and calculations we present an example parameter set of a GLSF SSMB light source which can deliver 1 kW-average-power EUV radiation. This 1 kW EUV solution given in Tab. 2 can be viewed as a summary of our investigations presented in this paper. Our work provides the basis for the future development of SSMB.

ACKNOWLEDGMENTS

We thank Chao Feng, Ji Li and Yujie Lu for helpful discussions on storage ring-based coherent light source, tilted laser modulation schemes, and the issue of quantum excitation contribution of damping wiggler to the horizontal beam emittance. Many helpful discussions with our colleagues in Tsinghua and other institutes are also much appreciated.

-
- [1] D. F. Ratner, A. W. Chao. Steady-state microbunching in a storage ring for generating coherent radiation. *Phys. Rev. Lett.* **105**, 154801 (2010). doi: [10.1103/PhysRevLett.105.154801](https://doi.org/10.1103/PhysRevLett.105.154801)
- [2] Y. Jiao, D. F. Ratner, A. W. Chao, Terahertz coherent radiation from steady-state microbunching in storage rings with X-band radio-frequency system. *Phys. Rev. ST Accel. Beams* **14**, 110702 (2011). doi: [10.1103/PhysRevSTAB.14.110702](https://doi.org/10.1103/PhysRevSTAB.14.110702)
- [3] A. Chao, E. Granados, X. Huang, et al. High Power Radiation Sources using the Steady-state Microbunching Mechanism. The 7th International Particle Accelerator Conference, Busan. 2016. p. 1048.
- [4] C. Tang, X. Deng, A. Chao, et al. An overview of the progress on SSMB. The 60th ICFA advanced beam dynamics workshop on future light sources, Shanghai. 2018. p. 166 doi: [10.18429/JACoW-FLS2018-THP2WB02](https://doi.org/10.18429/JACoW-FLS2018-THP2WB02)
- [5] X. J. Deng, A. W. Chao, W. H. Huang, et al., Single-particle dynamics of microbunching. *Phys. Rev. Accel. Beams* **23**, 044002 (2020). doi: [10.1103/PhysRevAccelBeams.23.044002](https://doi.org/10.1103/PhysRevAccelBeams.23.044002)
- [6] X. J. Deng, R. Klein, A. W. Chao, et al., Widening and distortion of the particle energy distribution by chromaticity in quasi-isochronous rings. *Phys. Rev. Accel. Beams* **23**, 044001 (2020). doi: [10.1103/PhysRevAccelBeams.23.044001](https://doi.org/10.1103/PhysRevAccelBeams.23.044001)
- [7] Y. Zhang, X. J. Deng, Z. L. Pan, et al., Ultralow longitudinal emittance storage rings. *Phys. Rev. Accel. Beams* **24**, 090701 (2021). doi: [10.1103/PhysRevAccelBeams.24.090701](https://doi.org/10.1103/PhysRevAccelBeams.24.090701)
- [8] X. J. Deng, A. W. Chao, W. H. Huang, et al., Courant-Snyder formalism of longitudinal dynamics. *Phys. Rev. Accel. Beams* **24**, 094001 (2021). doi: [10.1103/PhysRevAccelBeams.24.094001](https://doi.org/10.1103/PhysRevAccelBeams.24.094001)
- [9] Z. Li, X. Deng, Z. Pan, et al., Generalized longitudinal strong focusing in a steady-state microbunching storage ring. *Phys. Rev. Accel. Beams* **26**, 110701 (2023). doi: [10.1103/PhysRevAccelBeams.26.110701](https://doi.org/10.1103/PhysRevAccelBeams.26.110701)
- [10] C.-Y. Tsai, A. W. Chao, Y. Jiao, et al., Coherent-radiation-induced longitudinal single-pass beam breakup instability of a steady-state microbunch train in an undulator. *Phys. Rev. Accel. Beams* **24**, 114401 (2021). doi: [10.1103/PhysRevAccelBeams.24.114401](https://doi.org/10.1103/PhysRevAccelBeams.24.114401)
- [11] C.-Y. Tsai, Theoretical formulation of multiturn collective dynamics in a laser cavity modulator with comparison to Robinson and high-gain free-electron laser instability. *Phys. Rev. Accel. Beams* **25**, 064401 (2022). doi: [10.1103/PhysRevAccelBeams.25.064401](https://doi.org/10.1103/PhysRevAccelBeams.25.064401)
- [12] C.-Y. Tsai, Longitudinal single-bunch instabilities driven by coherent undulator radiation in the cavity modulator of a steady-state microbunching storage ring. *Nucl. Instrum. Methods Phys. Res. A* **1042**, 167454 (2022). doi: [10.1016/j.nima.2022.167454](https://doi.org/10.1016/j.nima.2022.167454)
- [13] Z. Zhao, N. Wang, H. Xu, et al., Calculations of space-charge tune shifts in storage rings with extremely short bunches and small bunch spacing. *Phys. Rev. Accel. Beams* **27**, 094201 (2024). doi: [10.1103/PhysRevAccelBeams.27.094201](https://doi.org/10.1103/PhysRevAccelBeams.27.094201)
- [14] X. Deng, A. Chao, J. Feikes, et al., Experimental demonstration of the mechanism of steady-state microbunching. *Nature* **590**, 576 (2021). doi: [10.1038/s41586-021-03203-0](https://doi.org/10.1038/s41586-021-03203-0)
- [15] A. Kruschniski, X. Deng, J. Feikes, et al., Confirming the theoretical foundation of steady-state microbunching. *Commun. Phys.* **7**, 160 (2024). doi: [10.1038/s42005-024-01657-y](https://doi.org/10.1038/s42005-024-01657-y)
- [16] Z. Pan, Research on optimization and design of advanced laser-driving storage ring. PhD thesis, Tsinghua University, Beijing, 2020.

- [17] X. Deng, *Theoretical and experimental studies on steady-state microbunching*. (Springer Nature, 2024). doi: [10.1007/978-981-99-5800-9](https://doi.org/10.1007/978-981-99-5800-9)
- [18] Y. Zhang, Research on longitudinal strong focusing SSMB ring. PhD Thesis, Tsinghua University, Beijing, 2022.
- [19] C. X. Tang, X. J. Deng, Steady-state micro-bunching accelerator light source. *Acta Phys. Sin.* **71**, 152901 (2022). doi: [10.7498/aps.71.20220486](https://doi.org/10.7498/aps.71.20220486)
- [20] R. Bonifacio, C. Pellegrini, L. M. Narducci, Collective instabilities and high-gain regime in a free electron laser. *Optics Communications* **50**, 373 (1984). doi: [10.1016/0030-4018\(84\)90105-6](https://doi.org/10.1016/0030-4018(84)90105-6)
- [21] A. W. Chao, Evaluation of beam distribution parameters in an electron storage ring. *J. Appl. Phys.* **50**, 595 (1979). doi: [10.1063/1.326070](https://doi.org/10.1063/1.326070)
- [22] M. C. Wang, G. E. Uhlenbeck, On the theory of the Brownian motion II. *Rev. Mod. Phys.* **17**, 323 (1945). doi: [10.1103/RevModPhys.17.32](https://doi.org/10.1103/RevModPhys.17.32)
- [23] N. Campbell, The study of discontinuous phenomena. *Proc. Cambridge Philos. Soc.* **15**, 117 (1909).
- [24] M. Sands, Synchrotron Oscillations Induced by Radiation Fluctuations. *Phys. Rev.* **97**, 470 (1955). doi: [10.1103/PhysRev.97.470](https://doi.org/10.1103/PhysRev.97.470)
- [25] K. W. Robinson, Radiation Effects in Circular Electron Accelerators. *Phys. Rev.* **111**, 373 (1958). doi: [10.1103/PhysRev.111.373](https://doi.org/10.1103/PhysRev.111.373)
- [26] E. D. Courant, H. S. Snyder, Theory of the alternating-gradient synchrotron. *Ann. Phys. (N.Y.)* **3**, 1 (1958). doi: [10.1006/aphy.2000.6012](https://doi.org/10.1006/aphy.2000.6012)
- [27] M. Sands, The Physics of Electron Storage Rings: An Introduction. SLAC report SLAC-121, 1970.
- [28] X. Deng, Optical Stochastic Cooling in a General Coupled Lattice. in Proceedings of the 67th ICFA Adv. Beam Dyn. Workshop Future Light Sources, Luzern, Switzerland (JACoW, Geneva, 2023), p. 143. doi: [10.18429/JACoW-FLS2023-TU4P30](https://doi.org/10.18429/JACoW-FLS2023-TU4P30)
- [29] L. C. Teng, Minimum emittance lattice for synchrotron radiation storage rings. Technical Note. No. ANL-LS-17. 1985.
- [30] X. J. Deng, A. W. Chao, J. Feikes, et al., Breakdown of classical bunch length and energy spread formula in a quasi-isochronous electron storage ring. *Phys. Rev. Accel. Beams* **26**, 054001 (2023). doi: [10.1103/PhysRevAccelBeams.26.054001](https://doi.org/10.1103/PhysRevAccelBeams.26.054001)
- [31] X.-Y. Lu, R. Chiche, K. Dupraz, et al., 710 kW stable average power in a 45,000 finesse two-mirror optical cavity. *Opt. Lett.* **49**, 6884 (2024). doi: [10.1364/OL.543388](https://doi.org/10.1364/OL.543388)
- [32] D. Ratner, A. Chao, Reversible seeding in storage rings. Proc. of the 33th International Free-electron Laser Conference. 2011. p. 57.
- [33] X. J. Deng, W. H. Huang, Z. Z. Li, et al., Harmonic generation and bunch compression based on transverse-longitudinal coupling. *Nucl. Instrum. Methods Phys. Res. A* **1019**, 165859 (2021). doi: [10.1016/j.nima.2021.165859](https://doi.org/10.1016/j.nima.2021.165859)
- [34] Dragt, Alex J. *Lie methods for nonlinear dynamics with applications to accelerator physics*. University of Maryland (2020).
- [35] L. H. Yu, Generation of intense uv radiation by subharmonically seeded single-pass free-electron lasers. *Phys. Rev. A* **44**, 5178 (1991). doi: [10.1103/PhysRevA.44.5178](https://doi.org/10.1103/PhysRevA.44.5178)
- [36] A. W. Chao, Focused laser. Unpublished Note. 2023.
- [37] H. Deng, C. Feng, Using off-resonance laser modulation for beam-energy-spread cooling in generation of short-wavelength radiation. *Phys. Rev. Lett.* **111**, 084801 (2013).
- [38] C. Feng, H. Deng, D. Wang, et al., Phase-merging enhanced harmonic generation free-electron laser. *New J. Phys.* **16**, 043021 (2014). doi: [10.1088/1367-2630/16/4/043021](https://doi.org/10.1088/1367-2630/16/4/043021)
- [39] C. Feng, Z. Zhao, A storage ring based free-electron laser for generating ultrashort coherent EUV and X-ray radiation. *Sci. Rep.* **7**, 4724 (2017). doi: [10.1038/s41598-017-04962-5](https://doi.org/10.1038/s41598-017-04962-5)
- [40] C.-Y. Tsai, Analytical study of higher harmonic bunching and matrix formalism in linear high-gain free-electron laser model. *Nucl. Instrum. Methods Phys. Res. A* **1048**, 167974 (2023). doi: [10.1016/j.nima.2022.167974](https://doi.org/10.1016/j.nima.2022.167974)
- [41] A. W. Chao, *Physics of collective beam instabilities in high energy accelerators*. (Wiley, 1993).
- [42] D. Xiang, W. Wan, Generating ultrashort coherent soft X-ray radiation in storage rings using angular-modulated electron beams. *Phys. Rev. Lett.* **104**, 084803 (2010). doi: [10.1103/PhysRevLett.104.084803](https://doi.org/10.1103/PhysRevLett.104.084803)
- [43] X. Wang, C. Feng, C. Yang, et al., Transverse-to-longitudinal emittance-exchange in optical wavelength. *New J. Phys.* **22**, 063034 (2020). doi: [10.1088/1367-2630/ab8e5d](https://doi.org/10.1088/1367-2630/ab8e5d)
- [44] Y. Lu, X. Wang, X. Deng, et al., Methods for enhancing the steady-state microbunching in storage rings. *Results Phys.* **40**, 105849 (2022). doi: [10.1016/j.rinp.2022.105849](https://doi.org/10.1016/j.rinp.2022.105849)
- [45] B. Jiang, J. G. Power, R. Lindberg, et al., Emittance-exchange-based high harmonic generation scheme for a short-wavelength free electron laser. *Phys. Rev. Lett.* **106**, 114801 (2011). doi: [10.1103/PhysRevLett.106.114801](https://doi.org/10.1103/PhysRevLett.106.114801)
- [46] K. Feng, C. Yu, J. Liu, et al., Coherent X-ray source generation with off-resonance laser modulation. *Opt. Express* **26**, 19067 (2018). doi: [10.1364/OE.26.019067](https://doi.org/10.1364/OE.26.019067)
- [47] X. Wang, C. Feng, C.-Y. Tsai, et al., Obliquely incident laser and electron beam interaction in an undulator. *Phys. Rev. Accel. Beams* **22**, 070701 (2019). doi: [10.1103/PhysRevAccelBeams.22.070701](https://doi.org/10.1103/PhysRevAccelBeams.22.070701)
- [48] W. Liu, C. Feng, Y. Jiao, et al., A coherent harmonic generation method for producing femtosecond coherent radiation in a laser plasma accelerator based light source. *J. Synchrotron Rad.* **28**, 669 (2021). doi: [10.1107/S1600577521002745](https://doi.org/10.1107/S1600577521002745)
- [49] X. Deng, J. Li, Y. Lu, Contribution of Wigglers to Radiation Integral in an Electron Storage Ring. arXiv 2410.12863 (2024). doi: [10.48550/arXiv.2410.12863](https://doi.org/10.48550/arXiv.2410.12863)
- [50] J. Zhao, Undulator in SLIM. Unpublished Note. Oct. 2023.
- [51] K. Bane, A simplified model of intrabeam scattering, in Proceedings of the 8th European Particle Accelerator Conference, Paris, France, 2002 (EPS-IGA and CERN, Geneva, 2002), p. 1443.
- [52] K. F. Bane, Y. Cai, G. Stupakov, Threshold studies of the microwave instability in electron storage rings. *Phys. Rev. ST Accel. Beams* **13**, 104402 (2010). doi: [10.1103/PhysRevSTAB.13.104402](https://doi.org/10.1103/PhysRevSTAB.13.104402)
- [53] J. Feikes, M. von Hartrott, M. Ries, et al., Metrology Light Source: The first electron storage ring optimized for generating coherent THz radiation. *Phys. Rev. ST Accel. Beams* **14**, 030705 (2011). doi: [10.1103/PhysRevSTAB.14.030705](https://doi.org/10.1103/PhysRevSTAB.14.030705)
- [54] X. J. Deng, Y. Zhang, Z. L. Pan, et al., Average and statistical properties of coherent radiation from steady-state microbunching. *J. Synchrotron Radiat.* **30**, 35 (2023). doi: [10.1107/S1600577522009973](https://doi.org/10.1107/S1600577522009973)
- [55] N. Nakamura, R. Kato, H. Sakai et al., High-power EUV free-electron laser for future lithography. *Jpn. J. Appl. Phys.* **62**, SG0809 (2023). doi: [10.35848/1347-4065/acc18c](https://doi.org/10.35848/1347-4065/acc18c)